Impact study of COVID-19 lockdown measures on air quality and climate

Impacts of COVID-19 lockdown measures on Air quality and Climate (ICOVAC)

Final Report

Title	ICOVAC Final Report
Reference	ICOVAC_S5pI_CHOCHO_CCN_FR
Contract	4000127610/19/I-NS CCN1
Issue	2.0
Date of issue	13/07/2021
Authors:	C. Lerot, M. Bauwens, I. De Smedt, T. Stavrakou, N. Theys (BIRA-IASB) R. van der A, J. Ding, H. Eskes, B. Mijling (KNMI) M. Buchwitz, K. Lange, A. Richter, O. Schneising (IUP-Bremen) T. Borsdorff (SRON) Coordinated by Christophe Lerot
Distributed to:	Christian Retscher, ESA ICOVAC Consortium

Table of Contents

1 Executive Summary

With the onset of the COVID19 pandemic in early 2020, significant restrictions, including closing of shops, pubs, and restaurants, limitations of displacement and social contacts, obligation of homeworking… have been implemented in many countries worldwide to limit the spread of the disease. Those lockdown measures have had a significant impact on human activities and therefore on anthropogenic emissions of pollutants into the atmosphere. The 1-year ICOVAC project is built following an ESA initiative upon experts from the Royal Belgian Institute for Space Aeronomy (BIRA-IASB), the University of Bremen (IUP-Bremen), the Royal Netherlands Meteorological Institute (KNMI) and the Netherlands Institute for Space Research (SRON) and aims at

- Evaluating the impact of COVID19-related restriction measures on atmospheric NO_2 concentrations in different regions of the world using satellite data products but also ground remote or in situ measurements. This activity is supported by models, which help to better interpret the observations by considering factors other than COVID-related emission changes affecting NO_2 concentrations. When possible, the changes in NOx emissions due to lockdowns are also estimated either using models or specific data analyses;
- Investigating whether any footprint of lockdown measures can be detected (and quantified) from space using other satellite atmospheric data products available to the consortium. The considered species are SO_2, CO, HCHO, CHOCHO as well as the climate-related gases CO_2 and CH_4.

The present report aims at describing the main findings of the study, which are summarized below.

Impact on NO_2 *tropospheric column and concentrations and on NOx emissions.*

- Significant reductions of NO_2 amounts have been observed and quantified in many locations worldwide during the local lockdowns. Space and ground measurements showed very consistent reductions in 2020 compared to 2019.
- In Europe, the strongest reductions (-40/-50%) have been observed during the most intense lockdown phase (March/April 2020) in Southern European and French cities. NO_2 reductions were more moderate in the Northern and Eastern European countries (-15/-25%). Using models, the contribution of meteorology on the year-to-year variability has been estimated to be as large as 15% for the NO_2 columns, and 21% for in-situ concentrations.
  NOx emissions derived from TROPOMI with the DECSO algorithm showed similar overall reductions in Europe. In many cities, they also showed reductions in the first months of 2020, before the implementation of any COVID19 restriction. Those are linked to a general long-term downward trend of NOx emissions in European cities, which needs to be considered in the analyses. This has also been highlighted by ground data in the cities of Bremen/Germany and Vienna/Austria, which show reduced NO_2 concentrations in 2020 due to both a long-term trend and the local lockdowns.
- In China, NO_2 columns and concentrations have been reduced by about -40% in many cities during the severe lockdown of February 2020, and then rapidly rebounded. In Wuhan, this reduction was even more severe (-60%) and lasted until June. The observed 2020/2019 NO_2 ratio in China could be reproduced with simulations realized with the CTM MAGRITTEv1.1 using a COVID19-optimized anthropogenic emission inventory, both during the most intense lockdown phase in February and later when the NO_2 returned to usual levels.
  Using TROPOMI observations, NOx emissions have also been inverted with the DECSO algorithm and were found to be lower by about -20/-50% in the urban areas of China and by -40% in the energy sector compared to last year. The inversion of those emissions at high

spatial resolution clearly indicated that the strongest NO_2 reductions took place in area where the traffic-related emissions dominate.

- NOx emissions have been derived directly from satellite observations for a series of cities worldwide: In Buenos Aires and New Delhi, they have been estimated to be respectively up to -56% and -89% lower in April 2020 compared to 2019. In New York, Riyadh, Kano and Madrid, despite larger uncertainties related to the analysis, lower NOx emissions were also often derived in 2020 with a timing depending on the local COVID19 waves.

Impact on other species.

- Based on a novel algorithm to retrieve SO_2 tropospheric columns from TROPOMI measurements with an improved detection limit, some significant reductions of SO_2 have been identified in Northern China (-75%) and in India (-40%) during their local lockdowns (February and April respectively).
- Similarly, reductions have been identified in the TROPOMI tropospheric columns of HCHO and CHOCHO in Northern China (-40%) and Northern Indo-Gangetic Plains (-20% and -25% respectively; -40% and -50% over New Delhi). Simulations realized with the CTM MAGRITTEv1.1 using a COVID19-optimized anthropogenic emission inventory indicate HCHO and CHOCHO reductions in China consistent with the observations.
- On contrary, the longer atmospheric lifetimes of CO and CH_4 and the large variability of CO prevented to identify any unambiguous signature of the COVID measures in their TROPOMI column measurements in any region worldwide.
- A thorough analysis of an ensemble of XCO_2 satellite data products indicated an emission reduction of a few percent over East China. However, the associated uncertainty, which is on the order of the derived emission change, makes this result statistically insignificant. Detecting and quantifying the impact of human-induced emission reductions via analysis of XCO_2 satellite data is challenging because of the weak signal, the impact of biospheric CO_2 fluxes, the sparseness of the data and remaining biases of the satellite data.

Finally, an important activity for the ICOVAC team was to contribute to outreach and communication to both public and experts on the impact on air quality and climate-related gas concentrations of the unprecedented measures taken to stem the new coronavirus. This has been largely achieved with contributions to 14 press articles and web stories and to 6 press releases. The consortium has also been significantly involved into the preparation of a specific MOOC module on this topic and one team member contributed to a BBC docuseries. Communication to the scientific community has also been intense with contributions to 19 peer-reviewed articles published or in preparation, as well as via at least 15 presentations at international conferences.

2 Introduction and overview of activities

The global crisis due to the pandemic spread of the coronavirus COVID-19 that the humanity is facing since early 2020 led to unprecedented measures taken by different governments worldwide in order to limit as much as possible the number of impacted persons. Those measures include social distancing, banning of people gathering and travels, encouragement for teleworking, closings of schools, universities, restaurants, pubs and non-essential product shops, border closings, etc. All those measures have been implemented by the individual countries at different moments, depending mostly on the virus outbreak timing in each territory. China has been the first country to be strongly impacted in January 2020 and lockdown measures have been taken at that time for trying to stem the spread. The virus then propagated to other countries. From early March 2020, European countries have been affected by the virus outbreak and most of them entered into a period of lockdown for a few weeks or months[1]. Very rapidly, the virus also propagated to countries in America and Africa. From May 2020 onwards, the virus propagation weakened, most likely resulting from all taken social distancing measures, which could be progressively lifted out during summertime. However, a second wave of the coronavirus struck many countries from early October 2020 onwards, which obliged many governments to reintroduce social restrictions to slow down again the virus propagation. Despite the restrictions in place, a third wave stroke again Europe in Spring 2021. In early summertime 2021, the benefit of vaccination has progressively improved the situation in the United States and Europe and most of the restrictions have been progressively lifted out. Many other countries such as India, Brazil where access to vaccination is more limited are still strongly impacted. Furthermore, the spread of different variants of the virus requires specific attention.

All those measures have a significant impact on the anthropogenic emissions in the atmosphere as they lead to drastic drops in road and air traffic and a strong reduction of industrial activities in non-essential sectors. On the other hand, other sectors might have faced increased demands, like domestic heating for example. Satellite measurements of nitrogen dioxide (NO_2) tropospheric columns are a direct proxy for anthropogenic emissions and a reduction of the NO_2 concentrations collocated with lockdown measures has been reported very rapidly at the early phase of the crisis. However, quantitative evaluations of the impact of lockdown measures on NO_2 quantities (and on NOx emissions) require accounting for the other factors impacting in a significant way NO_2 concentrations, such as the meteorology or longer-term emission changes. Besides NO_2, other atmospheric species such as CO, SO_2, glyoxal (prime product of the main contract), CO_2... originate, at least partly, from anthropogenic activity and might be impacted by the taken COVID-19 measures. It is beneficial to investigate whether such lockdown signatures are visible in the different available satellite atmospheric data products, and to quantify the observed changes, if possible.

The ICOVAC (Impacts of COVID-19 lockdown measures on Air quality and Climate) project is a response from a consortium built on experts from the Royal Belgian Institute for Space Aeronomy (BIRA-IASB), the University of Bremen (IUP-Bremen), the Royal Netherlands Meteorological Institute (KNMI) and the Netherlands Institute for Space Research (SRON) to an ESA initiative to address those questions. The 1-year ICOVAC study relied on three main activity components that were inter-related:

[1] For a description of the timing of different virus waves and lockdowns per region worldwide, see for example https://www.ft.com/content/a2901ce8-5eb7-4633-b89c-cbdf5b386938 or https://en.wikipedia.org/wiki/COVID-19_lockdowns.

- An analysis of satellite data products for tropospheric NO_2 columns and other trace gases including CO, VOC, and greenhouse gases (CO_2 and CH_4)… to investigate if they present signatures of the human emission reductions due to lockdown measures in the different regions worldwide (Asia, Europe, US,…).
- An analysis of collected remote sensing and in situ ground data in Europe and China to detect possible lockdown signatures in the time series. Results of this analysis have been confronted to the satellite data analyses and to models.
- A comprehensive modelling component based on CAMS, DECSO and MAGRITTE to support the interpretation of the observations. Those models allowed disentangling the changes in the satellite products caused by the meteorology or by actual human emission changes (possibly resolved per industrial sector). Optimized NOx emissions have also been derived in China and Europe using inverse modelling techniques. Those updated NOx emissions allowed to better estimate the impact of COVID-19 measures on air quality, but also on climate as they can be used as a proxy for fossil-fuel CO_2 emissions.

This final report aims at presenting and summarizing all the findings and activities carried out during the project.
Section 3 focuses on investigations related to species linked to the air quality aspect. A large part of this section is dedicated to the analysis of satellite and ground-based NO_2 measurements in many different locations worldwide and of their inter-consistency (section 3.1). A specific focus is on China and Europe where the consortium has the tools needed to go one step further and to evaluate and remove the contribution of meteorology from the observed NO_2 changes in order to better quantify the effect of emission changes. Furthermore, 2020 and 2019 NOx emissions, whether directly derived from the observations or based on inverse modelling techniques, are compared in different regions of the world.
Section 3.2 presents the findings of search for footprints of COVID-19 lockdowns in a series of other air quality-related satellite data products, including SO_2, CO, formaldehyde and glyoxal.
Section 4 focuses on the climate-related species CO_2 and CH_4 and presents the conclusions from the satellite data product analyses carried out for trying to detect a possible impact of emission changes on the corresponding measurements.
Finally, this unprecedented crisis generated a large interest of the public in the topic. Therefore, the consortium has also devoted a significant effort in outreach with a large number of contributions to interviews, general articles, press releases or web stories. Communication has not only been ensured for the public, but also for the scientific community with a number of presentations at workshops and conferences as well as the publication or the preparation of many peer-reviewed articles. All these contributions are listed in section 5.

3 Impact of lockdown measures on air quality

3.1 Nitrogen dioxide (NO_2)

3.1.1 Analyses of satellite observations

3.1.1.1 Sharp changes in NO_2 levels detected by TROPOMI over large cities (BIRA-IASB)

The TROPOMI data used for our analysis are L3 data for NO2 for the period from January 2019 to November 2020. The data, gridded at 0.05×0.05 degree, are based on the offline L2 data version 1.3.2 with the identifier "S5P_OFFL_L2__NO2", and are processed using the HARP software (https://atmospherictoolbox.org/harp/). Scenes with a quality flag lower than 0.75 are removed from the analysis. The time series shown in Figure 3.1.1 and Figure 3.1.2 are based on a daily average of all valid data within a 25×25 km2 square box around the city centre. A running mean is used to reduce the noise that is associated to meteorological variability. Since the day-to-day column variability is larger for the European cities, a longer period is used for the running average (28 days) in Figure 3.1.2 compared to Figure 3.1.1 (14 days).

The lockdown periods and the measures taken against the spread of the virus have been country- and often city-specific. Figure 3.1.1 illustrates the temporal evolution of NO_2 columns from January to May over large cities in different continents. The TROPOMI observations indicate substantial decreases in NO_2 during the lockdowns in all studied cities, but the reductions vary significantly from one city to another.

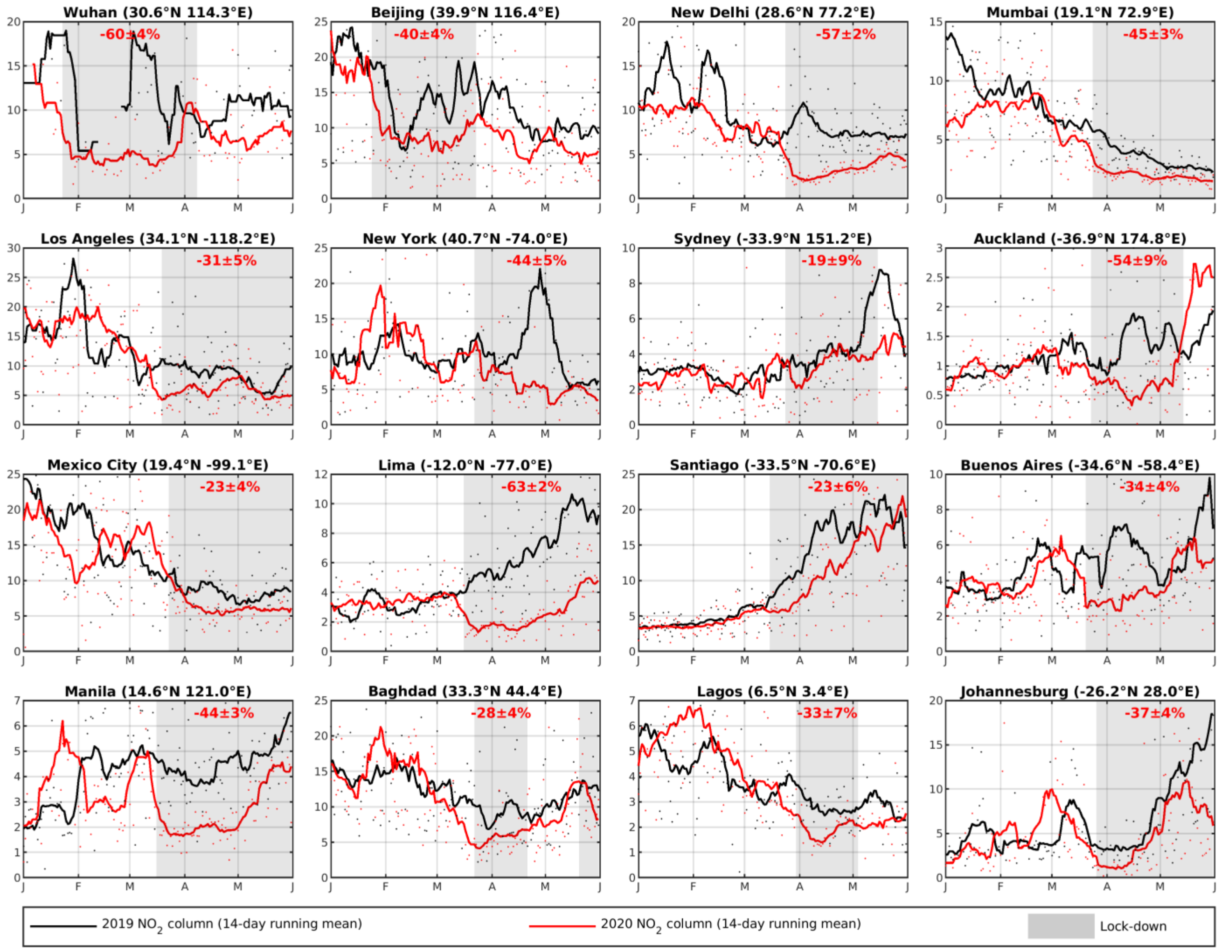

Figure 3.1.1: TROPOMI NO_2 column (in 10^{15} molec.cm^{-2}) time series from 1 January to 1 June for selected cities in 2019 (black dots) and 2020 (red dots). TROPOMI observations are averaged over a 25×25 km^2 box around the city centre. The lines indicate the 14-day running mean for 2019 (black) and 2020 (red). The grey zones indicate the official lockdown period for each city. The reduction of the average NO_2 column during the lockdown period relative to the same period in 2019 is given inset. The given uncertainties are standard errors calculated from the retrieval uncertainties, accounting for the number of days with valid data.

In Wuhan, the first city to issue quarantines and lockdown measures, the NO_2 column was drastically reduced (-60%) between 23 January and 8 April 2020 compared to the same period in 2019. This reduction is in good agreement with estimated reductions based on TROPOMI NO_2 over 11 February-2 March 2020 (-43%, Bauwens et al. 2020), and in situ NO_2 observations in Wuhan

(-55%, Shi and Brasseur, 2020). Note however, the strong day-to-day NO_2 column variability due to meteorological factors, as well as the missing data over Wuhan in February 2019 due to clouds. Model calculations by Liu et al. (2020) indicate that meteorological variability could have led to increased NO_2 columns in 2020 compared to 2019, suggesting that the observed NO_2 reductions underestimate the impact of emission reductions due to Covid-19. The lifting of the restrictions on 8 April led to a progressive increase of NO_2 levels, which however remained lower than in 2019, likely, because the population was still advised to stay at home as much as possible and schools remained closed. A similar response in NO_2 levels was observed in Beijing, but the decreases were less pronounced (-40%), in excellent agreement with the reported decrease based on in situ NO_2 measurements (-40%, Shi and Brasseur, 2020). The weaker response could be due to the less drastic measures adopted in Beijing, because locally sustained Covid-19 cases were lower than in the Hubei province. Strong NO_2 reductions were observed for other Chinese cities, like Nanjing, Qingdao and Zhengzhou, based on TROPOMI NO_2 observations (Bauwens et al. 2020).

The strongest NO_2 decline among all cities was observed in Lima (-63%), where very strict stay in-door orders have been enforced. A drastic NO_2 drop compared to the 2019 levels marked the start of the lockdown, and the levels remained very low throughout the entire lockdown period. The gradual increase of NO_2 columns in Lima and other Southern Hemisphere cities from January to May reflects the natural seasonal variation of NO_2 levels, which peaks in Southern Hemisphere wintertime due to longer lifetime in the winter season.

In Buenos Aires, the observed reduction was relatively weaker than in Lima over the entire lockdown period (-35%), but was particularly marked during the first month of the lockdown (20 March-20 April 2020), because of a compulsory quarantine period and near-total shutdown. Although a partial lifting of the measures was issued after 10 April for many provinces of Argentina, the measures in the Buenos Aires agglomeration were maintained due to the elevated number of cases. More moderate reductions are found for Mexico City (-23%) and Sao Paulo (-28%) during the lockdown in comparison to the same period in 2019, that could be attributed to the pressure of the population and the reluctance of their governments to strictly implement the coronavirus guidelines.

Strong reductions were observed over the entire lockdown period in the heavily hit cities in south-west Europe, Los Angeles and New York, with reductions ranging between -32% and -54% (Bauwens et al. 2020). Note however, that in these regions, the start of the lockdown period is generally less marked partly because the lockdowns were not as strictly enforced in Europe and the U.S. as in China and India. Moreover, the satellite signal displays a strong variability attributed to meteorology, e.g. over Paris, New York and Los Angeles in 2019. This variability is estimated at about 13% for European cities, as discussed in section 3.1.1.4. In Sydney, the reduction was moderate (-14%) and delayed with respect to the onset of the measures. This delay could be due to the initial disrespect of the bans on gatherings and social events, obliging the government to issue new legislation on people movement.

A quick and strong response of the NO_2 columns to the lockdown measures was observed in Auckland, New Zealand (-55%). The lockdown in New Zealand was swift and tight, with effectively communicated and largely accepted rules. The end of the lockdown coincided with a strong increase in NO_2 pollution, from 1.8×10^{15} molec.cm^{-2} to 3×10^{15} molec.cm^{-2} in the last 3 weeks of May.

In Africa, Nigeria was among the countries with the highest number of cases (Ekienabor, 2020). The locking down of Lagos for two weeks was announced on 30 March. The NO_2 column declined by -33% during the lockdown with respect to the same period of last year, and remained lower than in 2019 after the lifting of restrictions on 4 May. An NO_2 column decrease of similar magnitude (-37%) was observed in Johannesburg, where a national lockdown was enacted on 26 March 2020, and a gradual easing from 1 May. In Sub-Saharan Africa the emissions reductions in April were

significant, larger in populous and industrialized areas, whereas no noticeable drop was found in less developed regions (Masaki et al. 2020).
Finally, the Iraqi capital Baghdad faced an initial lockdown starting on 22 March until 21 April and a second partial lockdown from 20 May and for two weeks in reaction to a spike in infections since restrictions were relaxed in late April to ease the Ramadan celebration. The NO_2 column responded quickly, as confirmed by the rapid drop upon issuing the curfew measures.

3.1.1.2 Up-to-date time series over European cities (BIRA-IASB)

Figure 3.1.2 shows the temporal evolution of the NO_2 columns in a 25×25 km^2 box around 4 European cities between January and November 2019 and 2020 as well as their relative changes.
In London, we observe very low columns at the end of January 2020 associated with specific meteorological conditions (Gaubert et al., 2020). Shortly after the announcement of the lockdown on 23 March 2020, the NO_2 columns reduced by 40%, but bounced back at normal levels in May. Moreover, we did not observe abrupt changes due to the announcement of the second lockdown in November. Overall, the variation in 2020 NO_2 in London are close to the 2019 variations, and cannot be clearly linked to the COVID-19 measures. Moreover, in January-February 2019 very few TROPOMI NO_2 data are available over London due to cloudy conditions. Therefore, the use of a running mean generates an artificial plateau around the few days with observations. In Paris as well, meteorology is responsible for extremely low NO_2 columns observed in February and March 2020, before the onset of the lockdown. The start of the lockdown on 17 March 2020 led to a decrease of NO_2 columns to values up to 60% lower as in 2019. A slow recovery was observed afterwards, but the announcement of a second lockdown on 30 October might have induced a new reduction in NO_2.
In Madrid, a strong NO_2 column reduction (60%) is observed after the first lockdown. NO_2 columns recovered by the end of July, but a new lockdown announced on 20 August resulted in a significant column decline by the end of September.
In Rome, NO_2 columns stayed low since the start of the COVID-19 crisis. The columns that were about 50% lower in the beginning of April 2020 compared to April 2019, gradually increased, but until today, they are about 20% lower on average than in 2019.
Figure 3.1.2 also shows that NO_2significant reductions in NO_2 columns were found in Northern Europe in January-February, in addition to the NO_2 decrease in response to the later economic slowdown. Since no lockdown was imposed at that time in Europe, these changes are the result of meteorological variability. Barré et al. (2020) and Goldberg et al. (2020) stress that meteorology complicates the analysis of observed data and that such natural variations have a large impact, sometimes competing with or even exceeding the effects of the Covid-19 shutdowns.

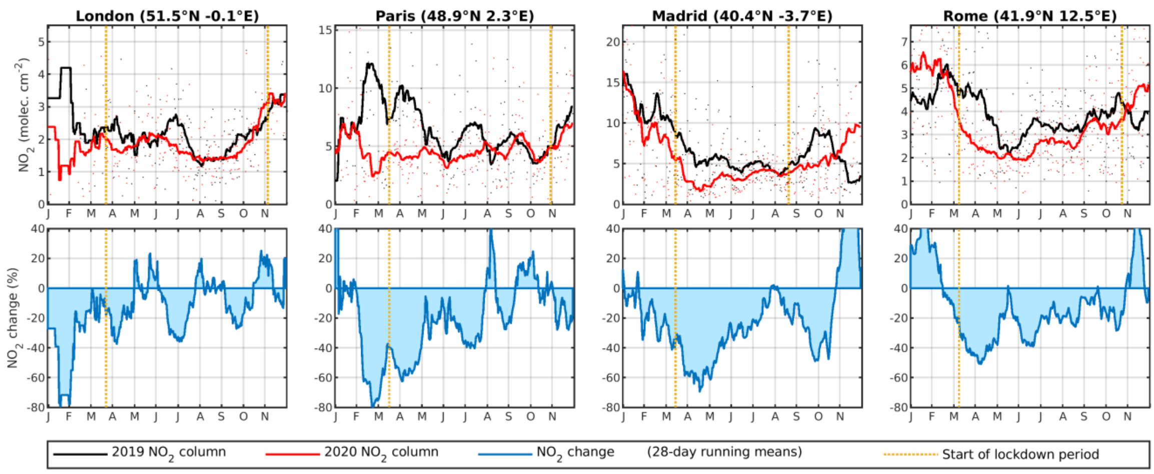

Figure 3.1.2: The upper panels show the 28-day running mean of the NO_2 columns over four European cities between January and November 2020 in 2019 and 2020. The lower panels show the relative reduction of NO_2 in 2020 compared to 2019. The yellow lines indicate the starting day of lockdown periods. The coordinates of the city centres are obtained from the https://geonames.org.

3.1.1.3 Examples of NO_2 reductions observed by TROPOMI (KNMI)

In relation to all the media attention in 2020 a large number of plots were generated comparing lockdown periods with similar periods in 2019 (as reference). All around the globe TROPOMI has detected major decreases in NO_2NO_2, and graphical material was produced for China, South-West Europe, North-West Europe, Eastern Europe, India, Middle East, Africa, North America and several countries and cities in South America (see also section 5).

One example of such a plot is the composite shown in Figure 3.1.3. This image was produced for the Levelt et al. 2021 preprint.

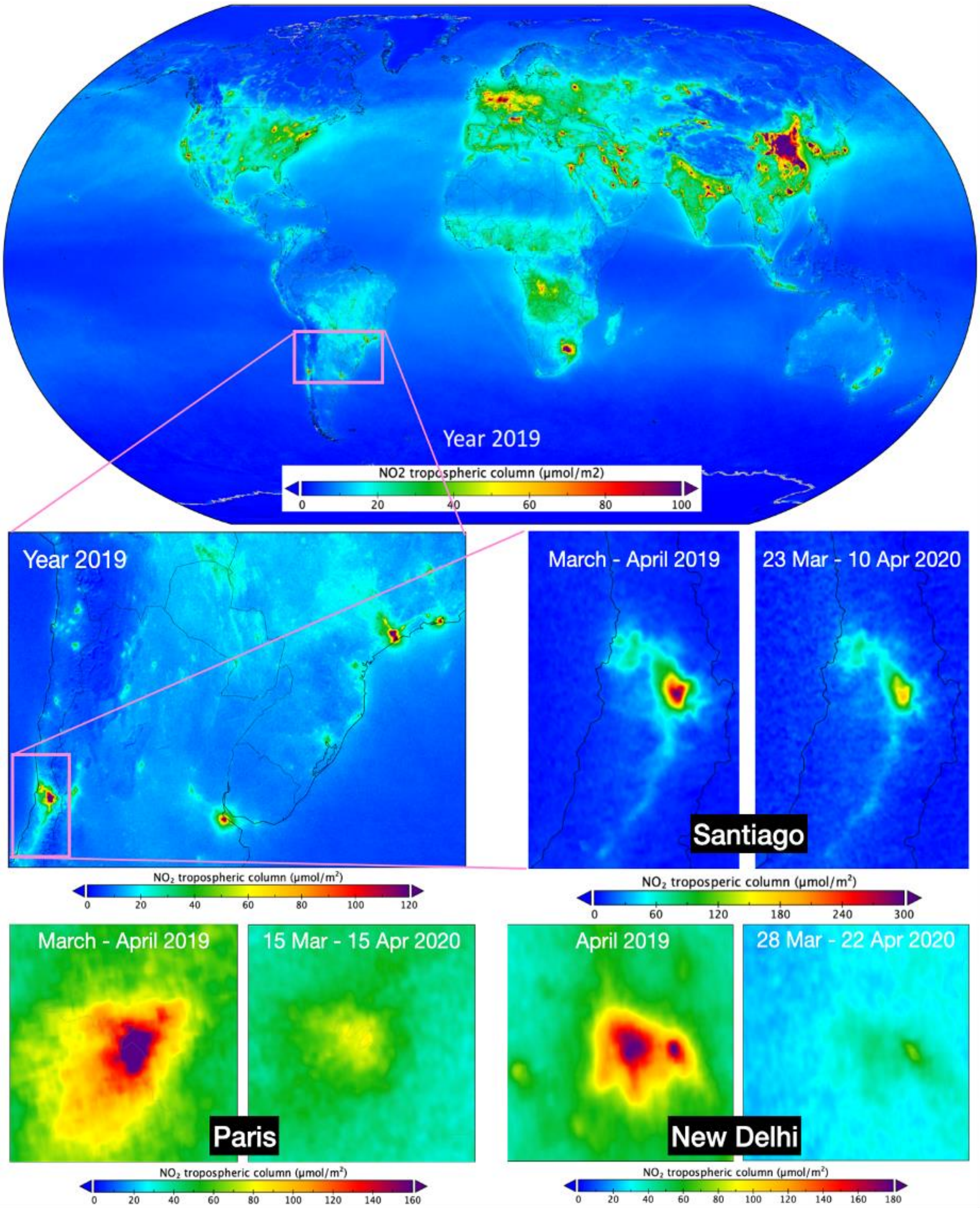

Figure 3.1.3: Global distribution of NO_2NO_2 based on the annual average of tropospheric column amounts of NO_2NO_2 measured by TROPOMI for 2019 (top panel) shown in units of micromole per m2. Using the same data, several zoom-in plots are shown in the middle and bottom panels: regional zoom-in for central South America (middle left) and a city-scale zoom-in over Santiago, Chile (middle right panels, comparing 23 March to 10 April 2020 with March-April 2019), over Paris (lower left, comparing 15 March to 15 April 2020 with March-April 2019) and over New Delhi (lower right, comparing 28 March to 22 April 2020 with April 2019). Note the different color scales in the three subpanels. The domain size of the panels is 1.5 x 1.0 degree for Paris, and 1.1 x 1.0 degree for New Delhi. Reference: Levelt et al., 2021.

3.1.1.4 Correction for the meteorology contribution to observed NO_2 changes in Europe (KNMI)

The TROPOMI NO_2 observations were analysed on a month-by-month basis, starting 15 March. In March-April 2020 we observe the strongest impacts of the lockdowns, with 40-50% reductions in the NO_2 tropospheric columns over major cities in south-west Europe (Madrid, Rome, Milan, Paris) compared to 2019. These large reductions lasted until early May, after which the strict lockdowns have been relaxed. This can be seen in Figure 3.1.4, where we observe a recovery of the 2020 concentrations relative to 2019. However, also in May-June there is still a clear indication that concentrations did not reach the values observed in 2019.

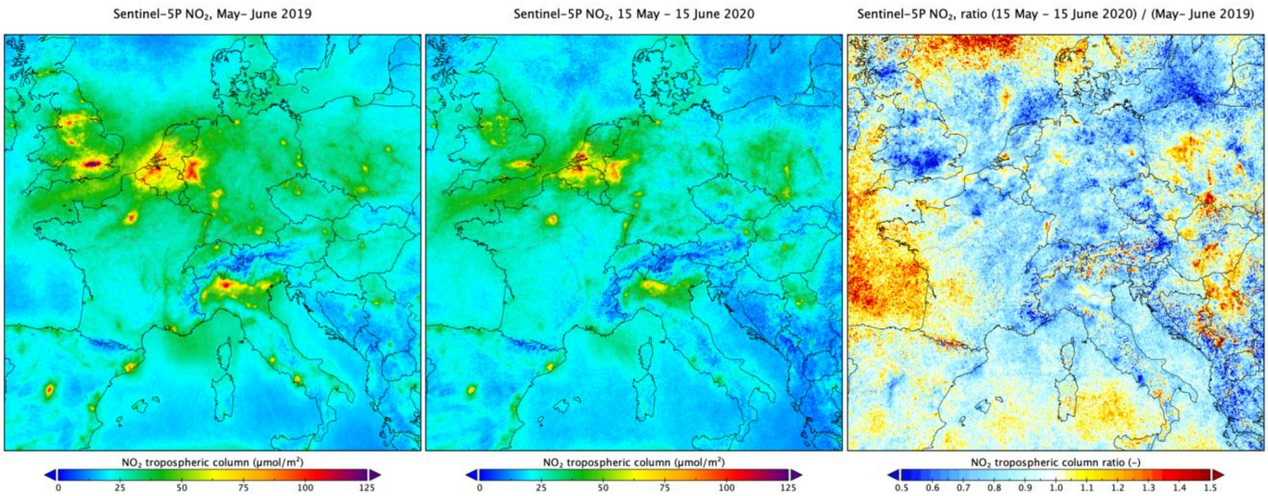

Figure 3.1.4: TROPOMI NO_2 tropospheric columns in May-June 2019 (left), 15 May to 15 June (middle), and the reductions calculated from the ratio between vertical column concentrations in 2020 and 2019.

Locally, changes in the weather, even when averaged over a full month, can still be substantial and will impact the 2020/2019 ratio. So only part of the observed differences between the years may be attributed to the COVID-19 measures and related emission reductions. In order to estimate the impact of the weather we performed model runs with the LOTOS-EUROS model version 2.2 (CAMS configuration) for 2019 and 2020 with fixed emissions at a resolution of 0.1 x 0.1 degree. The hourly model fields were post-processed: the model profiles were co-located to the location and time of each of the cloud-cleared (qa_value > 0.75) TROPOMI observations. The profiles were integrated to 3 km altitudes and convoluted with the TROPOMI averaging kernels. A tropospheric column was generated by adding the profiles of the CAMS-global forecasts from 3km altitude up to the tropopause. Next, these columns were averaged over the month to represent the satellite observations (like shown in Figure 3.1.4) as good as possible. Subsequently these 2D column fields were averaged over boxes of 0.6 degree longitude x 0.4 degree latitude, centered over the city centers of major towns in Europe.

Figure 3.1.5 shows the results of these simulations. On average, the standard deviation is 13%. However, in some cases the difference may be larger. We looked in more detail at London in May-June. We find that the mean wind direction is different in 2019 and 2020, shifting the maximum of NO_2 of the pollution cloud over the city to different suburbs. The fixed choice of the box used to average the data is a second reason for (substantial) differences from year to year, adding to the total variability observed. A better approach would be to analyze the city plumes and time-average over the plumes accounting for the changes in location and wind speed.

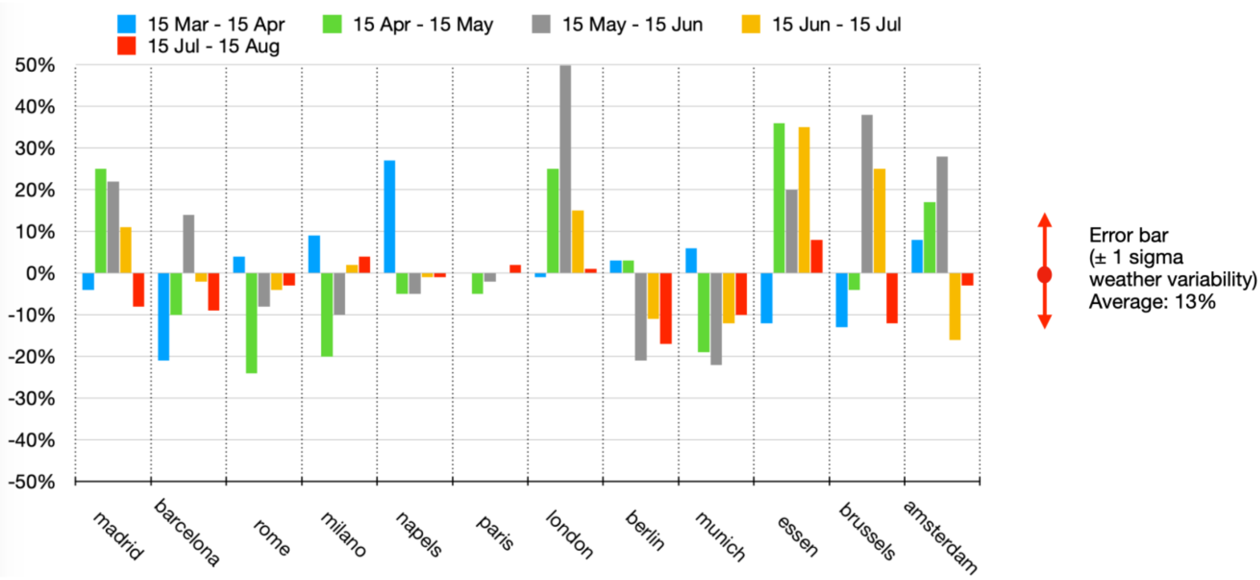

Figure 3.1.5: LOTOS-EUROS simulations of the ratio of monthly-mean NO_2 tropospheric column observations for 2020/2019, using a fixed emission inventory in the model. The simulations have been averaged over boxes around the centres of major cities in Europe (horizontal axis), and for 5 monthly periods (legend on top). The mean variability, attributed to differences in weather between the two years, is 13% (1 sigma) for the 12 cities/agglomerates shown.

In Figure 3.1.6 we show the TROPOMI observed relative reductions in 2020 compared to 2019 on a monthly basis. The dashed line shows the TROPOMI results corrected for the weather impact (by multiplying with the ratios shown in Figure 3.1.5. Correcting with the LOTOS-EUROS simulations does not change the main conclusions: in south-west Europe, we observe major decreases in NO_2 of 35-50% over the large cities compared to 2019. These decreases become less, but a significant reduction compared to 2019 remains of the order of 20%, indicating impacts of the relaxed lockdowns and impacts on the economy. In north-west Europe, the impact of the lockdowns was a reduction in NO_2 of the order of 15-20%, and the reduction stays around 15% also for the later months (May-August). The LOTOS-EUROS corrected results sometimes show unexpected values, like the strong reduction in May-June in N-W Europe. This may indicate problems in the model to accurately simulate the year-to-year variability.

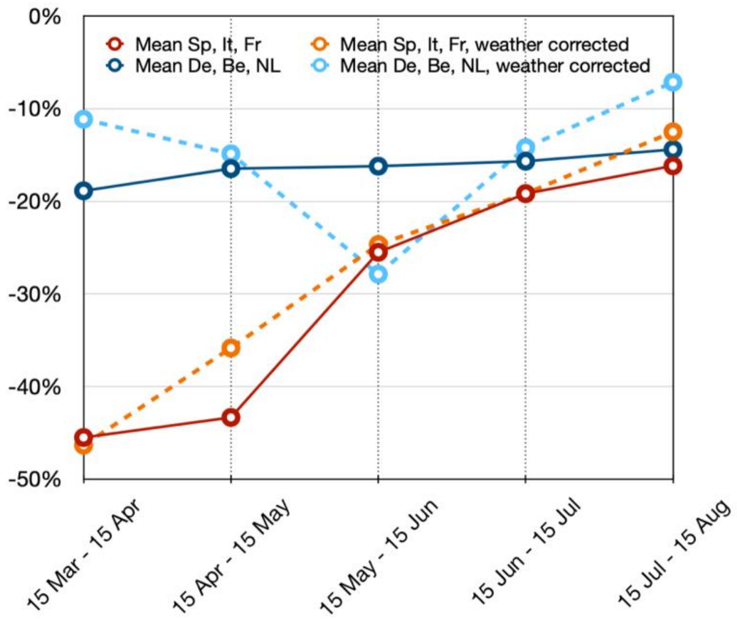

Figure 3.1.6: NO_2 reductions calculated from the ratio between satellite tropospheric column observations in 2020 and 2019. The solid line are the satellite ratios. The dashed line are the same ratios but corrected for weather influences using the LOTOS-EUROS model with fixed emissions. The results are averaged over major cities in Spain+Italy+France (red/orange), and Germany+Belgium+Netherlands (blue, light blue).

3.1.1.5 Correction for the meteorology contribution to observed NO_2 changes on global scale (KNMI)

KNMI have contributed to a recent review paper (Gkatselis et al., 2021) on the impact of COVID-19 measures on air quality. The abstract of this paper is reproduced here:

"The coronavirus-19 (COVID-19) pandemic led to government interventions to limit the spread of the disease which are unprecedented in recent history; for example, stay at home orders led to sudden decreases in atmospheric emissions from the transportation sector. In this review article, the current understanding of the influence of emission reductions on atmospheric pollutant concentrations and air quality is summarized for nitrogen dioxide (NO_2), particulate matter (PM2.5), ozone (O3), ammonia, sulfur dioxide, black carbon, volatile organic compounds, and carbon monoxide (CO). In the first 7 months following the onset of the pandemic, more than 200 papers were accepted by peer-reviewed journals utilizing observations from ground-based and satellite instruments. Only about one-third of this literature incorporates a specific method for meteorological correction or normalization for comparing data from the lockdown period with prior reference observations despite the importance of doing so on the interpretation of results. We use the government stringency index (SI) as an indicator for the severity of lockdown measures and show how key air pollutants change as the SI increases. The observed decrease of NO_2 with increasing SI is in general agreement with emission inventories that account for the lockdown. Other compounds such as O3, PM2.5, and CO are also broadly covered. Due to the importance of atmospheric chemistry on O3 and PM2.5 concentrations, their responses may not be linear with respect to primary pollutants. At most sites, we found O3 increased, whereas PM2.5 decreased slightly, with increasing SI. Changes of other compounds are found to be understudied. We highlight future research needs for utilizing the emerging data sets as a preview of a future state of the atmosphere in a world with targeted permanent reductions of emissions. Finally, we emphasize the

need to account for the effects of meteorology, emission trends, and atmospheric chemistry when determining the lockdown effects on pollutant concentrations."

Data from 150 papers was digitized for this review. Of these 150 papers, about 50 reported satellite observations (a majority of papers was of course based on surface observations). Of these 50 papers, the vast majority used the TROPOMI NO_2 product, which demonstrates the huge increase of interest in this satellite dataset in 2020.

For the paper we produced a comparison between April 2020 (with the exception of China, where we focused on February 2020) and April 2019. The Copernicus Atmosphere Monitoring Service (CAMS) reanalysis results (Inness et al., 2019) were used to correct for changes in NO_2 caused by the variability of the meteorology between the months of April 2019 and April 2020. The emissions used in the CAMS reanalysis were based on "business as usual" scenarios, unaffected by COVID-19 reductions. The CAMS 3-D NO_2 fields were interpolated to the location and time of all the individual TROPOMI observations in April 2019 and 2020 used to construct the monthly mean. The averaging kernels were applied to obtain CAMS simulations of all the individual TROPOMI observations. These data were subsequently averaged over the month of April, and the CAMS ratio 2019/2020 was applied to the TROPOMI April 2020 monthly mean to correct for the expected meteorological impact on NO_2 between the two years.

The results of this procedure led to the figure in the Gkatselis paper reproduced below (Figure 3.1.7). In some regions we see a clear positive impact of the procedure (e.g. the North Sea area), while in other regions the results of the procedure are less conclusive.

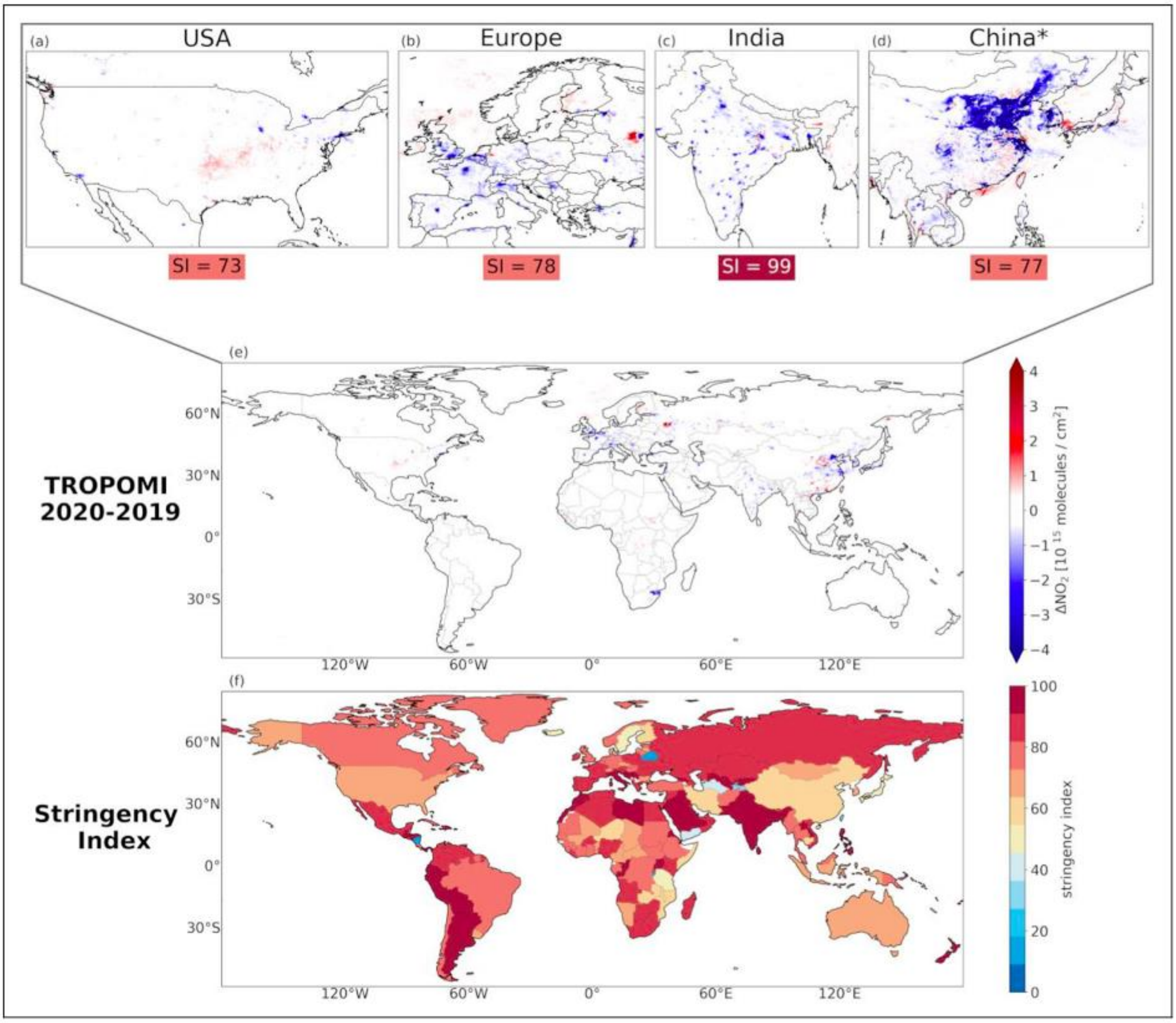

Figure 3.1.7: Meteorologically corrected TROPOMI NO_2 column difference between April 2020 and 2019 using the global Copernicus Atmosphere Monitoring Service-Integrated Forecasting System reanalysis in (a) the United States, (b) Europe, and (c) India at 0.1 x 0.1 resolution, as well as (d*) for the three post-Chinese New Year weeks in 2020 and 2019 in China at a 2 x 2 km resolution, (e) globally between April 2020 and 2019 at 0.4 x 0.4 resolution, and (f) the national stringency index as an indicator for the severity of lockdown averaged over April 2020. The corresponding stringency indices of the regions (a)–(d) are provided below the individual panels. Reproduced from Gkatselis et al., 2021, https://doi.org/10.1525/elementa.2021.00176.

3.1.1.6 Increasing the spatial resolution of TROPOMI NO_2 observations using oversampling over China (BIRA-IASB)

The large amount of TROPOMI observations at high resolution (3.5×5.5 km^2) allows us to generate data at even higher spatial resolution by performing temporal averaging on a spatial grid finer than the pixel resolution of the instrument. This method is referred to as *oversampling* and consists in increasing the spatial resolution of the observations at the expense of temporal resolution. It has proved to be useful to better characterize pollutants emissions from urban point sources (de Foy *et al.*, 2009; Zhu et al., 2014).

Here we applied this technique to generate monthly TROPOMI NO2 data at 0.02° × 0.02° over eastern China (20-44°N, 110-130°E) from February to June in 2019 and 2020. Figure 3.1.8

illustrates the resulting dataset. It also displays the average NO_2 columns and the corresponding relative NO_2 decrease over 2 regions (northeastern China, in black, and the city of Wuhan, in red). Over northeastern China, we find a reduction of -40% to -20% in February and March, respectively, followed by moderate reductions from April onwards. At the scale of the city of Wuhan, we detect much stronger reductions in March (-60%), and NO_2 columns stay lower than usual until June. Note that NO_2 columns over Wuhan were not available in February due to the presence of clouds.

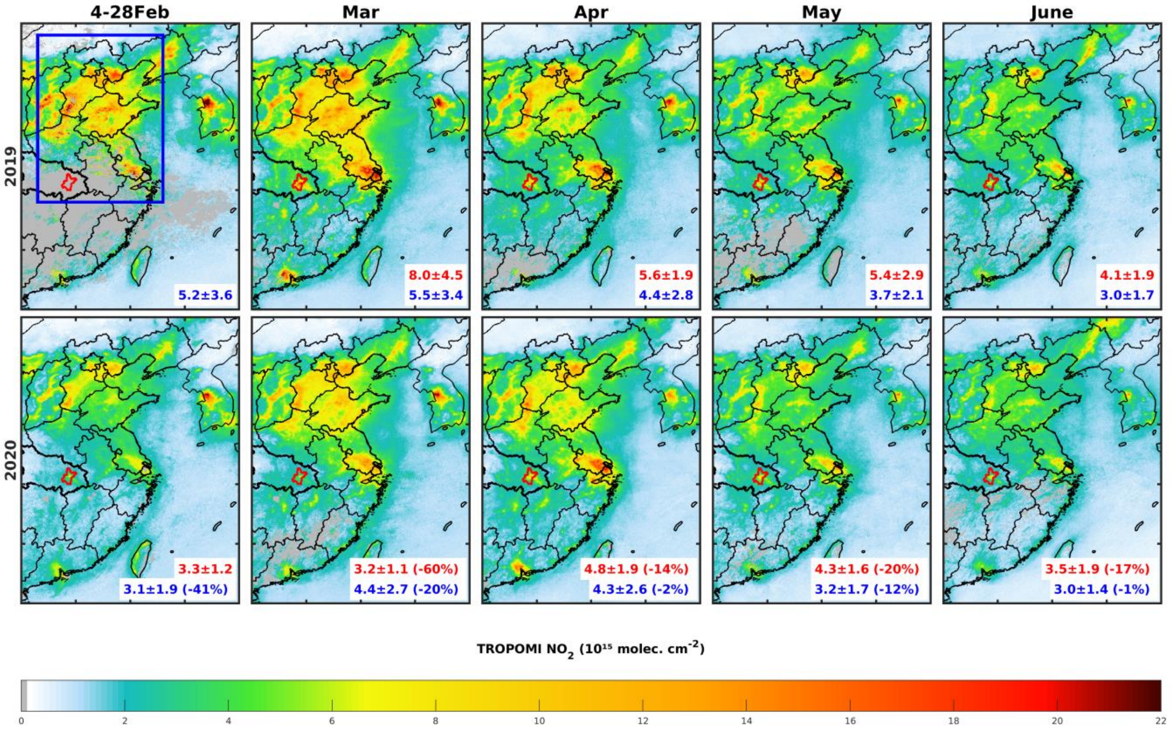

Figure 3.1.8: TROPOMI NO_2 data at 0.02° × 0.02° obtained by applying an oversampling method for the 5 periods indicated in the titles. The values shown in the right corner denote the average and the standard deviation of the NO_2 columns over the rectangular region indicated in blue (29-43°N and 111.5-123°E) and over the city of Wuhan in red. The percentages in parentheses indicate the relative NO_2 reduction over the respective region for the specific period.

The oversampled TROPOMI data are used in order to conduct a more detailed comparison with the in situ measurements, as described in section 3.1.2.3. Overall, the NO_2 reductions observed by TROPOMI are similar to the reductions observed using in situ data (see Figure 3.1.9). TROPOMI reductions agree quite well with in situ reductions in March, but are more pronounced in February and May. TROPOMI also observes a slight increase of NO_2 columns in April, which is not seen in the in situ data. On average, the NO_2 change observed by TROPOMI over February-June is equal to -19%, in close agreement with the in situ change (-16%).

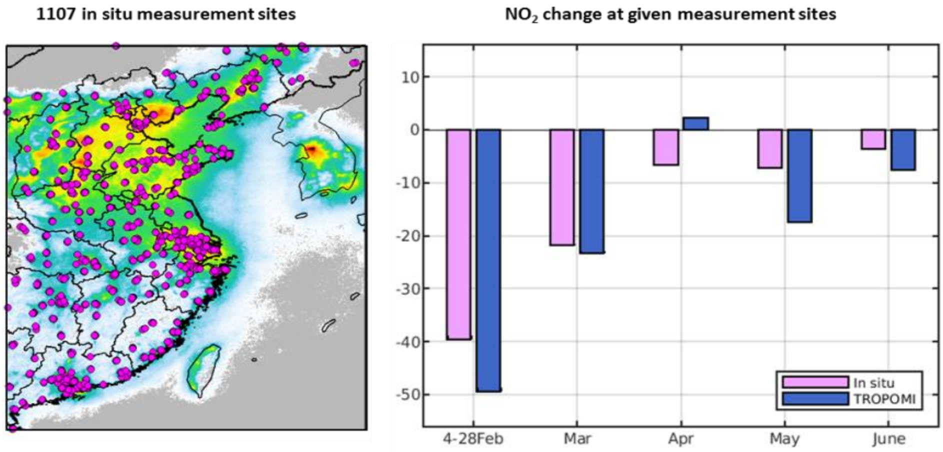

Figure 3.1.9: Left: Location of the in situ measurement sites (pink) and oversampled TROPOMI data at 0.02° × 0.02°. Right: Relative change in NO_2 observed using in situ measurements (pink) and oversampled TROPOMI dataset.

3.1.1.7 Comparison with NO_2 changes over China simulated with the CTM MAGRITTEv1.1

MAGRITTEv1.1 (Model of Atmospheric Composition at Global and Regional scales using Inversion Techniques for Trace gas Emissions, Müller et al., 2019) is run at 0.5°×0.5° over China and surrounding areas (73-150°E, 17-54°N) for February and May 2019 and 2020. Meteorological fields are from the ERA5 reanalysis (Hersbach et al., 2020). Biomass burning fluxes are taken from the GFED4s database (van der Werf et al., 2017, https://www.geo.vu.nl/~gwerf/GFED/GFED4), and biogenic emissions from the MEGAN-MOHYCAN model (Stavrakou et al., 2018; Opacka et al., 2021). Baseline anthropogenic emissions are provided by the CAMS-GLOB-ANT_v4.2-R1.1 inventory (Granier et al., 2019, Elguindi et al., 2020), which provides emissions from 2000 to 2020. The anthropogenic emissions during the pandemic are obtained from the CONFORM (COvid adjustmeNt Factor fOR eMissions) global dataset, which accounts for the slowdown of human activities through adjustment factors based on activity data, which are applied for all economic sectors and geographical regions (Doumbia et al., 2021). For China, on average, the adjustment factors for the main sectors, i.e. road transport, power generation, industry, and residential are estimated at 0.4, 0.6, 0.65, and 1.1, respectively, in February 2020, and at 1.0, 0.9, 0.8, 1.0 in May 2020 (Doumbia et al., 2021). The factor for air traffic emissions is estimated at 0.44 in February 2020 and 0.67 in May 2020. Figure 3.1.10 illustrates the emission ratio (E_{2020}/E_{2019}) for anthropogenic NO_x and VOC fluxes in February and May, as well as the difference in biomass burning VOC and isoprene fluxes between 2020 and 2019. Besides the average adjustment factors, the CONFORM dataset provides low and high estimates of those factors accounting for uncertainties due to lack of data or limited information for some activity sectors (Figure 3.1.11).

The modeled columns are sampled for the same days as the satellite observations, and account for the averaging kernels. We conduct the following simulations (Table 1): (i) R1, using the average CONFORM estimate; (ii) R1H and R1L, using the CONFORM high and low adjustment factors, respectively; (iii) R2, using the baseline anthropogenic emissions for 2020, which neglect the pandemic-induced disruptions.

Table 1: Description of the model simulations. All simulations use the same emissions for 2019 but differ regarding their 2020 emissions.

Short name	*Description*
R1	Use average estimates of CONFORM adjustment factors for anthropogenic 2020 emissions (Doumbia et al., 2021)
R1H	Use high estimates of CONFORM adjustment factors. The resulting anthropogenic fluxes for 2020 are higher than in R1.
R1L	Use low estimates of CONFORM adjustment factors. The resulting anthropogenic fluxes for 2020 are lower than in R1.
R2	Use 2020 baseline anthropogenic emissions from CAMS-GLOB-ANT_v4.2-R1.1 (Granier et al., 2019, Elguindi et al., 2020). These emissions do not account for pandemic-induced disruptions.

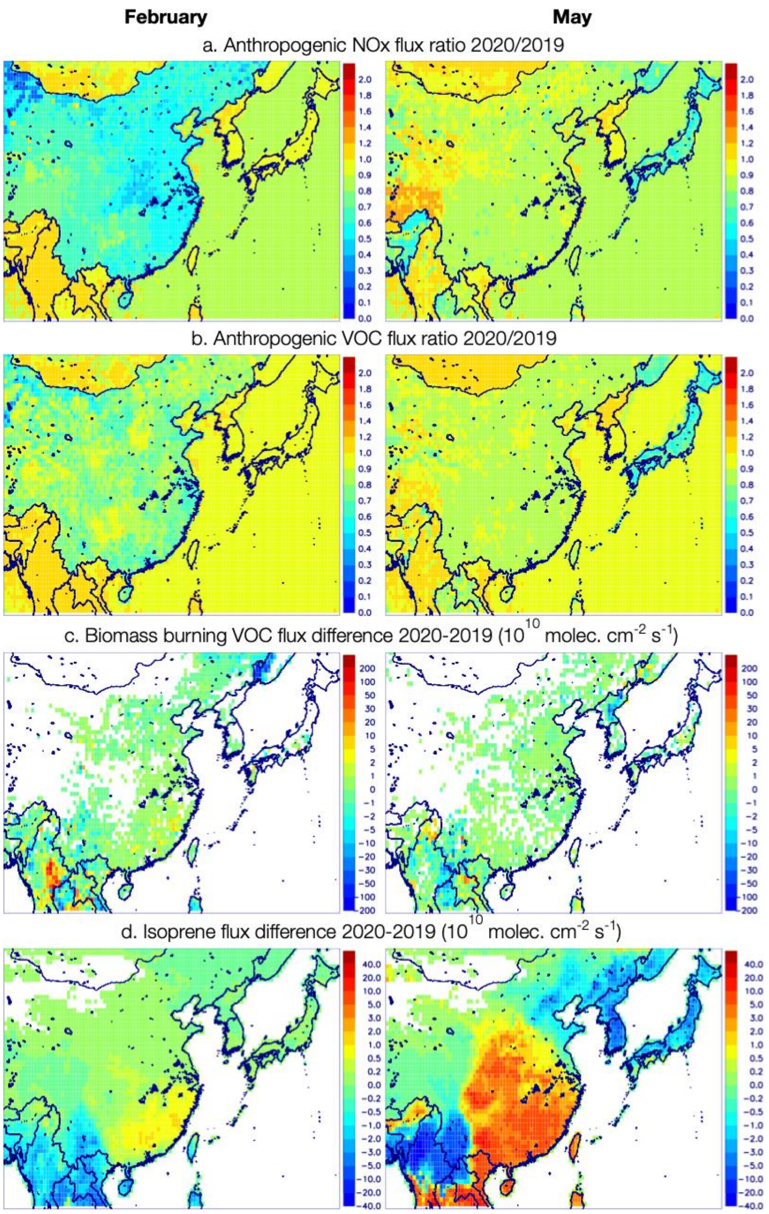

Figure 3.1.10: (a) Ratio of anthropogenic NO_x fluxes, February 2020 to February 2019 (left) and May 2020 by May 2019 (right). (b) Idem for anthropogenic VOC fluxes. The anthropogenic fluxes for 2020 are those of the CONFORM dataset (Doumbia et al., 2021). (c) Absolute flux difference 2020-2019 for biomass burning VOCs in February (left) and May (right). (d) Idem for isoprene biogenic fluxes.

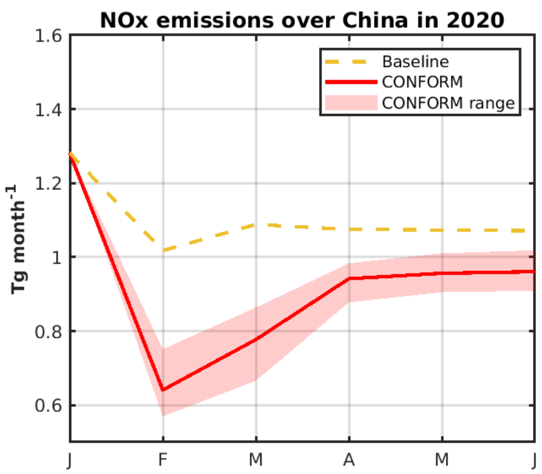

Figure 3.1.11: NOx emission estimates over China according to the baseline inventory CAMS-GLOB-ANT_v4.2-R1.1 (dashed), and the CONFORM emissions which account for the slowdown of economic activities due to the crisis (red). The pink shading represents the uncertainty ranges of the CONFORM emissions.

Figure 3.1.12 illustrates the ratio of NO_2 columns in February 2020 to those of February 2019, observed by TROPOMI and simulated by MAGRITTEv1.1 using the adjustment factors from the CONFORM dataset. The modeled and observed ratios show a good degree of consistency, both in terms of spatial patterns and percentage changes. In February the NO_2 column ratio is generally smaller than 1 (blue), in line with Figure 3.1.8 that shows higher columns in 2019. One exception is the north-western part of China where NO_2 columns are higher in 2020. Note however that the NO_2 columns are very low in this region ($< 3\times10^{15}$ molec.cm-2) as seen in Figure 3.1.8. Over eastern China, defined as 22-42°N, 108-125°E (Figure 3.1.13), the column decrease estimated by the R1 experiment (-38.8%) is in excellent agreement with the observed decrease (-39.5%), whereas the simulations R1H and R1L, using high and low CONFORM factors (Figure 3.1.11) result in underestimated (-31.4%) or overestimated (-47%) changes, respectively (Table 2). These declines respond almost linearly to the anthropogenic NOx flux decreases of the CONFORM dataset in the R1 simulation (-41%), as well as in the R1H (-33%) and R1L (-51%) simulations. The strongest column reduction is observed in the Hubei-Hunan (HH) region (-42%, Figure 3.1.13), encompassing the Hubei province where some of the most severe lockdowns were enforced, and Wuhan, the city where the pandemic was first detected. The R1 experiment leads to a slightly weaker decrease over this region (-37%), suggesting that the CONFORM factors are likely too high. The opposite is found in the Yangtze River Delta (YRD), where the modeled change is slightly stronger than observed (-43% in R1 vs. -38% in TROPOMI). An excellent match is found between the observed and modeled decreases in the densely populated North China Plain (NCP) with an average reduction of -46%. The baseline R2 scenario predicts a column decrease of 2%, due to the 2% lower NOx emissions in 2020 with respect to 2019 in the CAMS-GLOB-ANT_v4.2-R1.1 dataset, while the R3 (same anthropogenic NOx flux for 2019 and 2020) and R5 (same emissions in 2019 and 2020) simulations lead to small NO_2 column changes (less than 5%).

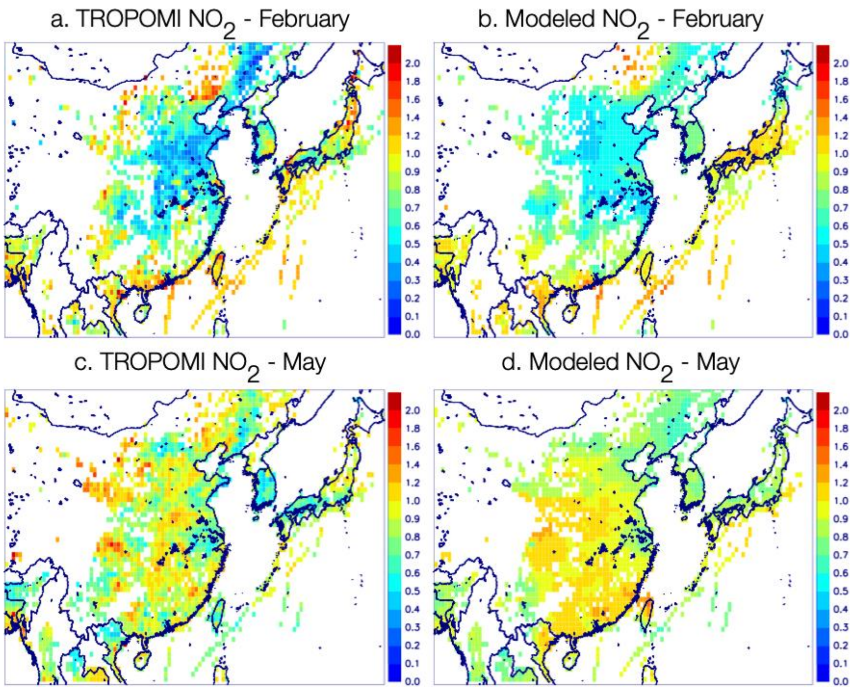

Figure 3.1.12: (a,b) NO_2 column ratio, February 2020 divided by February 2019, according to TROPOMI (left) and to the R1 simulation (right). (c,d) Idem for May. Invalid data and areas with very low NO_x emissions (less than 2×10^{10} molec.cm^{-2}s^{-1}) are left blank.

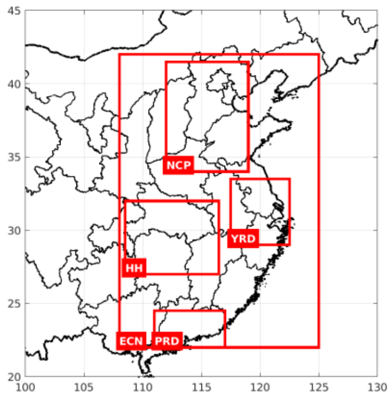

Figure 3.1.13: Regions used in this study. ECN=eastern China (22-42°N, 108-125°E); NCP= North China Plain (34-41.5°N, 112-119°E); YRD=Yangtze River Delta (29-33.5°N, 117.5-122.5°E); HH=Hubei-Hunan (27-32°N, 108.5-116.5°E); PRD=Pearl River Delta (22-24.5°N, 111-117°E).

After the sharp decline in economic activity during the first three months of 2020, China's economy recovered in the following months, reaching almost normal levels by mid-May, as suggested by numerous indicators, like traffic density, energy consumption and business reopening (Al-Haschimi et al., 2020; Doumbia et al., 2021). By the beginning of May 2020, the resumption levels were estimated at ~90%, marking a swift normalization of economic activity, even though some sectors restarted somewhat later, e.g. the services sector (Al-Haschimi et al., 2020). According to the average CONFORM estimate for May 2020, the anthropogenic NO_x and VOC fluxes over China were respectively about 15% and 13.5% lower than in May 2019 (Figure 3.1.10), while the high (low) CONFORM estimate suggests decreases of 7% (18%) for NOx and 5% (20%) for VOCs.
Figure 3.1.12 demonstrates an overall close agreement between the observed NO_2 column changes and the R1 simulation in May (-15.5% vs. -11%, Table 2), and indicates that the use of the low

CONFORM values (R1L) brings the model even closer to the observed change (Table 2). We find very similar decreases in R1 and the observations in the NCP (-15%) and in YRD (-21%), although the observed decreases in PRD (-22%) are slightly stronger compared to R1 (-10%), possibly indicating that the CONFORM distribution of NO_x emission decreases (Figure 3.1.10) might be too homogeneous. The change in NO_2 column due to the COVID-19 restrictions is estimated at about 10% in May (difference between R1 and R2 changes).

Table 2 Percentage changes of monthly columns between 2020 and the same month in 2019 ((2020-2019)/2019), based on observed and modelled columns from simulations R1 (CONFORM emissions), R1H and R1L (high and low CONFORM emissions), and R2 (baseline emissions). All values are calculated for the eastern China region shown in Figure 3.1.13 delimited by 22-42°N, 108-125°E.

	TROPOMI	R1	R1H	R1L	R2
February	-39.5	-38.8	-31.4	-47.0	-2.1
May	-15.5	-11	-4.0	-13.2	-2.5

3.1.1.8 Direct estimation of NOx emission changes from TROPOMI data (IUP-Bremen)

Satellite observed NO_2 columns are not directly proportional to NOx emissions but rather depend on emissions, meteorology and photochemistry. Estimation of emissions from satellite columns can either be done by inverse modelling at different levels of complexity or by estimating fluxes directly from the data by combining them with wind information. An elegant method to derive both NO_2 fluxes and lifetimes from satellite data was introduced by Beirle et al. (2011) and later refined by Pommier et al. (2013) and Valin et al. (2013). It is based on three steps: First, a time series of daily measurements around an emission hot-spot is averaged after rotating each day's measurement in the direction of the wind vector. Only scenes with wind speeds > 2 m/s are used. In the second step, data is converted to NOx using modelled NO_2/NOx ratios, averaged across the plume over a region wide enough to cover the plume, but small enough not to include any other sources, converting a mean map to a line integral. In the third step, this curve is fitted by the product of a Gaussian and an exponential decay, resulting in an estimate of the emission and of the lifetime. This method has been applied to operational NO_2 lv2 data from TROPOMI observations. Details can be found in Lange et al., 2021.

Since the EMG (exponentially modified Gaussian) method can only be used to investigate point sources, the range of possible study areas is limited. Here we focus on several cities which can be considered to be point sources and have an appropriate number of days with satellite data available during the comparative periods using the recommended quality assurance value of 0.75. The EMG method was used and monthly means of emissions from 2019 and 2020 were calculated and compared for the month January to November. In December, the FRESCO version used in the operational S5P NO_2 retrieval changed which has a significant impact on the NO_2 columns and therefore prevents direct comparisons of data after this point with earlier retrievals.

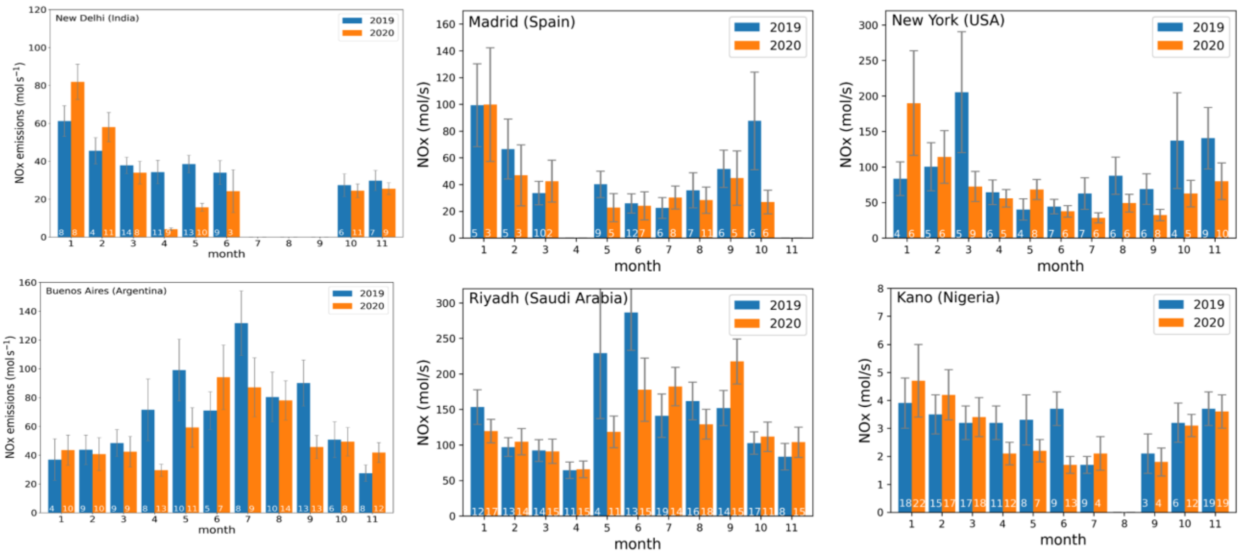

Figure 3.1.14: Monthly NOx emissions calculated with the EMG method based on TROPOMI data from 2019 (blue) and 2020 (orange) for (a) January to November for New Delhi (India), Madrid (Spain), new York (US), Buenos Aires (Argentina), Riyadh (Saudi-Arabia) and Kano (Nigeria). The numbers in the bars give the number of days available for the monthly mean.

Figure 3.1.14 shows the monthly means of the NOx emissions calculated from TROPOMI data for 2019 and 2020 for New Delhi (India), Madrid (Spain), new York (US), Buenos Aires (Argentina), Riyadh (Saudi-Arabia) and Kano (Nigeria) The same months in 2019 and 2020 can be compared, as well as the pre COVID-19 period with the period of containment measures. However, in the latter case the seasonality of NO_2 emissions must be considered. Due to seasonality effects, the NOx emissions calculated for Buenos Aires, Madrid and New York show lower emissions during respective summer months and are increasing towards the winter months. The emissions for New Delhi do not show such a strong seasonality as those for Buenos Aires, but in general the emissions are also higher during the winter months January and February (months 1-2) and decrease towards the summer months.

On 20 March 2020, a nationwide strong lockdown started in Argentina, which remained in place for Greater Buenos Aires until October 2020. From January to March, NOx emissions from 2020 are comparable with those from the same months in 2019. In April 2020, the first complete month in lockdown, the emissions are 56 % lower than in April 2019, and also in May 2020, the emissions are 48 % reduced compared to 2019. In June, however, emissions are higher in 2020 than in 2019, although there has been no major change in the containment measures by the government. A possible explanation is that the June 2019 emissions are lower than expected from the seasonal cycle comparing to May and July 2019 but it is also possible that June 2020 emissions are unexpectedly high due to a cold winter month and people starting to burn waste for heating due to new poverty. The emissions in July behave similarly as in March and April, only with a somewhat smaller decrease of 32% compared to 2019.

In India, a nationwide strict lockdown started on 24 March 2020. The reductions in NO_2 columns when comparing April 2020 and 2019 were strong all over India but very pronounced for New Delhi. In January and February, the calculated NOx emissions are higher in 2020 than in 2019. In this time period, there is no impact of COVID-19 yet, and India's rapidly growing economy is probably the explanation for the upward trend in NOx emissions. In April 2020, the first complete month in lockdown, the emissions are 89 % lower than in April 2019, and also in May and June, the emissions are much lower (70 % and 47 %) than in 2019. For July, comparisons are not possible as less than four days of measurements are available per month due to persistent clouds. In October and November, NOx emissions are lower in 2020 than in 2019 but less so than in spring.

In New York, Riyadh and Kano and Madrid, lower NOx emissions are found in 2020 than in 2019, but with different seasonal patterns. This is related to the different timing of the Covid-19 infection waves and the differences in lockdown severity. There is however also variability in the data, which is probably linked to differences in sampling due to clouds and uncertainties introduced by measurement errors and inaccuracies in the wind fields used.

Despite the shortness of the periods available for analysis, it was possible to investigate short-term variability of NOx emissions induced by COVID-19 with TROPOMI NO_2 data and the EMG method. Strong decreases due to lockdown measures of 56 % in Buenos Aires and 89 % in New Delhi are shown for April 2020 compared to April 2019. These emission estimates account for wind conditions and can therefore give a better estimate of the COVID-19 on NOx emissions than direct comparisons of NO_2 column measurements. For some cities and months, the number of days in monthly means is very limited due to cloud cover, which also is a problem when comparing monthly NO_2 levels, even if days with lower wind speeds are also included.

3.1.2 Analyses of ground-based/in situ measurements

3.1.2.1 Analyses of ground-based observations in Bremen, Germany (IUP-Bremen)

The city of Bremen operates a network of air quality monitoring stations (BLUES, https://www.bauumwelt.bremen.de/umwelt/luft/luftqualitaet-24505) measuring key pollutants including NO_2. Data of this network can be used to investigate a possible reduction of NO_2 levels during the first lockdown phases in Germany first in March and April 2020 and then in January – May 2021. These data are complemented by observations of the MAX-DOAS instrument located on the roof of the IUP building, University of Bremen at the northern outskirts of the city.

The approach used for the analysis is a simple comparison of data from 2021 and 2020 with the corresponding values for 2019. This analysis is oversimplified for an assessment of the Covid19 measures on NOx emissions as not only emissions, but also meteorology plays an important role in determining pollutant levels at ground level. Nevertheless, similar comparisons have widely been used in the literature and the media, and it is interesting to evaluate it for a mid-sized (560 000 inhabitants) industrial city in Northern Germany.

For the air quality network, data from 8 stations is used. The NO_2 instrument operated in BLUES is a Cavity Attenuated Phase Shift (CAPS) measuring at 450nm. Three of the stations are located at road-side to represent traffic situations while the other 5 are located in residential areas measuring background levels. All data shown are 24 hour averages without distinguishing between day and night.

The MAX-DOAS instrument on the roof of the IUP building is a scientific grade two channel instrument equipped with a telescope which can point at any position of the sky. Measurements at different elevation angles are performed routinely in three azimuthal directions covering different parts of the city. Data from the visible channel are used and the geometric approximation is applied to convert measurements under 15° elevation to vertical tropospheric columns. All valid measurements from all three directions are averaged to obtain representative daily mean values.

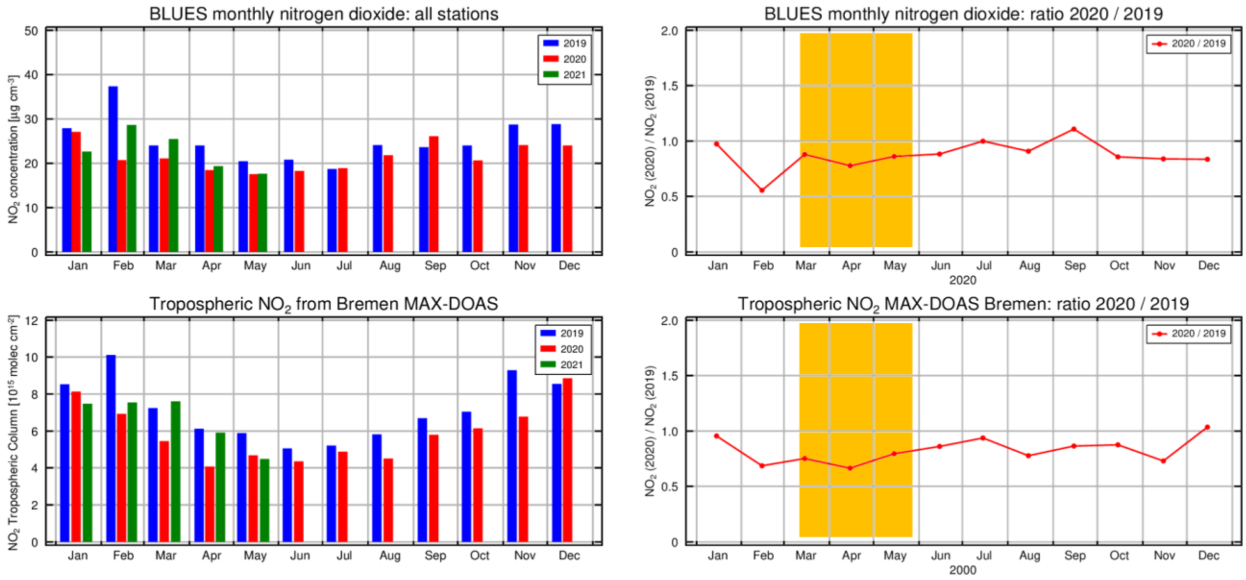

Figure 3.1.15: Comparison of the NO_2 measurements in Bremen for 2021, 2020 and 2019. The top panel shows mean concentrations measured by the in-situ instruments of the air quality network BLUES, the bottom panel shows mean tropospheric columns observed by the MAX-DOAS instrument on the IUP building. Left figures show absolute values for the three years, right figures the ratio between 2020 and 2019. The shaded area indicates qualitatively the time period with restrictions in 2020 due to the Covid-19 pandemic.

In Figure 3.1.15, measurements for 2019 and 2020 are compared for both data sets. Data from 2021 is also included in the left column. As expected, both in-situ NO_2 measurements at ground level and MAX-DOAS tropospheric columns were lower during the lockdown period in early 2020 than at the same months in 2019. The difference is of the order of 20% (in-situ) and 30% (MAX-DOAS). Over the course of the year, values increased and the ratio was back to being close to 1 in October. One unexpected result was, that already in February, NO_2 levels in Bremen were clearly lower in 2020 than in 2019, a result that cannot be related to the Covid19 measures, which had not started by then. This reduction was probably linked to unusual weather conditions with an exceptional number of clear-sky days in February 2020. In 2021, the lockdown in Germany was not as strict as in 2020 until mid-March, when it became more stringent but arguably still less efficient than in 2020. Consequently, NO_2 values were mostly larger than in 2020 but lower than in 2019. However, there is clear variability from month to month because of the impact of weather.

Both data sets are in good agreement with respect to the temporal evolution in 2020 and 2021, indicating that surface NO_2 dominates the MAX-DOAS measurements. There appears to be a larger seasonality in MAX-DOAS derived columns than in the in-situ observations, but this can in part be the effect of using 24-hour averages for the in-situ data while the MAX-DOAS observations are limited to daytime where photolysis plays an important role.

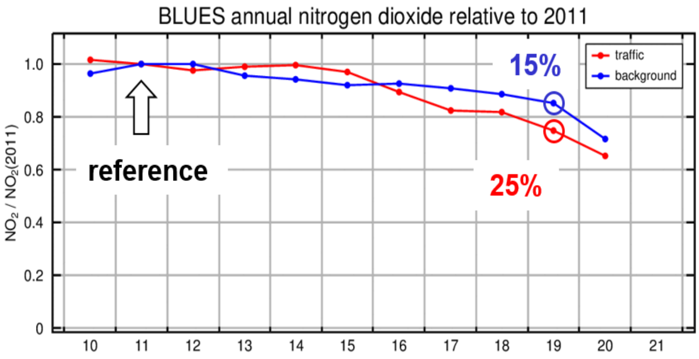

Figure 3.1.16: Evolution of mean NO_2 concentrations in Bremen as measured by the BLUES air quality network, separated by traffic and residential area background measurements. Reference is the year 2011.

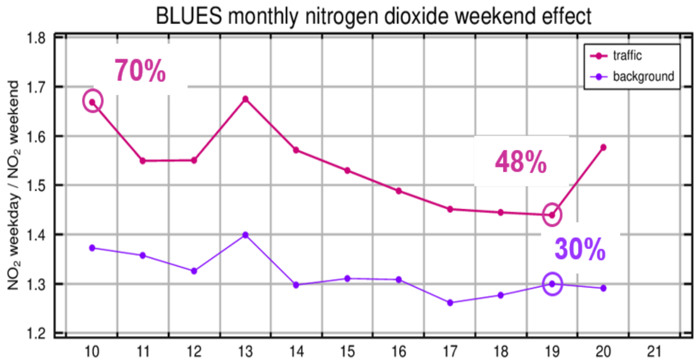

Figure 3.1.17: Ratio of weekday to weekend (Saturday + Sunday) NO_2 concentrations measured by the BLUES air quality network in Bremen for the years 2010 to 2020, separated by traffic and residential area background measurements. The year 2011 was chosen as reference as for this year, all BLUES stations covered a full seasonal cycle.

Overall, both data sets have a tendency to show lower values in 2020 than in 2019 even outside the time period affected by lockdown measures. This could be part of a longer downward trend in NO_2 concentrations in Bremen as shown in Figure 3.1.16. Relative to the year 2011, NO_2 measurements in 2019 were lower by 15% at background stations and even more in 2020. The decrease was even 25% for 2019 at traffic stations, followed by more than 35% in 2020. For the traffic stations, the decrease happened in the 4 years since 2015, indicating recent rapid improvements in NOx emissions from cars. This link to traffic is further confirmed by an interesting trend in the weekday to weekend ratios shown in Figure 3.1.17. While this ratio is stable and around 1.3 for background stations, it significantly decreased from 1.7 in 2010 to 1.48 in 2019, indicating a decreasing importance of traffic. In 2020 however, the ratio increased strongly. This was driven by larger reductions during the weekends, arguably because the lockdown mainly affected private activities and much less work related traffic. Also, because of the lower NO_2 levels on weekends, a similar absolute decrease on all days would result in an increase in the ratio of weekday to weekend values.

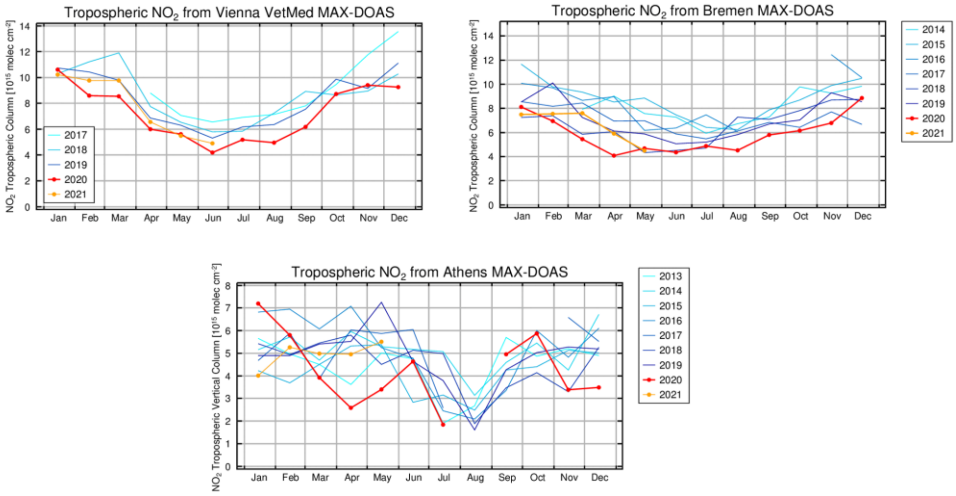

Figure 3.1.18: MAX-DOAS observed tropospheric NO_2 columns in Vienna (top left), Bremen (top right) and Athens (bottom) for several years.

The general decrease in NO_2 levels over recent years is further illustrated in Figure 3.1.18 where MAX-DOAS measurements at three stations are shown for several years. Like for the Bremen data, all valid measurements in Athens and Vienna from all azimuthal directions are averaged to obtain representative daily mean values. The clear reduction from year to year is apparent both in the Bremen data and in the observations in Vienna, 2021 data being the exception but still at the same or a lower level than 2019. The low values in 2020 are therefore probably a combination of the long-term downward trend and the effects of Covid-19 measures taken. In Athens, the situation is less clear – while there is a small downward trend, variability between years is large and the pattern is less obvious. The effect of the strict lockdown in March – May 2020 is however clearly visible, while NO_2 columns for the same period in 2021 are back to normal.

In summary, analysis of in-situ and MAX-DOAS measurements in Bremen, Vienna and Athens show that

- a reduction in NO_2 levels by 20 – 30% was seen during the lockdown in 2020 relative to 2019 and a smaller effect in 2021,
- lower NO_2 columns are also found in February 2020, probably due to unusual weather conditions,
- a long-term downward trend in NO_2 is found which is in particular linked to traffic and needs to be taken into consideration when estimating Covid-19 effects in Germany and Austria, but probably also in other European countries. This effect is large and on an annual basis could be comparable or even more important than the reductions in NOx emissions from Covid-19 abatement measures.

3.1.2.2 Analysis of NO_2 concentration changes in Europe and correction for the meteorology contribution (KNMI)

In-situ measurements for major European cities have been retrieved from the central database of the European Environmental Agency (EEA – available at https://www.eea.europa.eu/data-and-maps/data/aqereporting-8). The NO_2 surface concentration reductions due to COVID in 2020 have been determined by a direct comparison with corresponding periods in 2020 and 2019, see Figure 3.1.19. To avoid the influence of non-representative local sources, we use the average of background stations (i.e. discarding street stations).

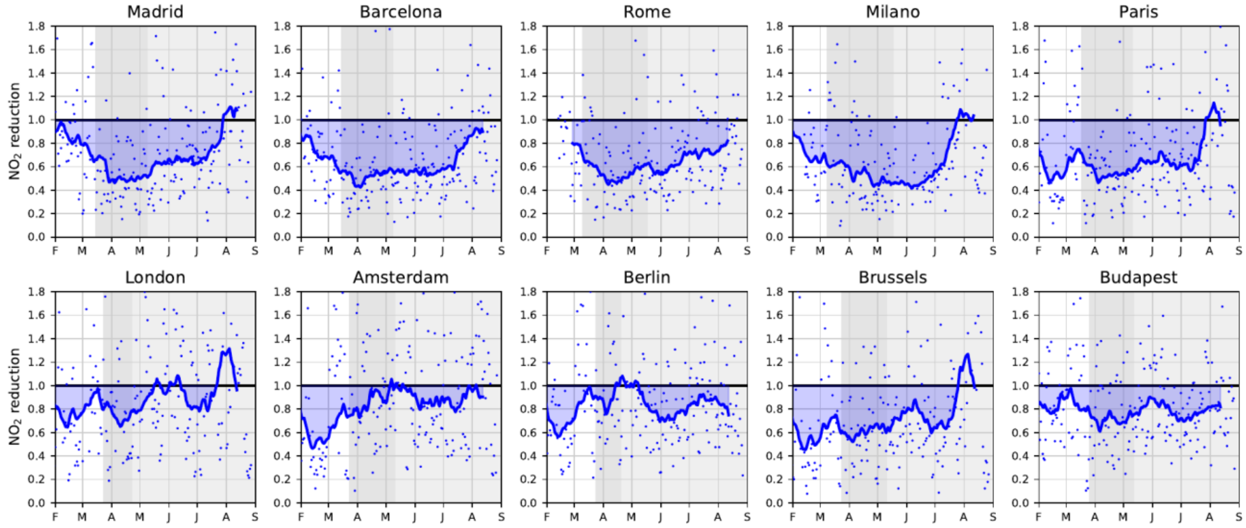

Figure 3.1.19: NO_2 reductions calculated from the ratio between background concentrations in 2020 and 2019. The dots indicate daily average reductions, while the thick lines represents a 31-day moving average. The dark grey area indicates the period with strict lockdown measures, while the light grey area correspond to the following with less strict measures.

As expected, the NO_2 reductions are highest during the period with strict lockdown measures. For cities in Spain, Italy, and France, NO_2 was reduced by 50%-60% during this period. The reductions are found to be less for Northern and Eastern Europe, as a combined effect of less strict measures and stronger meteorological variability. Towards the summer, when measures become less strict, NO_2 concentrations start to increase again, although generally they are still behind their pre-COVID levels.

Agreement analysis from space and from ground

The NO_2 reduction analysis from in situ-observations compares well with the analysis from space based on TROPOMI NO_2 tropospheric columns, as can be seen in Figure 3.1.20. This reconfirms the sensitivity of the TROPOMI instrument to concentrations at the boundary layer of the atmosphere.

The comparison between the two approaches can also be summarized as scatter plots in Figure 3.1.21. The derived NO_2 reductions agree within 5%, with the exception of Paris (9%) and London (14%). As stated before, the largest reductions are found in Southern Europe. In the post-lockdown period (July-August) the NO_2 concentrations increase again, but generally are still around 15% behind their pre-COVID levels.

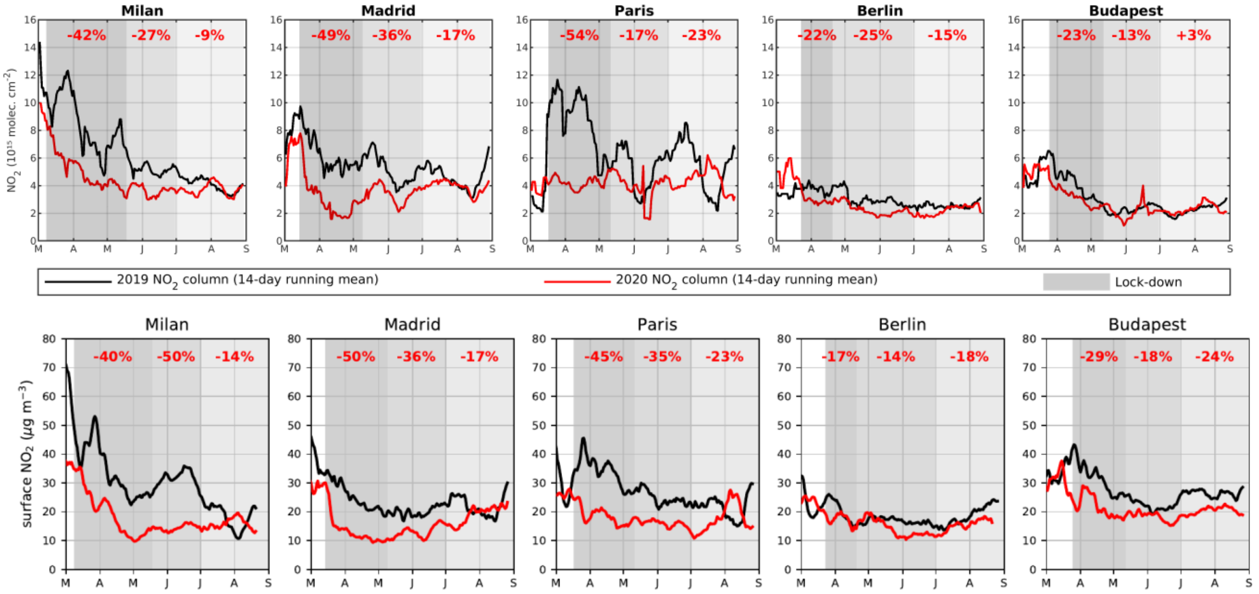

Figure 3.1.20: Time series of NO_2 concentrations for 2019 (black) and 2020 (red) for selected European cities. The upper panels show daily tropospheric NO_2 columns, while the bottom panels show concentrations of in-situ background stations. The grey areas indicate the lockdown period; the different shades indicate the strength of the lockdowns measures.

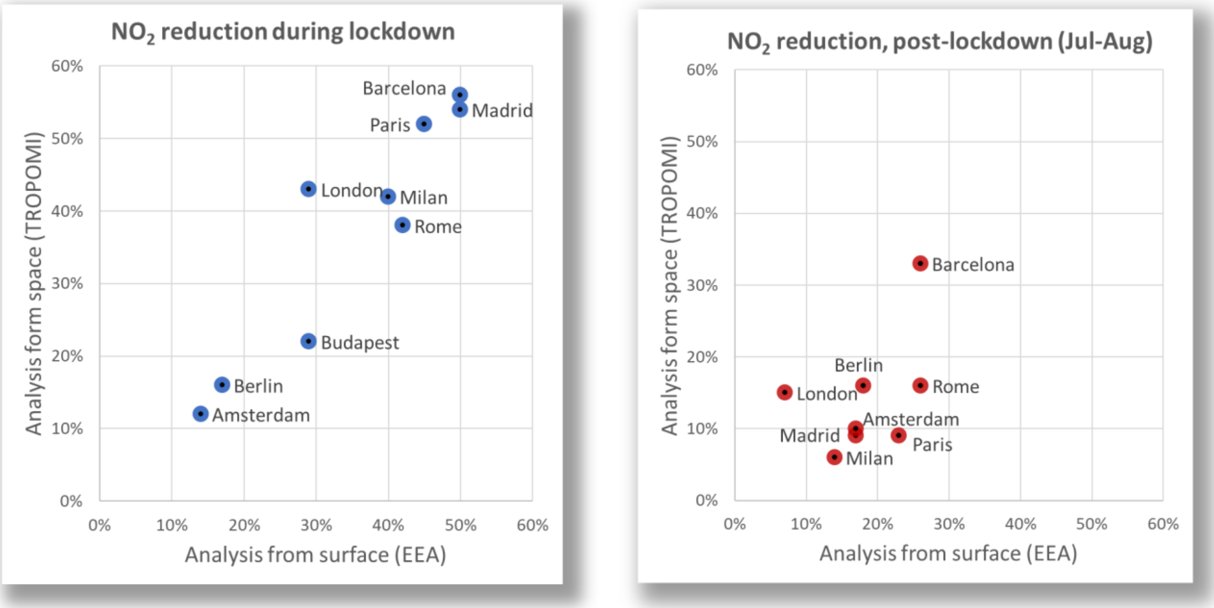

Figure 3.1.21: Comparison of NO_2 reductions determined from space and from in-situ observations.

This direct approach does not account for meteorological variability, which can be substantial on a year-to-year basis. To estimate the meteorological influence, we analyzed simulated surface concentrations by LOTOS-EUROS with a fixed emission inventory.
Table 3 lists the monthly ratios between 2020 and 2019 for 10 cities. From the different time series, we estimate the standard deviation to be 21%. This number is higher than the standard deviation found in simulated tropospheric NO_2 columns (see Section 3.1.1.4), as column concentrations are insensitive to changing vertical distribution of NO_2 by e.g. different boundary layer heights.

Table 3: Ratios of surface concentrations by LOTOS-EUROS (mean2020-mean2019)/mean2019

	Rome	Milan	Madrid	Barcelona	Paris	Brussels	Amsterdam	London	Berlin	Budapest
Jan	0.27	0.22	0.58	0.37	-0.07	-0.10	0.07	0.07	0.02	0.62
Feb	0.12	-0.14	0.22	-0.07	-0.41	-0.44	-0.50	-0.38	-0.46	-0.37
Mar	-0.04	-0.08	0.26	0.10	0.05	-0.11	-0.17	0.14	-0.00	0.18
Apr	0.28	0.34	0.06	0.02	0.12	-0.09	0.10	0.30	0.03	0.22
May	0.13	-0.02	-0.07	-0.20	-0.16	-0.11	0.01	-0.07	-0.01	-0.11
Jun	-0.05	0.07	-0.14	0.03	-0.07	0.02	0.03	-0.16	-0.02	-0.04
stdev	**0.14**	**0.18**	**0.26**	**0.19**	**0.19**	**0.16**	**0.23**	**0.24**	**0.19**	**0.34**

The meteorological variability is further illustrated in Figure 3.1.22, which shows monthly averaged surface concentrations simulated by LOTOS-EUROS, based on a fixed (2019) emission inventory. Especially in February large differences are found in NO_2 concentrations in North West Europe, when comparing 2020 with 2019 (see also corresponding values in Table 3).

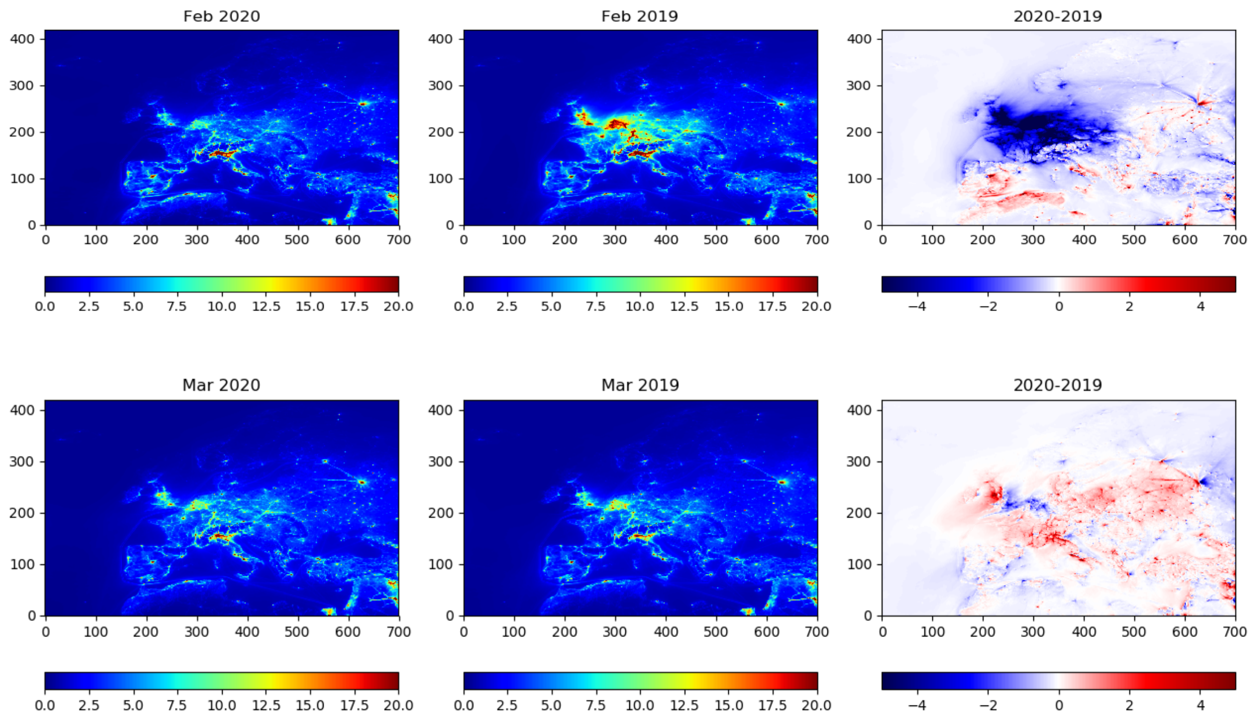

Figure 3.1.22: Monthly averaged surface NO_2 concentrations, as simulated with LOTOS-EUROS with a fixed emission inventory for February and March. The right-hand panels show the difference between the 2020 and 2019 concentration fields.

Chemical transport model runs with unchanged emission inventories can provide the "business as usual" scenario, i.e. what would the NO_2 concentration be without lockdown measures. Having 4 quantities, obs_{2019} (the observation in 2019), obs_{2020} (the observation in 2020), fc_{2019} (the model forecast in 2019), and fc_{2020} (the model forecast in 2020, with 2019 emission inventory), we can calculate

$$\frac{fc_{2019}}{fc_{2020}}\frac{obs_{2020}}{obs_{2019}}$$

which can be interpreted as

$$\frac{obs_{2020}}{obs^*_{2019}}$$

in which obs^*_{2019} is the observation from 2019 corrected for meteorology with a weather correction factor fc_{2020} / fc_{2019}, or alternatively as

$$\frac{obs_{2020}}{fc^*_{2020}}$$

in which fc^*_{2020} is the forecast for 2020 corrected for representation error with a factor obs_{2019} / fc_{2019}.

In our assessment we used two model runs to study the meteorological correction: the forecast of the CAMS regional ensemble, and the before-mentioned LOTOS-EUROS model with a fixed 2019 emission inventory. The results for both runs are not satisfying. The CAMS consortium introduced important emission inventory revisions in the ensemble members during 2019-2020, therefore not providing a consistent dataset. On the other hand, LOTOS-EUROS is not able to simulate urban NO_2 concentrations sufficiently realistically, i.e. it suffers from meteorology and location dependent biases. This is illustrated for Paris in Figure 3.1.23. The upper panels show the observed surface concentrations for 2019 and 2020. The middle panels show the ratio between observation and forecast. The CAMS ensemble forecast corresponds well with the observation in the first 6 months of 2019 (note the thick blue line is close to 1). Due to a switch to a different (generally lower) emission inventory in June 2016, this fixed relation is broken. As a consequence, the corrected concentration reduction for the pre-lockdown period in January and February are strongly biased, as can be seen in the lower left panel. The blue line for LOTOS-EUROS reveal a strong seasonal dependency during 2019. The corrected concentration reductions (bottom right panel) seem more realistic that for CAMS, but still a strong emission reduction is visible in the pre-lockdown period (January to half March).

Using LOTOS-EUROS for meteorological correction, the time series of Figure 3.1.19 change into the time series of Figure 3.1.24. For cities in Spain, Italy, and France, NO_2 reduction remain 50%-60%.
The model is able to correct partially the strong NO_2 differences found in the pre-lockdown months for Northern-European cities. The COVID-19 measures taken in Berlin were of the order of 20% in the first period and remain similar in the months up to August 2020. This behaviour is typical for cities in North-West Europe. Also in Eastern Europe the impact of the measures has been less drastic than in Southern Europe and France, with reductions of the order of 15-25%.

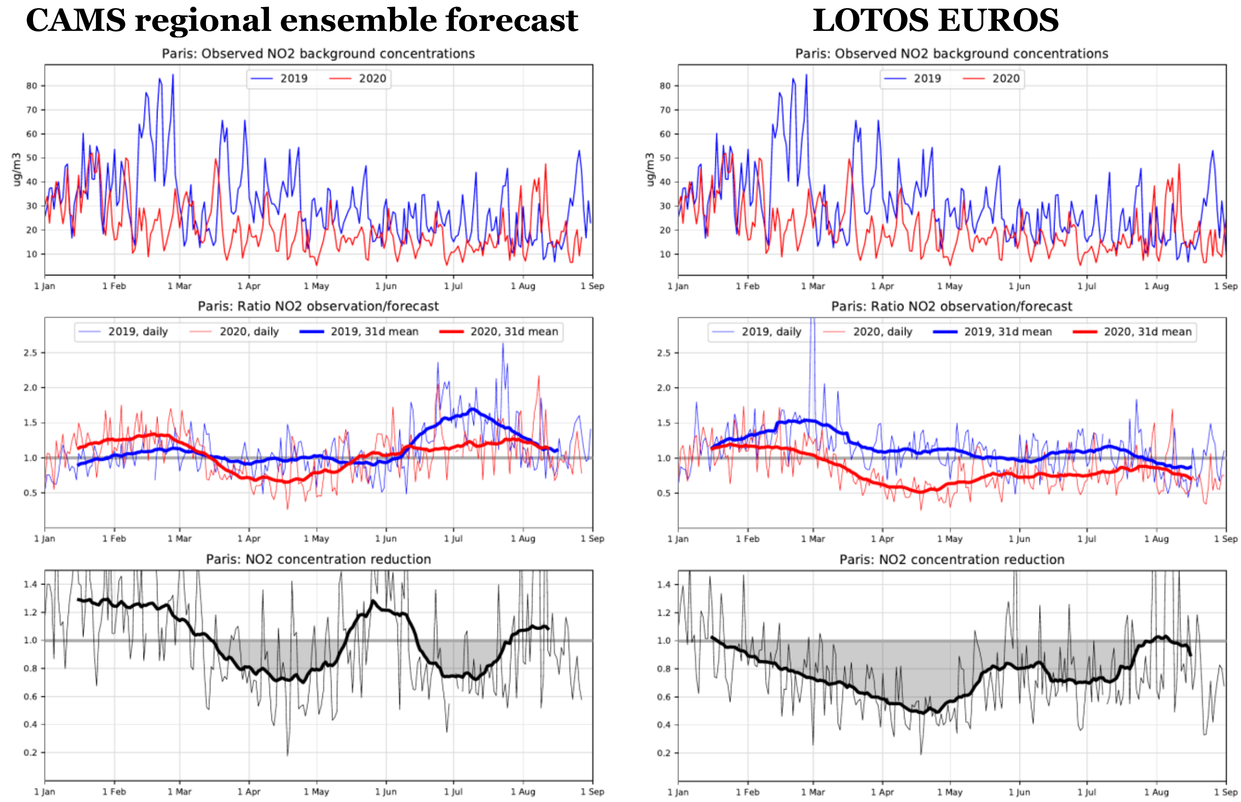

Figure 3.1.23: Observations and model corrections by CAMS (left) and LOTOS-EUROS (right)

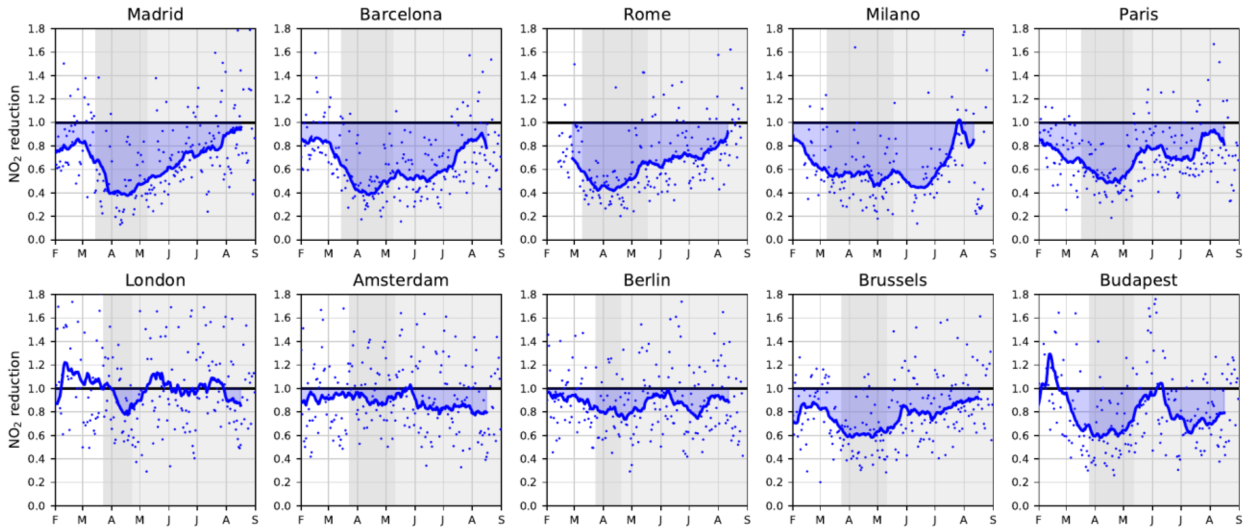

Figure 3.1.24: NO_2 reductions found in selected European cites, after correcting for meteorological variability by LOTOS-EUROS. The dots indicate daily average reductions, while the thick lines represents a 31-day moving average.

3.1.2.3 Comparison between TROPOMI and in situ data in China (BIRA-IASB).

The availability of ground based NO_2 measurements in 1643 stations well distributed over China allows to compare the time series of temporal evolution of TROPOMI columns and in situ concentration measurements focusing and in particular on the NO_2 reduction observed during the lockdown. The observed concentrations of NO_2 were obtained from the China National Environmental Monitoring Center (Liu and Wang, 2020, courtesy of Y. Liu). The stations monitor the air quality at a half-hour resolution, providing measurements of various pollutants including NO_2, SO_2, CO, O_3, and $PM_{2.5}$.
Here we compare the in situ NO_2 observations to TROPOMI NO_2 daily gridded columns at 0.05° × 0.05° from the operational product, obtained via the Copernicus open data access hub (https://s5phub.copernicus.eu, van Geffen et al., 2020). In order to allow meaningful comparison between in situ concentrations and the satellite data, we proceed as follows:

- for each of the 0.05° × 0.05° TROPOMI grid cells including one of the 1643 in situ stations, we extracted the daily TROPOMI NO_2 columns and generated daily satellite data series per site;
- we considered only in situ data within a two-hour time-window around the TROPOMI overpass time (12-14h);
- we considered comparisons for days where both in situ and TROPOMI data are available.

Figure 3.1.25 shows the average NO_2 concentrations for all measurements stations in 2019 (dotted line) and 2020 (solid line) for in situ measurements (black) and TROPOMI observations (red). The right panel displays the relative NO_2 reduction observed from both datasets, the lines representing a 21-day running mean. Both in situ data and TROPOMI data show an NO_2 reduction between January and April, with the strongest reduction of -40% observed by the end of February. However, the NO_2 levels were reduced in January 2020, before the start of the lockdown. This is partly due to the Chinese New Year festivities, which kicked off on 25 January 2020. Important reductions in air pollutant concentrations were reported during the New Year holidays in China (Tan et al., 2009). Between May and July, both datasets show a negligible NO_2 reduction of about -5%. Overall, the in situ and TROPOMI data show a good agreement in the observed NO_2 change (r =0.88), however TROPOMI suggests a stronger reduction at the end of January.
Figure 3.1.26 shows the change in NO_2 over the same period, for individual provinces affected by the shutdowns. Overall, for all provinces, the NO_2 changes observed by TROPOMI and by monitoring stations are very well correlated. The strongest correlations are found in Hubei, Shandong, and Guangdong provinces (>0.9), followed by high correlations (0.8-0.9) in other Chinese provinces, like Fujian, Zhejiang, Hunan, and Jiangxi, all strongly affected by the lockdowns. Weaker correlations are found in Beijing and Shanghai (0.5-0.6), which might be related to the small number of measurement stations. Based on these comparisons, we note that most provinces have undergone a pronounced NO_2 decrease of -40% to -60% in the month of February, which vanishes by the beginning of April.
The stronger NO_2 reduction observed by TROPOMI at the end of January occurs in several central and northern provinces (e.g. Liaoning, Henan and Shandong), whereas the higher NO_2 observed by TROPOMI in April occurs in other provinces (e.g. Guangdong). Local dynamics play in important role and might account for a large part of these differences. Models accounting for meteorological variability and chemical interactions are needed to help understand these discrepancies.

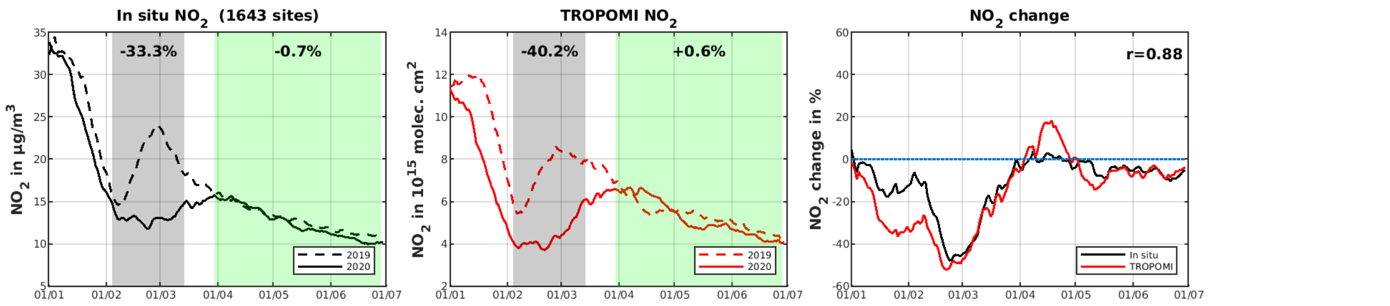

Figure 3.1.25: ***Left:*** **Average NO_2 concentration over all 1643 in situ measurement sites in China.** ***Middle:*** **Average NO_2 column observed by TROPOMI over the grid cells with in situ measurement stations.** ***Right:*** **Relative change in NO_2 between 2020 and 2019. The black and red lines represent the changes derived from in situ and from TROPOMI data, respectively. The correlation between both is given in the top right corner. The curves correspond to 21-day running averages.**

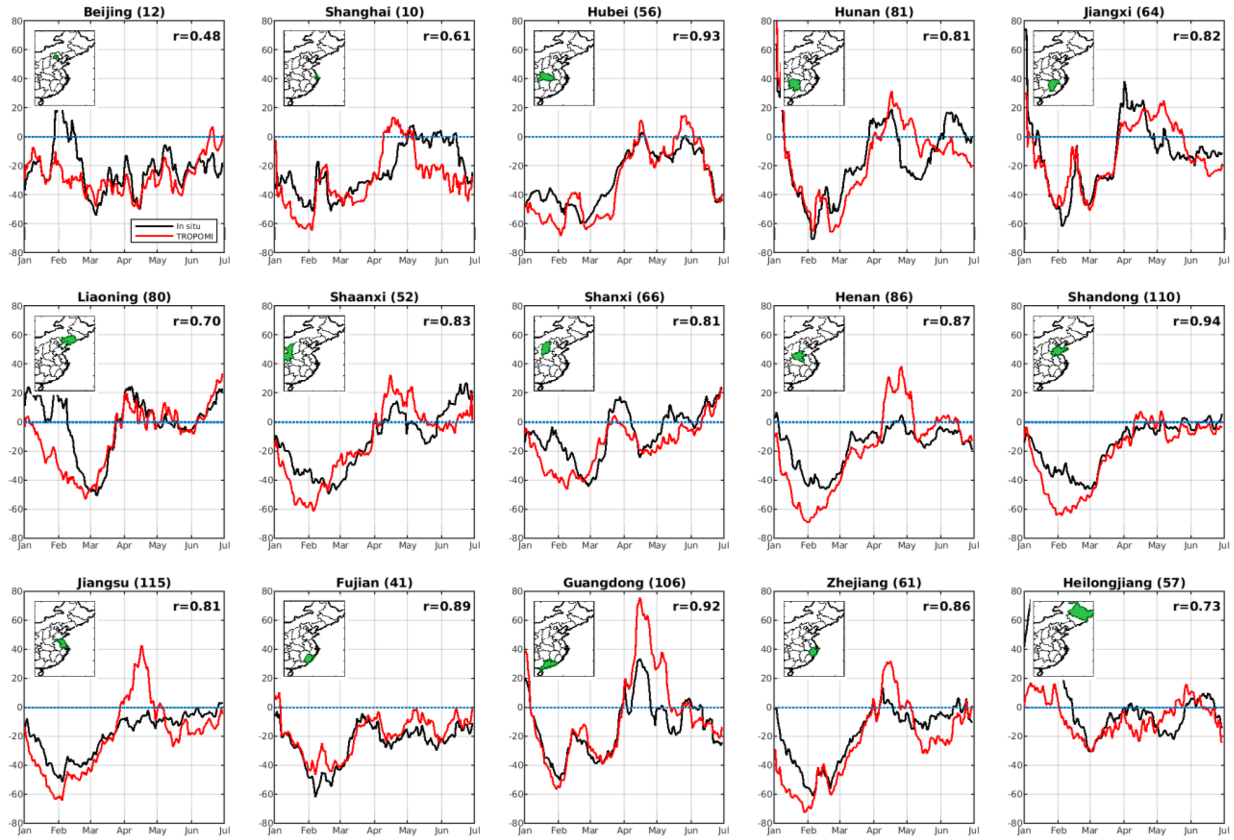

Figure 3.1.26: The relative changes in NO_2 between 2020 and 2019 per province based on in situ (black) and TROPOMI NO_2 data (red). The Pearson's correlation coefficients calculated between the two datasets. The number of in situ sites per province is indicated between brackets in the title. The curves correspond to 28-day running averages.

3.1.2.4 Analysis of NO_2 concentration changes in China and correction for the meteorology contribution (KNMI)

We daily collect the data of more than 1500 in-situ stations covering all major cities in China that are published by the China National Environmental Monitoring Centre. They provide hourly observations of the pollutants PM10, PM2.5, O3, NO_2, SO_2, and CO. NO_2 is measured by a chemi-luminescence technique (Zhang & Cao, 2015). Data can also be accessed via websites of third parties, such as www.pm25.in and www.aqicn.org. For this study, we have averaged the various in situ NO_2 observations in a city to a single value per hour for each of 36 selected major cities (with a population of more than 3 million. For comparison with model results, we calculated a daily value based on the observations from 10:00 to 18:00 local time. The daytime selection is due to large inaccuracies in simulations of the night time boundary layer height.

To eliminate the effect of meteorology and transport we compare these measurements of in situ stations with an ensemble model for air quality developed for urban areas of China (Brasseur et al., 2019, Petersen et al., 2019, http://www.marcopolo-panda.eu). The ensemble service has a typical resolution of about 20 km. The model is driven by emission inventories, which are not corrected for the effects of either Spring Festival or the COVID-19 crisis and hence are considered the business-as-usual situation. A possible bias between measurements and model is corrected for by normalizing the results for the first two weeks of January. In Figure 3.1.27, the ratio between in-situ measured NO_2 and the modelled NO_2 is shown. The concentration reductions are shown as green area, while increased concentrations are shown in red. The reduction starts around the Chinese New Year and ends in March. Exception is the concentration level of Wuhan that becomes similar to that of the business-as-usual scenario after the first week of April. The average concentration reduction of all 36 cities is 41%, comparable to the emission reduction of 35 % shown in section 3.1.3. A striking difference between Wuhan and the other Chinese cities is the longer duration (by about one month) of the concentration reductions.

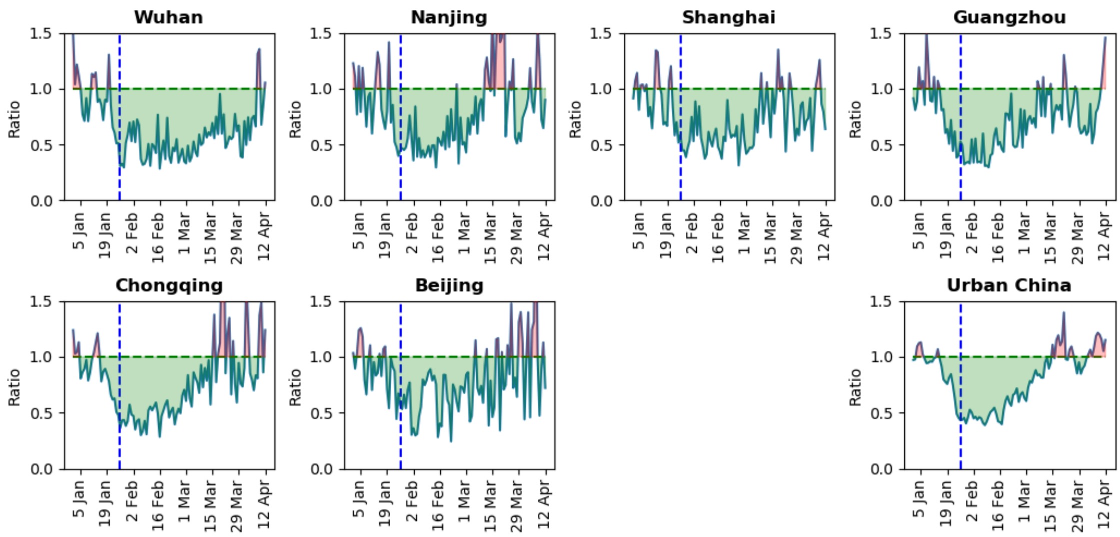

Figure 3.1.27: Ratio of measured NO_2 concentrations (from 1 January to 12 April 2020) to concentrations of the business-as-usual scenario. The Chinese New Year is indicated by the blue dashed line.

3.1.3 Impact on NOx emissions in China (KNMI)

During the COVID-19 lockdown in China, air quality had strongly improved. Here we study what sources were reduced and how much the reduction per city was. We used TROPOMI observations of the Sentinel-5P satellite, which monitors the Earth's atmosphere daily. We focused on observations of the pollutant “nitrogen dioxide,” an important precursor of air pollution in the atmosphere. With our novel methodology we are able to calculate the pollution back to the sources of the emissions, whether these are big cities, industrial regions, power plants, or busy shipping lanes. We applied this method to East China, we see strong emission reductions of 20–50% in the cities during the lockdown in February 2020. Besides urban China, we found an average emission reduction of 40% over coal power plants and a reduction in maritime transport by 15–40% depending on the region. The period of reduced emissions lasted until around the end of February, and the emissions slowly returned to normal during the month March 2020. Exception is the region Wuhan, the center of the COVID-19 crisis, where emissions started to rebound since 8 April, the end of their lockdown period.

From the observations of the TROPOMI instrument on the Sentinel-5P satellite, over China we see Tropospheric NO_2 column concentrations decrease about 35% and some areas up to 60% during the COVID-19 regulation period compared to the same period of 2019 (see Figure 3.1.28 a and b). The concentrations alone provide only an indication of the impact of the COVID-19 measures on air pollution. The inverse modeling system allows us to quantify the impact of the COVID-19 measures and distinguish emissions from cities, power plants, and maritime transport separately.

DECSO is a state-of-the-art inverse algorithm developed by Mijling and van der A (2012) updating daily emissions of short-lived atmospheric constituents using an extended Kalman filter, in which emissions are translated to concentrations via a CTM and compared to the satellite observations. The sensitivity of concentrations to emissions is calculated from a trajectory analysis to account for transport of the short-lived gas by using a single CTM forward run. DECSO has been successfully applied to NO_2 observations from OMI and TROPOMI over different regions. In this project, daily NO_x emissions from January 2019 to April 2020 over East Asia (102–120°E, 18–50°N) are derived with DECSO using the Eulerian regional off-line CTM CHIMERE v2013 (Menut et al., 2013) and TROPOMI NO_2 observations. The implementation of CHIMERE v2013 in DECSO is described in Ding et al. (2015). We apply DECSO to the super-observations of TROPOMI instead of directly using individual TROPOMI observations. Super-observations are representing the integrated average of the TROPOMI observations over the grid cells of the model after filtering for clouds. Figure 3.1.28 (c and d) shows the mean NOx emissions derived from TROPOMI for the same period as in Figure 3.1.28 (a and b) in 2019 and 2020 after the Chinese New Year. We see lower NO_x emissions in February 2020.

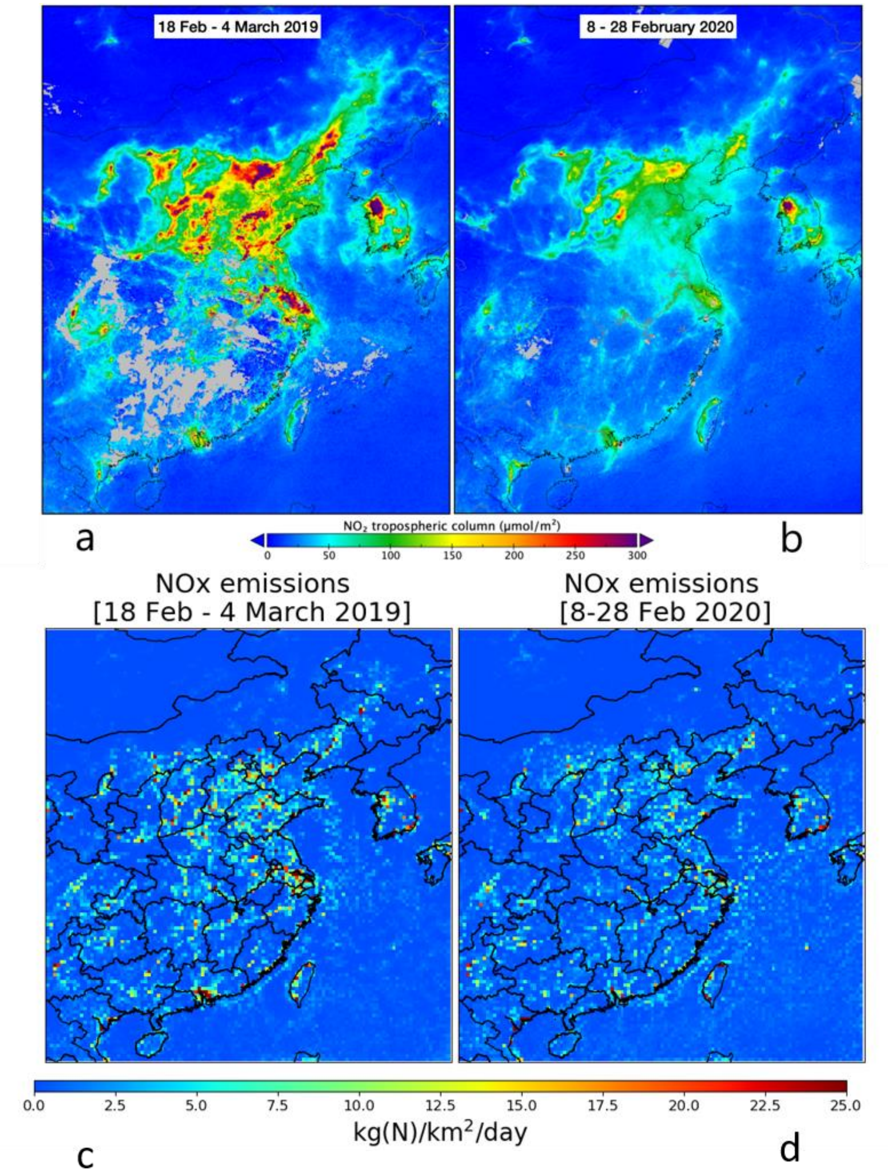

Figure 3.1.28: TROPOMI NO_2 columns over East China after the Chinese New Year in 2019 (a) and 2020 (b). NOx emissions for the same period in 2019 (c) and 2020 (d) derived with DECSO.

NO_x emissions have been affected since the strict regulations started in China, especially in Hubei. We select three periods to quantify the impact of the COVID-19 regulations. The first period (P1) is three weeks before the implementation of the COVID-19 regulations, 3 to 23 January in 2020, which is also just before the Chinese New Year. The second period (P2) is 8 to 28 February, which is regarded as the regulation period. The third period (P3) is from 18 March to 7 April, when most regions in China resumed working. We calculated the average of NO_x emissions derived with DECSO in each period and compare their differences. Figure 3.1.29 shows the relative changes of NO_x emissions during the selected 3 periods over the grid cells with high anthropogenic (above 3kg N/km^2/day) NO_x emissions. We observe a strong decrease by at least 30% of NO_x emissions over China in P2 compared to P1. In P3, NO_x emissions increased compared to P2 but are still lower than in P1 because of the step-wise resumption of work and social life. In Figure 3.1.29, we see that the NO_x emissions over sea also decrease. The emissions due to sea-transport from Shanghai to Guangzhou are less affected than the transport over land and are found to decrease by about 25% in

P2 and increase again with 18% in P3 in comparison to P2. A more significant emission decline was found in the Yellow Sea and Bohai area, where NO_x emissions reduced by about 41% in P2 and continued decreasing by 6% in P3.

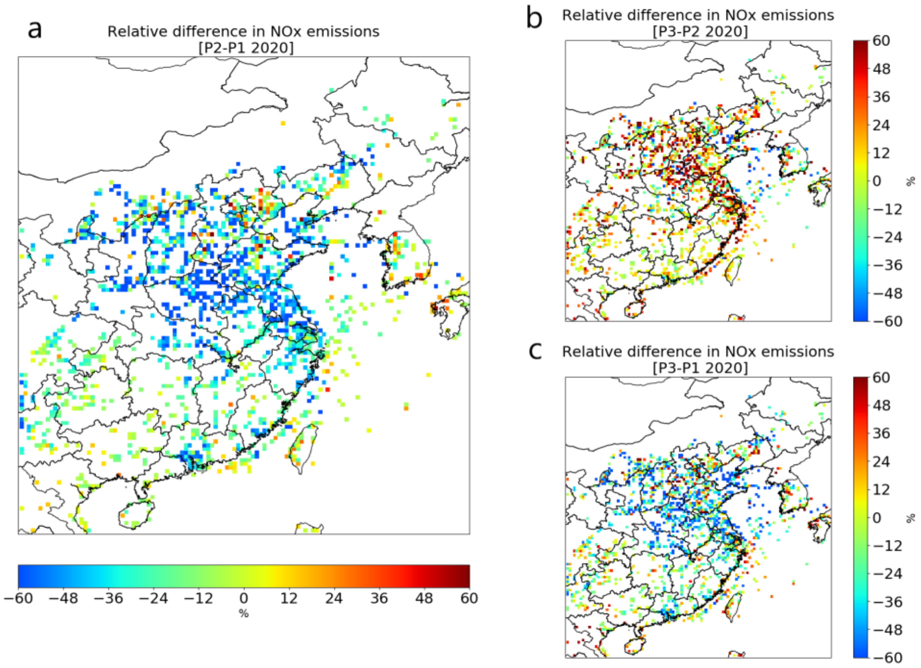

Figure 3.1.29: The relative difference in NOx emissions between (a) P2 and P1; (b) P3 and P2 (c) P3 and P1. P1 is 3-23 January. P2 is 8-28 February. P3 is 18 March to 7 April. The changes in emissions are shown in the figure for emissions higher than 3 kg(N)/km2/day in P1 to remove areas with dominating biogenic emissions or rural areas.

At city level changes in NO_x emissions started from January 2019. We infer a very strong NO_x emission decrease of more than 50% during and after the 2020 Chinese New Year in Wuhan, where the COVID-19 outbreak was first recorded and very strict lockdown regulations were adopted. At the other five Chinese cities, we also observe a much stronger decrease after the Chinese New Year in 2020 than in 2019. In addition, the duration of the period with low emissions is much longer. We also calculate the average reduction of grid cells containing urban. The inferred emission reduction is about 35% in urban areas. Besides the urban emissions, we find strong reductions of NO_x emissions from coal power plants. Figure 3.1.30 shows time series of NO_x emissions from the Ningxia Province, where the main sources of NO_x are fossil fuel power plants (van der A et al., 2017). Our inversion results indicate that after the 2020 Chinese New Year, NO_x emissions dropped about 40% in this province, 20% more than in 2019 New Year period. This shows the impact of the COVID-19 regulations on the energy production, especially in the industrial sector.

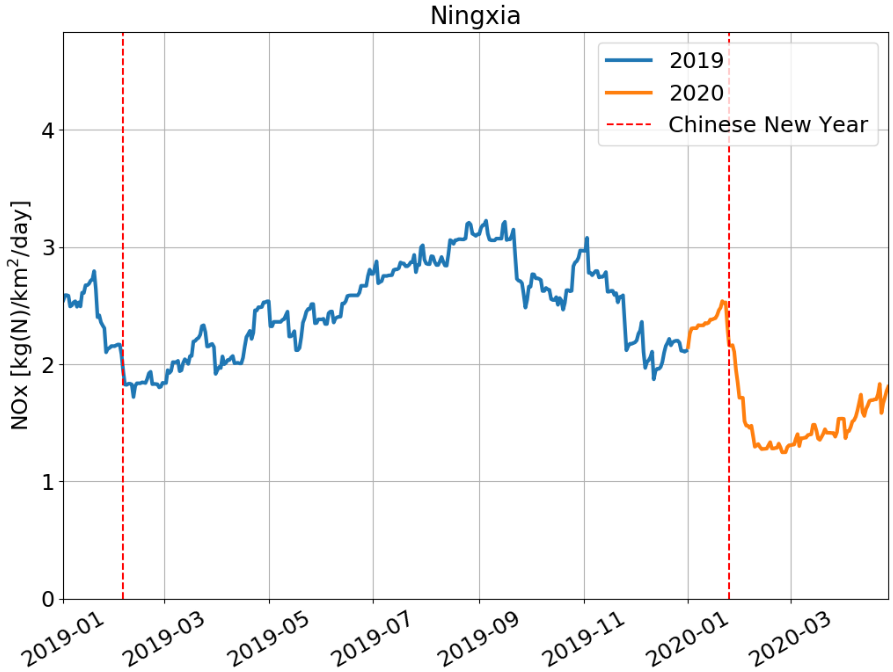

Figure 3.1.30: Time series (1 January 2019 to 28 April 2020) of daily NOx emissions in Ningxia Province.

To study the impact of the COVID-19 regulations on NO_x emissions (one of the key ingredients determining air pollution), we derived daily NO_x emissions at a resolution of 0.25° × 0.25° over East Asia from 2019 to March 2020 by applying the inverse algorithm DECSO to observations from TROPOMI. By grouping the emission into three periods of before, during and after the COVID-19 regulations, we quantified the emission changes on the small spatial scale of city level and from different emission sources such as sea-transport and the energy sector. The observations suggest emission reductions of 20% to 50% for cities. The emissions reduction of 40% in the Ningxia province reflects the impact of the lockdown measures on the energy sector. Maritime transport is also affected during the COVID-19 regulations, although its emissions reductions are dependent on the region. With the NO_x emissions derived from DECSO using observations from TROPOMI, we are able to get detailed information about the impact on emission changes due to the COVID-19 regulations by accounting for the influence of meteorology, lifetime and transport of the air pollutants. As the COVID-19 crisis progressively affects all continents, the public health regulations implemented by various countries may have different contributions to air quality. Applying our methodology to different regions can help to quantify the impact of the NO_x emission reductions by the different regulations on not only the improvement of air quality from urban to local to regional scale.

Yangtze River Delta (YRD)

For the Yangtze River Delta (YRD) we have applied DECSO with a higher resolution of 0.1 x 0.1 degree using TROPOMI data. The overall effect of the lockdown is clearly visible in Figure 3.1.31 where the NOx emissions are shown for a day just before the lockdown and a day in the middle of the lockdown period of China. The calculated emission reductions for individual cities like Shanghai, Nanjing, Wuhan and Hefei are consistent with the earlier results on 0.25x0.25 degree resolution.

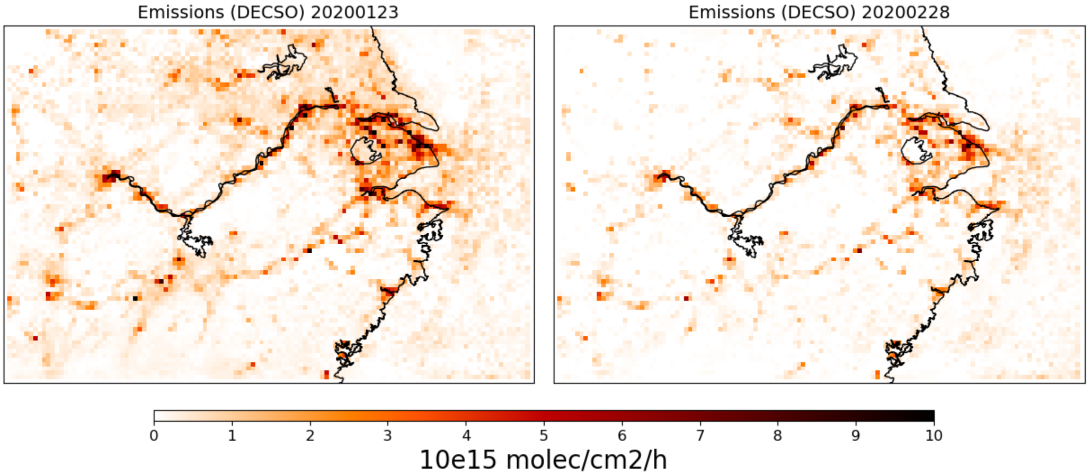

Figure 3.1.31: The NOx emissions in the YRD just before the lockdown, on 13 January (left) and during the lockdown on 28 February (right)

To understand more details of emission reductions for the cities, we have chosen the City of Nanjing and analysed the emissions per grid cell of about 10 x10 km. The nine grid cells presented in Figure 3.1.32 cover most of the city of Nanjing. For each part of the city a time series is made and the reduction calculated of P2 compared to P1. The reductions vary from 32% to 56%. The biggest reductions are seen in those parts of the city with dominating traffic, while more industrial regions (grid cell 1, 2, 3 in Figure 3.1.32) show slightly smaller reductions.

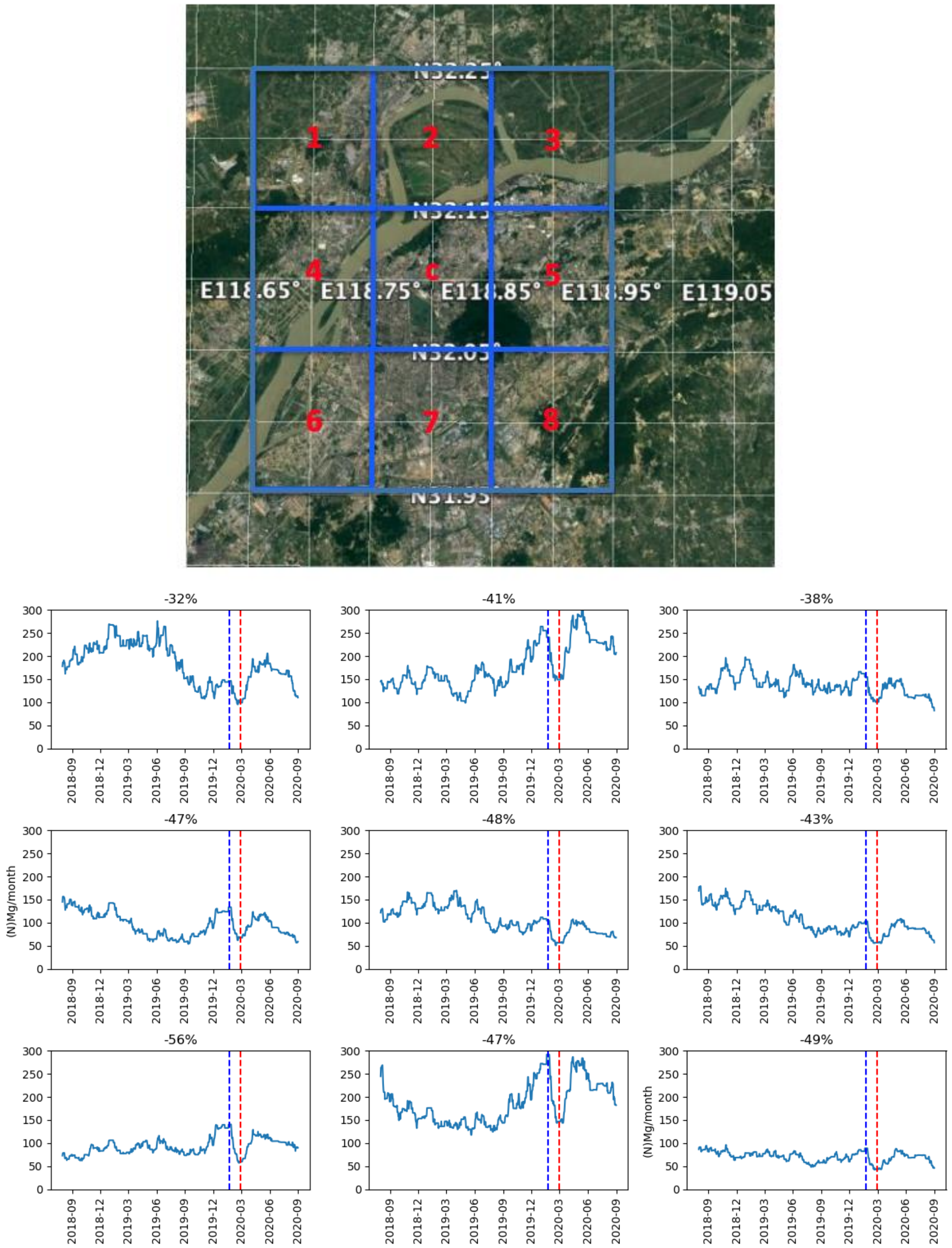

Figure 3.1.32: The top panel shows the city of Nanjing with the grid cells overlaid. For each grid cell a time series is plotted below in the same order as the blue grid cells. Blue line indicates 23 January 2020, just before the regulations and the blue line 28 February 2020 when strict regulations were enforced.

3.1.4 NOx emission reductions and relation to NO_2 concentration reductions in Europe (KNMI)

The DECSO algorithm, described in section 3.1.3, has also been applied to derive the NOx emissions in Europe in the period 2019-2020. We have derived emissions for Europe on a 0.2 x 0.2 degree grid and a separate run for Spain with resolution of 0.15 x 0.1 degree. Analysing emissions has the advantage that the derived emission reductions are hardly affected by changes in meteorological conditions.

For the same cities as analysed in section 3.1.2.2 we have plotted in Figure 3.1.33 the ratio of the NOx emission in 2020 and the emissions in 2019. We see that the emission reduction is rather large in some cities and this reduction is likely not only a result of COVID-19 regulation but also an effect of the general trend of reduced NOx emissions in the European cities. The left plot of Figure 3.1.34 gives the ratio of 2020 over 2019 of the average NOx emissions in the urban areas of Europe, showing a clear down-wards trend of emissions (of about 5-10%). A trend that was also reported by Georgoulias et al. (2019) and Zara et al. (2021). The right plot of Figure 3.1.34 shows that the trend varies a lot over the European cities. To minimise the effect of this trend we used as baseline the two and half month just before the COVID-19 period that started roughly half March in Europe. Plotting the emissions relative to this period, in Figure 3.1.35, shows us a different picture. The reductions still vary a lot from one city to another, but the reductions are in general much less, and in the cities Amsterdam, Berlin, Brussels and Budapest the reduction is not significantly higher than its annual trend. Note however that we make the assumption here that urban emissions are constant over the seasons, while in fact several cities show an increase in summer because of biogenic emissions from the green districts in the city.

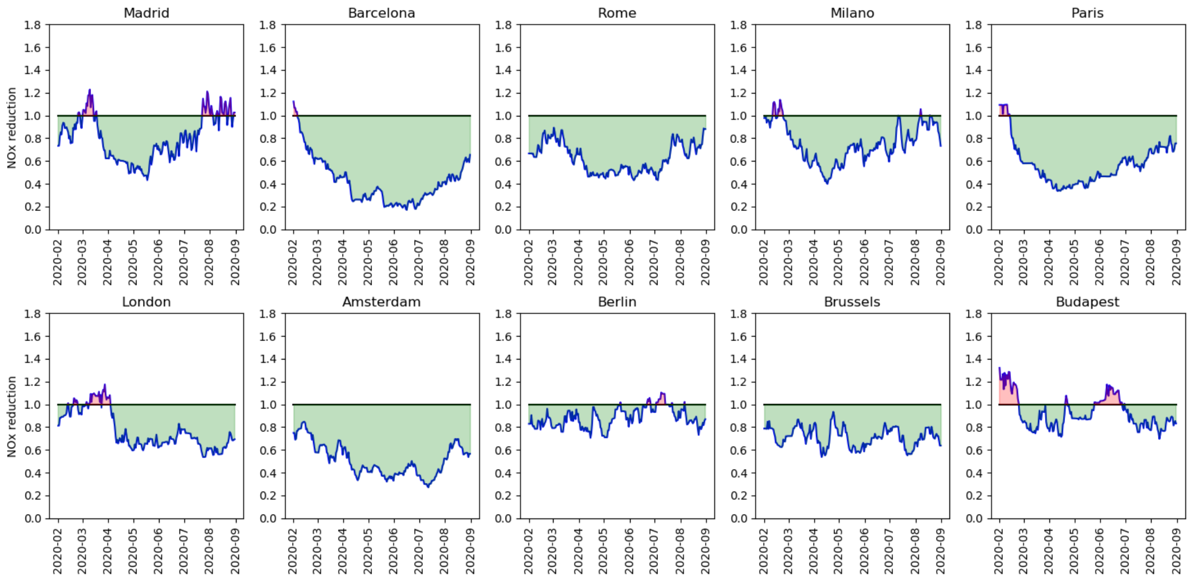

Figure 3.1.33: The NOx emission reduction by comparing the emissions in 2020 with the emissions in 2019 for the same day.

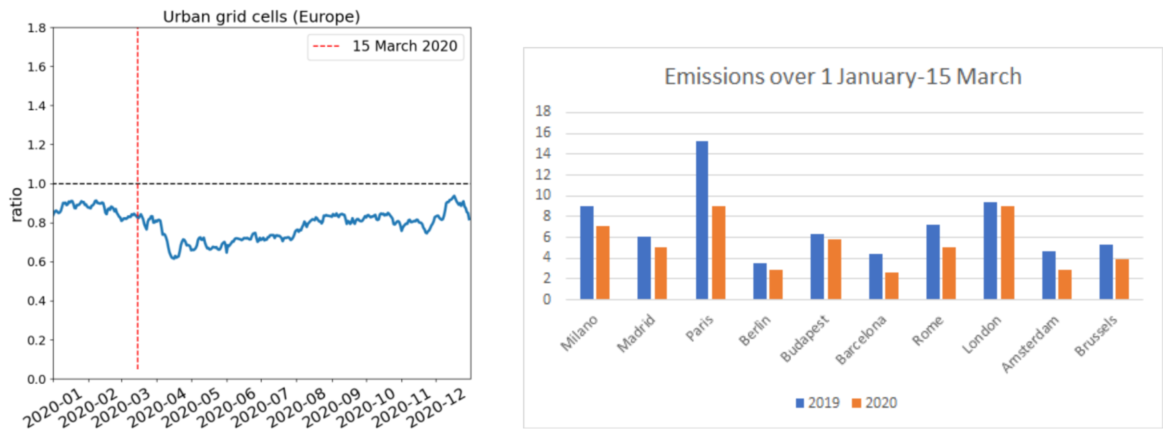

Figure 3.1.34: (left) Time series of the ratio of 2020 over 2019 of the average NOx emissions in European urban areas. The red line marks the start of the COVID-19 period on 15 March. (right) The emissions in the first months of 2019 and 2020 of the selected 10 European cities.

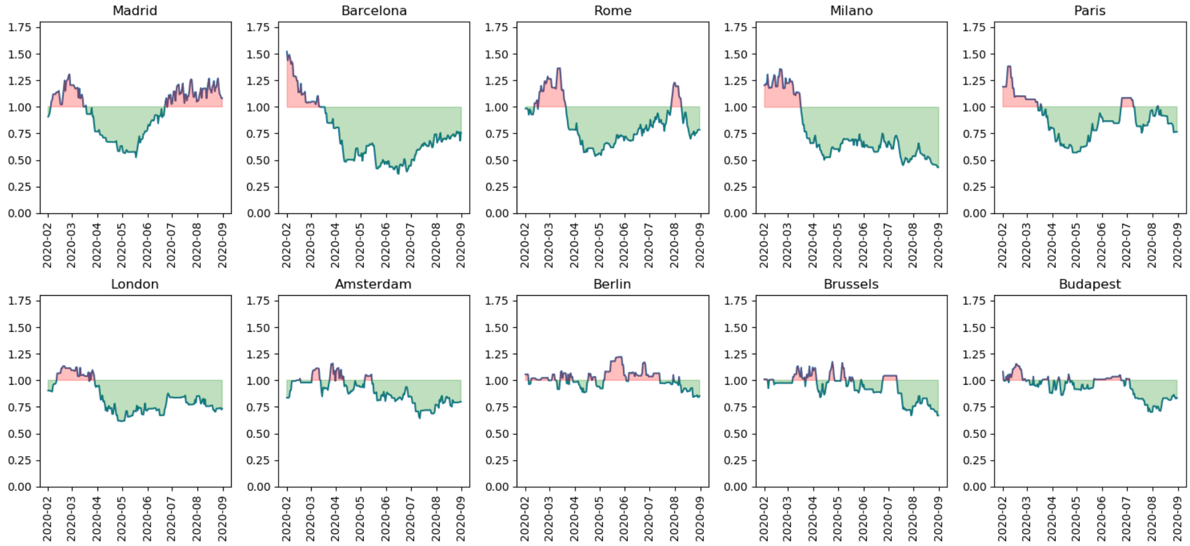

Figure 3.1.35: The NOx emission reduction by comparing the emissions in 2020 with the average emissions in the period 1 January 2020 to 15 March 2020.

Figure 3.1.36 shows the relationship of NOx emission fluxes with the corresponding NO_2 concentrations in cities, averaged in 14-day time intervals. As the COVID lockdown measures provoked a drop in NOx emissions causing lower NO_2 concentrations, this allows us to study this relationship for a wider range of values.

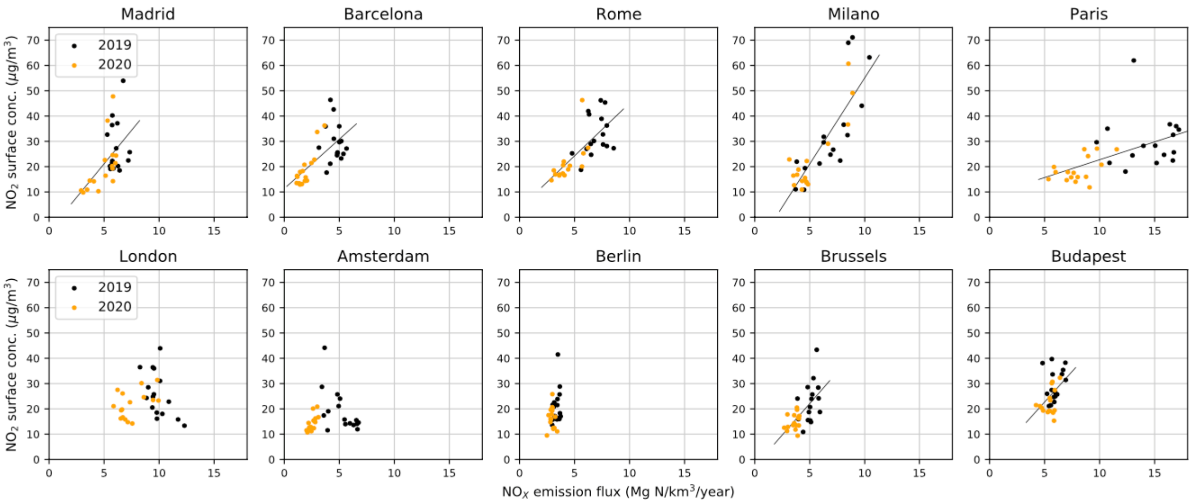

Figure 3.1.36: The relation between NOx emission flux and NO_2 concentrations in 10 European cities. The data is averaged in 14-day time intervals.

There is not always a clear relation visible in the scatter plots. Part of the scatter is caused by fluctuating concentrations due to variability in meteorology (estimated in Section 3.1.2.2 to be 21%). Cities like Amsterdam and Berlin show relatively high concentrations of NO_2 while having low local NOx emission fluxes, indicating that the NO_2 air pollution is largely affected by high background values (i.e. pollution being transported towards the city center).

A linear regression line has been drawn for cities where the correlation was found larger than 0.4. Note that this regression line does not capture any non-linear effects, probably caused by different chemical regimes (e.g. VOC-limited chemistry). This effect is especially visible for Madrid and Milan.

From the slope of the regression line, we can estimate for various cities by which fraction the local NOx emissions must be reduced to establish a reduction of NO_2 concentrations of 1 $\mu g/m^3$, based on 2019 levels.

Table 4: Correlation between NOx emission flux and NO_2 surface concentrations and linear regression results

city	n	correlation	slope=1/ΔE	E_{2019}	ΔE/E_{2019} x 100%
Madrid	32	0.52	5.30	6.10	3.1%
Barcelona	32	0.67	3.91	4.69	5.5%
Rome	31	0.72	4.16	7.01	3.4%
Milano	32	0.84	6.81	7.02	2.1%
Paris	32	0.55	1.41	14.63	4.8%
London	32	0.14	-	9.93	-
Amsterdam	32	0.07	-	5.28	-
Berlin	32	0.36	-	3.39	-

Brussels	32	0.63	4.97	5.10	3.9%
Budapest	32	0.46	4.83	5.96	3.5%

From Table 4, we can see that the impact of emission abatement policy will be largest in Milan, where a reduction of 1 μg/m^3 in NO_2 surface concentrations can be established by a reduction of 2.1% in NOx emissions. For the same effect, emission must be reduced by 5.5% in Barcelona, and 4.8% in Paris. For cities like Amsterdam and Berlin, NO_2 concentration reduction can best be achieved by policy targetting the reduction of imported background concentrations.

3.1.5 Conclusions on NO_2 analyses.

Significant reductions of NO_2 measurements (columns or concentrations) have been observed and quantified in many locations worldwide in phase with the local lockdown measures. In Europe and China, an excellent consistency is found between relative 2020/2019 differences observed from space with TROPOMI and from available ground in situ data. For most cities, they agree within 5%.

In Europe, the following conclusions can be drawn:

- The strongest reductions of 40-50% are found in the first phase of the lockdown in Southern European and French cities. The period up to 1 July can be seen as a transition period with weaker reductions. In July-August we find evidence that the concentrations are still 10% to 20% lower than pre-COVID levels.
- The COVID-19 measures taken in Berlin led to NO_2 reductions of the order of 20% in the first intense lockdown period, which remain similar in the months up to August 2020. This behavior is typical for cities in North-West Europe.
- Also in Eastern Europe, the impact of the measures has been less drastic than in Southern Europe and France, with reductions of the order of 15-25%.
- The contribution of meteorology on the NO_2 amount variability is high and explains for example much lower NO_2 concentrations in early 2020 compared to 2019 in Northern Europe, before any lockdown measure has been taken. Meteorological year-to-year variability is estimated to be 15% for NO_2 columns, and 21% for in-situ concentrations. Although using the LOTOS-EUROS model to correct for the meteorological contribution helped to better interpret the observations in many locations, such a correction has not always been optimal: in particular the CAMS ensemble had major emission inventory updates preventing to compare the 2019 and 2020 modelled fields, and LOTOS-EUROS shows weather (season) dependent biases. A stronger modelling effort with a consistent “business-as-usual” emission inventory could improve the results.
- In addition to meteorology, a downward trend of NO_x emissions in many European cities also contribute to lower NO_2 levels in 2020, which needs to be accounted for when trying to disentangle the different effects. When deriving NOx emissions with DECSO for Europe we find a strong annual trend in NOx emissions for many cities before the COVID regulations started, which can make the reduction look larger than they actually are. After correcting for this, we still find reductions of up to 40-50% in several Spanish, Italian and French cities.
- The COVID lockdown measures provoked a wider range of values of NOx emissions and NO_2 concentrations. This enables an assessment of the impact of emission abatement policies in various cities. In Milan, it is estimated that a reduction of 1 μg/m^3 in NO_2 surface concentrations can be established by a reduction of 2.1% in NOx emissions. For the same effect, emission must be reduced by 5.5% in Barcelona, and 4.8% in Paris. For cities like

Amsterdam and Berlin, NO_2 concentration reductions can best be achieved by policy targetting the reduction of imported background concentrations.

In China, we found that:

- Both satellite and in situ NO_2 observations in the biggest cities of China show reductions of about 40% during the lockdown. Then they rebound quickly to the original levels after the lockdown period. In Wuhan, the observed NO_2 reductions were larger (up to 60%) and last longer (until June).
- Simulations with the CTM MAGRITTEv1.1 using an anthropogenic emission inventory optimized for the effect of the different lockdowns worldwide allowed to reproduce reasonably well the 2020/2019 NO_2 column ratio as observed with TROPOMI in February when the reductions were the most important, but also later in May when local restrictions were much lighter.
- NOx emission estimates with the DECSO algorithm show a reduction of 20-50% in the urban areas of China and of 40% in the energy sector. Reductions of emissions in the maritime sector are also seen, but these are smaller and strongly depend on the region.
- When deriving 0.1 degree resolution emissions, we see that the various city quarters of Nanjing show similar reductions, but with slightly less reductions in the more industrial areas of the city as compared to the zones with only traffic.

NOx emissions have also been estimated for 2019 and 2020 by exploiting the correlation between the TROPOMI NO_2 column spatial variability and the wind conditions over a series of cities worldwide, considered as point sources. In Buenos Aires, NOx emissions in 2020 were 50-60% smaller in April 2020 than in 2019, while comparable in the first three months of the year. In New Delhi, derived NOx emissions were lower by 89% in April 2020 compared to April 2019 and remained significantly lower in May (70%) and June (47%). After the period July-September during which the analysis was not possible due to the limited amount of valid data, the NOx emissions derived in October/November were still lower in 2020 than in 2019. A similar analysis has been performed in New York, Riyadh, Kano and Madrid. Despite some variability in the data linked to sampling due to clouds and limitations in the analysis, lower NOx emissions have been found in 2020 than in 2019, but with different seasonal patterns, which is related to the different timing of the Covid-19 infection waves and the differences in lockdown severity.

3.2 Other species

3.2.1 Sulphur dioxide (SO_2) (BIRA-IASB)

In a first step, the TROPOMI offline operational SO_2 column product has been used to detect changes in SO_2 emissions related to the COVID-19 sanitary crisis, over China and India. However, it became soon evident that no robust conclusions could be drawn, because of biases in the product that are typically higher than the decrease in vertical column due to COVID-19 lockdown measures. Therefore, we have developed a new SO_2 algorithm that efficiently reduced VCD offsets and that can be used to study “weak” changes (~0.05-0.1 DU) in SO_2 vertical column levels. The algorithm is named COBRA (Covariance-Based Retrieval Algorithm) and makes use of a set of SO_2-free spectra to build a covariance matrix of the radiance in the 310.5-326 nm wavelength range to optimally represent the radiance background variability (except that of SO_2). The SO_2 SCD is retrieved as a single fit parameter (Theys et al., 2021) and the AMF needed to convert SCD into

VCD is taken 'as is' from the operational SO_2 product. Compared to the (DOAS) operational product, the COBRA is improved both in terms of noise level and bias reduction (see Figure 3.2.1). One additional advantage of the COBRA scheme is its computational speed (an order of magnitude faster than DOAS-type algorithms), and we have taken advantage of this to reprocess the full TROPOMI data record.

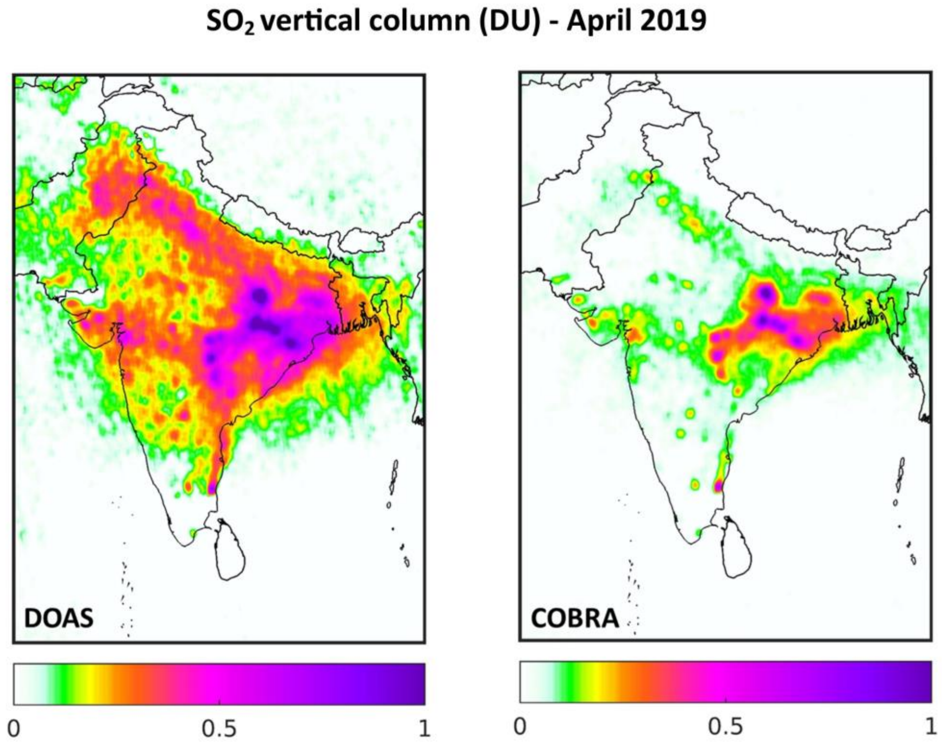

Figure 3.2.1: Monthly averaged TROPOMI SO_2 columns over India for April 2019, from (left) DOAS operational product and (right) COBRA scientific product. The noise and offsets reduction is clear from the maps. The individual point sources (power plants) can be better discerned in the COBRA SO_2 map.

The effect of COVID-19 measures on SO_2 columns has been investigated in details for China and India. The selection of pixels was performed based on strict cloud filtering and product quality indicators, and in an effort to align with other species, in particular NO_2. Figure 3.2.2 and Figure 3.2.3 presents the observed decrease of SO_2 VCDs over India and China.

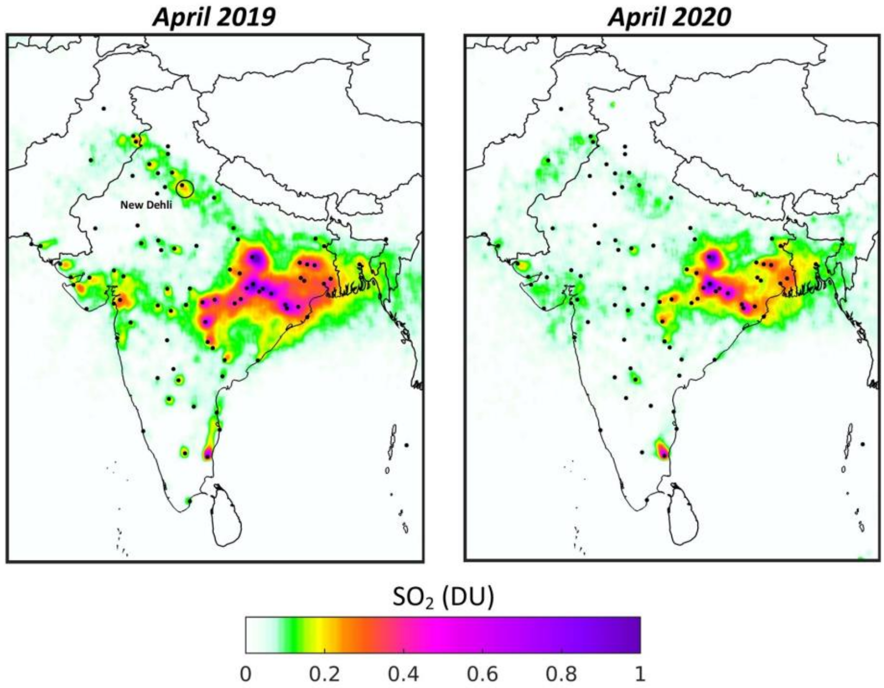

Figure 3.2.2: Monthly averaged TROPOMI SO_2 columns over India for April 2019 and April 2020.

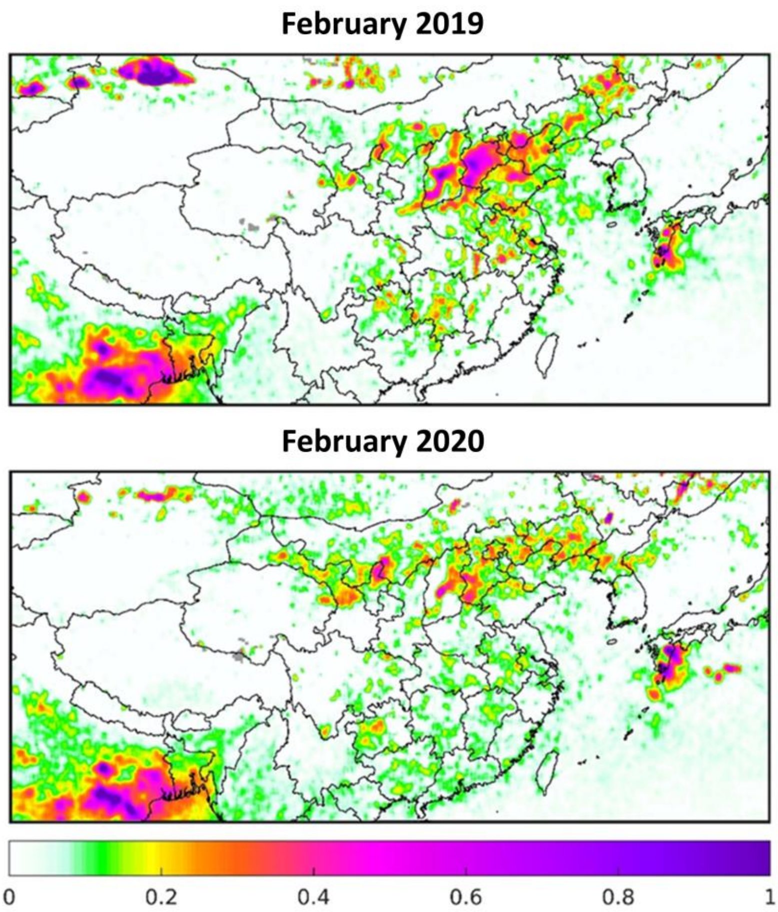

Figure 3.2.3: Monthly averaged TROPOMI SO_2 columns over China for February 2019 and February 2020.

Figure 3.2.4 gives a summary of the exercise. As can be seen, a clear COVID-19 related effect on SO_2 is observed with a decrease up to -75% (second half of February) and -40 % (April), respectively over China and India.

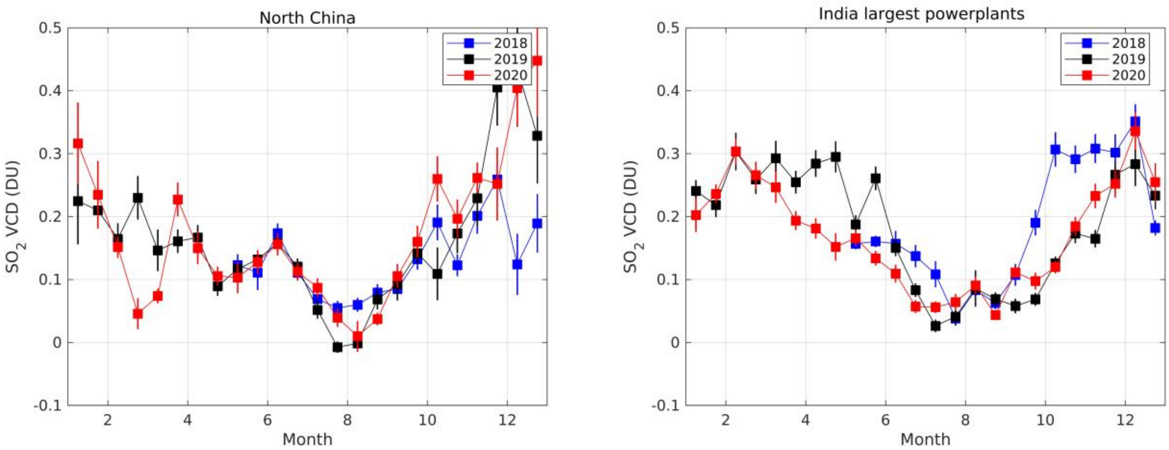

Figure 3.2.4: Time-series of bi-weekly mean SO_2 vertical columns for 2018-2020 over (left) North China (34°N-40°N; 110°E-120°E) and (right) India 59 largest power plants (0.5°x0.5° domain centered around each station, of which the coordinates are provided in Annex A).

As a note, we find that observed SO_2 VCD reduction is most often hard to separate from inter-annual variability and short-term variability (out of COVID-19 periods). Other regions in the world have been investigated (e.g., Turkey, South Africa) but no firm conclusions could be drawn on the possible link between observed variability and local lockdowns.

3.2.2 Carbon monoxide (CO)

3.2.2.1 Analysis using the operational product algorithm (SRON)

The operational TROPOMI CO dataset provides total column measurements of CO in the atmosphere with daily global coverage and a high spatial resolution of about 7x7 km^2 (Veefkind et al. (2012)). The retrieval deploys the SCIOR algorithm that retrieves trace gas columns together with effective parameters describing the cloudiness of the observed scene (cloud altitude and optical thickness) from the SWIR measurements of the instrument (Landgraf et al. (2016, 2016a)).

The TROPOMI CO dataset fulfils the mission requirements (precision < 10%, accuracy < 15%) (Borsdorff et al. (2018a, 2019)), has proven to be useful for the monitoring of CO enhancements above mid-sized cities, and even along main traffic roads (Borsdorff et al. (2018)). In combination with simulation of regional models like WRF-chem, the TROPOMI CO dataset has the potential to further improve emission inventories by distinguishing CO emissions on a fine spatial resolution e.g. emissions from different suburbs in Mexico City (Borsdorff et al. (2020)).

In this study, we use the offline CO retrievals (version 01.01) under clear-sky and optical thick low altitude cloud conditions. This corresponds to filtering the data by (qa_value > 0.5). TROPOMI CO clear-sky retrievals show a very good sensitivity throughout the atmosphere. By validation with TCCON measurements it was shown that the retrievals under low altitude cloud conditions are comparable to clear-sky measurements in unpolluted scenes (Borsdorff et al. (2018a, 2019)), but can lead to an underestimation of CO enhancements above pollution hot-spots (Borsdorff et al. (2018)). This so called smoothing or null space error (Borsdorff et al. (2014)) can become even higher than 30% (Borsdorff et al. (2017)), but can be completely avoided when comparing with vertical profiles e.g. from models by considering the vertical sensitivity of the retrieval (averaging kernel) that is supplied by the dataset for each retrieval (Borsdorff et al 2018b). Even though this is an additional error contribution to this study, we need to use cloudy retrievals to get a better data coverage.

We analysed the operational TROPOMI CO dataset from 2019 to 2020 to search for reductions in the CO concentration caused by COVID-19 lockdown measures. The regions considered are Italy, India, and China. For Italy, major cities like Milano, Turin, and Venice were studied and the Po valley as a whole. Figure 3.2.5 shows monthly means of TROPOMI CO from December 2019 to March 2020. CO enhancements over industrial areas near Venice can be sensed, but it is hardly possible to identify any isolated pollution hot spots like major cities in the area. One of the reasons for this is the satellite observation geometry at the time of the year with lower solar zenith angles leading to more noise in the data, but also the general high variability of CO over Europe. Figure 3.2.6 shows a time series of TROPOMI CO daily means over the Po Valley as a whole in the lat/lon box [45.45, 8.20, 44.89, 12.15]. The 60-day running average indicates that the seasonality of CO over the region is highly variable from year to year. Furthermore, the scatter of the daily means is so high that no COVID-19 lockdown signals can be identified (see lower panel of Figure 3.2.6).

For China, we analyzed different industrial regions (North, South, corridor between Beijing and Wuhan), the city of Wuhan, as well as power plants. Figure 3.2.7 compares the CO concentration over China in February 2019 with the one of February 2020. This clearly shows significantly reduced CO values in 2020. However, it seems that the variability of CO in the first months of each year is generally high over China as shown by Figure 3.2.8 presenting time series of CO over Northern China (lat lon box [41.42, 103.99, 34.63, 121.91]) and the corridor between Beijing and

Wuhan (lat lon box [42.33, 112.99, 29.64, 117.09]). For example, in January 2018, detected CO values are even lower than in 2020, apparently without any COVID-19 lockdown measures. The variability of CO could be driven by the meteorological situation and atmospheric transport. Hence, also for China, we find no significant COVID-19 lockdown signals in the TROPOMI CO data.

We analyzed India as a whole, but with a deeper focus on the Northern part of the country. Time series of major cities like New Delhi, Mumbai, and Bangalore as well as the Indo-Gangetic plain were considered. Figure 3.2.9 shows the monthly averaged CO concentration over India in April 2019 and 2020. For April 2020, we do not find reduced, but instead enhanced CO values over the southern part of India. The reason for this could be CO from biomass burning that accumulates in the atmosphere. This is possible due to the relatively long resistance time of CO that varies between weeks and months depending on the atmospheric OH concentration (Holloway et al. (2013)). Hence, the challenge to identify COVID-19 lockdown signals is to separate the background CO variability which is driven by pollution transport worldwide, from reduced local emissions. This is hardly possible without applying regional models like WRF-Chem. As can be seen in Figure 3.2.9 the Northern part of India is less affected by the CO enhancements observed in the South. However, the time series of CO over New Delhi and the Indo-Gangetic plain in Figure 3.2.10 still contain too much noise to detect a significant reduction of CO in April 2020 compared to former years. Furthermore, Figure 3.2.11 shows that most of the retrievals in April 2020 are cloud contaminated. This could also be a reason for reduced CO values during that time, since clouds in the observation geometry of the satellite are reducing the sensitivity for CO at the ground. Hence, again model calculations would be needed to better account for the sensitivity reduction of the retrieval. Consequently, for India we cannot conclude either on the presence of a possible COVID-19 lockdown signal.

We have developed a software framework to collocate the whole TROPOMI CO data product for 2020 with the simulations of the ECMWF-IFS forecast product. This control run of ECMWF-IFS is not assimilating other satellite measurements that could possible detect COVID-19 lockdown signals. We tried to use the model calculation to estimate the background variability of CO and to facilitate the extraction of a possible COVID-19 lockdown signal in the TROPOMI CO data. However, the bias between TROPOMI and the simulation is much too high and even scaling the simulation to the TROPOMI data is not enough to bring them in agreement as is shown in Figure 3.2.12. Furthermore, the bias between TROPOMI and ECMWF-IFS shows a significant dependency with latitude and time, which could exceed possible COVID-19 lockdown signals.

In conclusion, we find that COVID-19 signals are not easy to detect in the TROPOMI CO data. The challenge is to separate such signals form the high background variability of CO that is driven by atmospheric transport of pollution worldwide and additionally to account for the vertical sensitivity of the TROPOMI CO retrieval that can be degraded due to cloud contamination of the measurements. In future, regional modeling e.g., with the WRF-Chem model could possibly help to detect COVID-19 lockdown signals in the TROPOMI CO data. Furthermore, a correlation of TROPOMI CO with trace gases like NO_2, that are more sensitive to lockdowns, could give a better insight into the question whether COVID-19 lockdowns had an impact on the atmospheric CO concentrations.

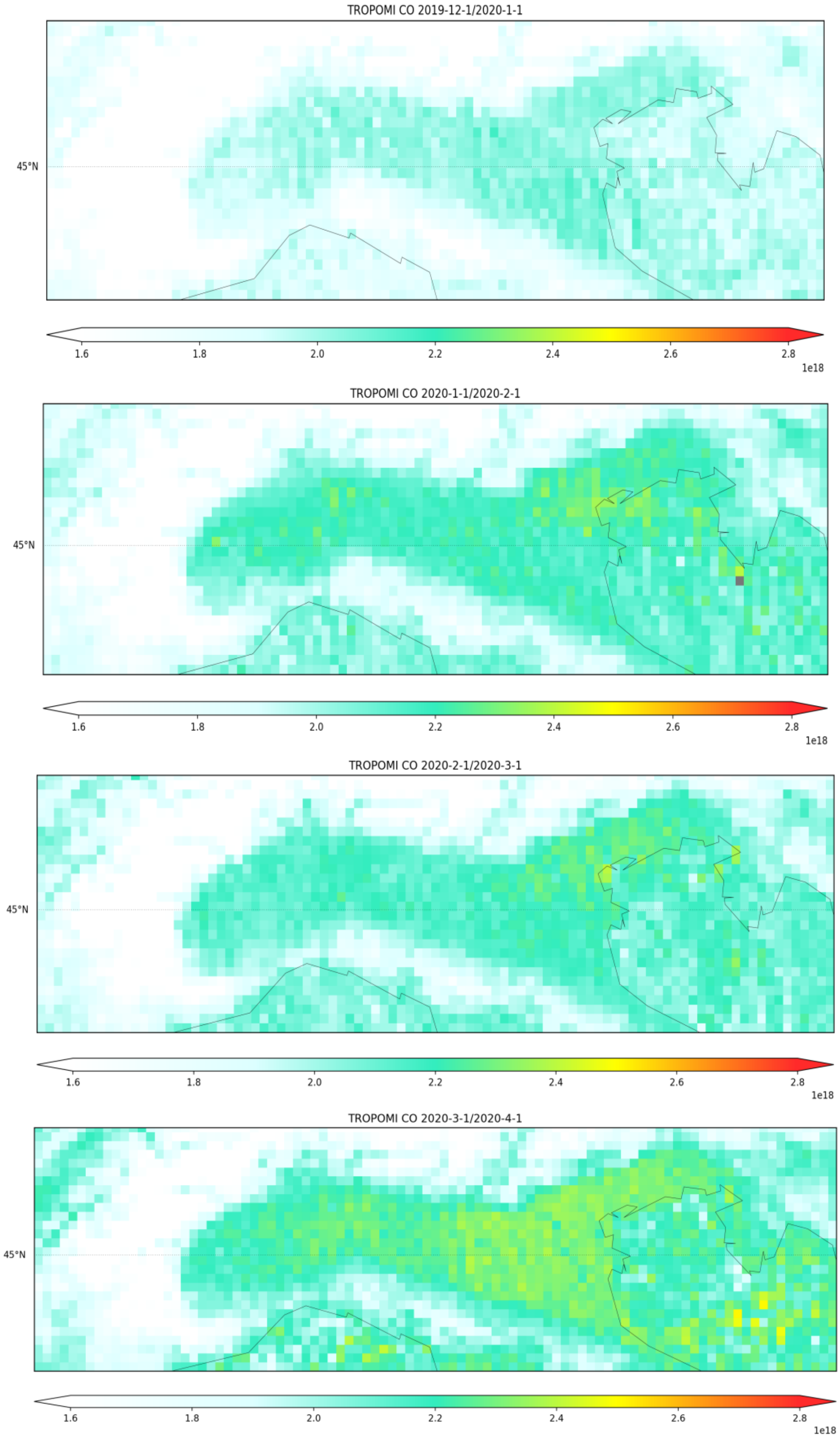

Figure 3.2.5: Monthly averaged TROPOMI CO retrieval over Northern Italy. From top to bottom December 2019 – March 2020. Vertical column densities in molecules/cm^2 are shown.

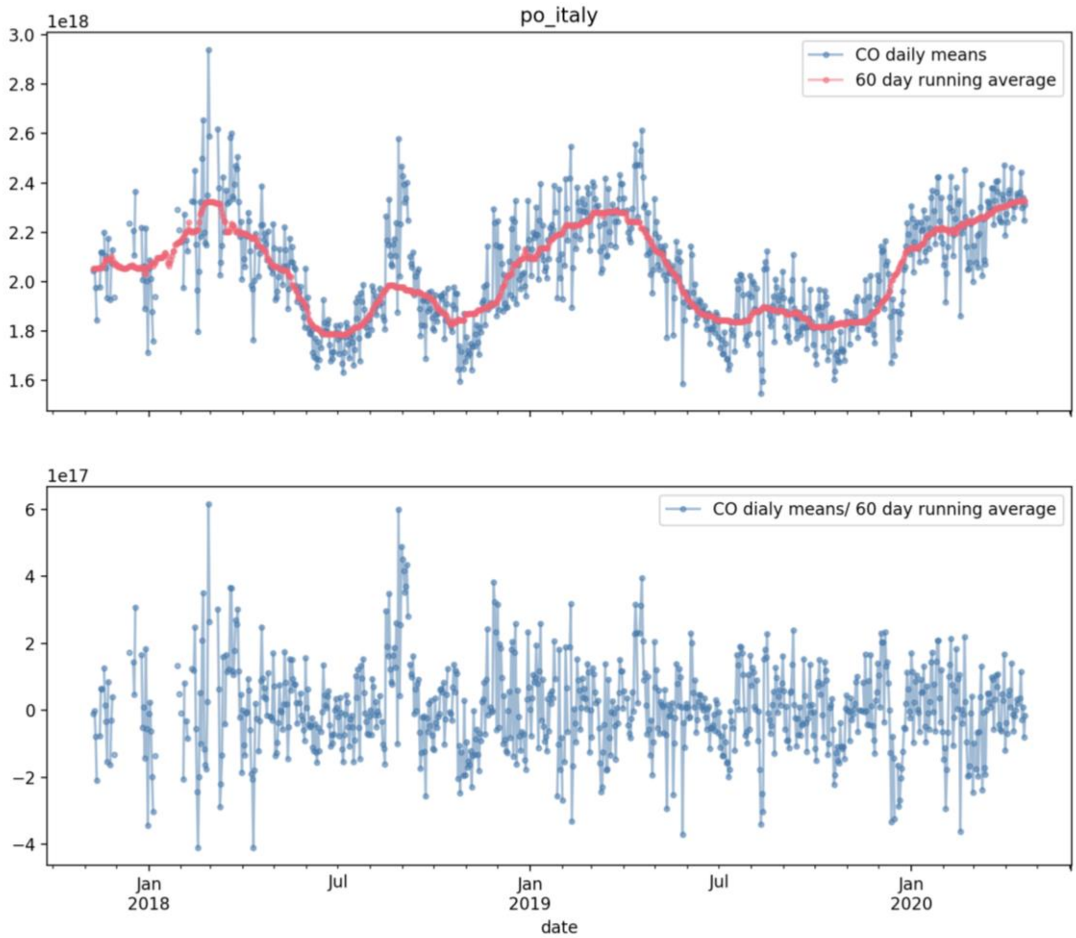

Figure 3.2.6: Time series of TROPOMI CO retrievals from 2018-2020 over the Po Valley [45.45, 8.20, 44.89, 12.15] (top panel). Daily means are shown with the standard deviation of the mean as error bars. The red line is a 60-day running mean. The lower panel shows the differences of the daily means and the 60-day running mean. Vertical column densities in molecules/cm^2 are shown.

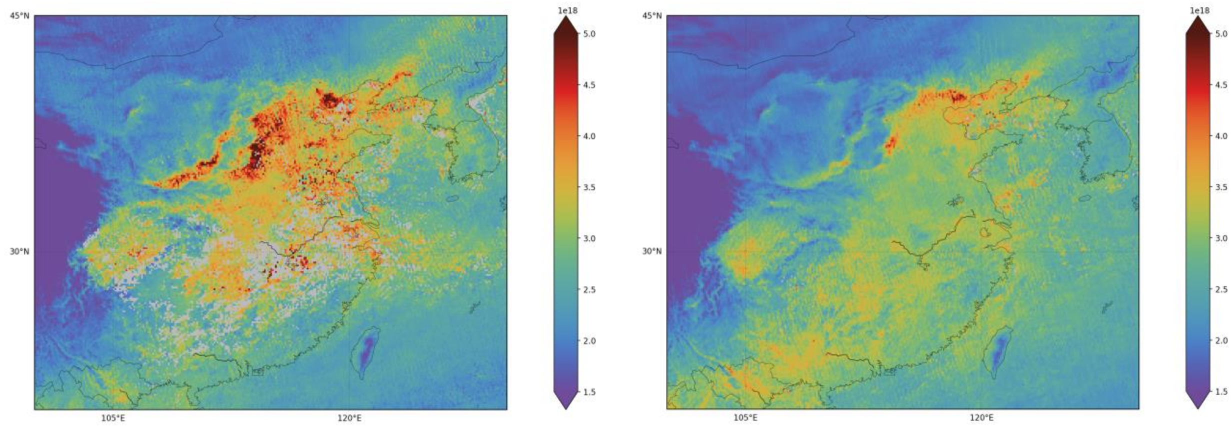

Figure 3.2.7: Monthly averages of the TROPOMI CO retrievals over China. From the 11th-28th February 2019 (left panel) and 8th-28th February 2020 (right panel). Vertical column densities in molecules/cm^2 are shown.

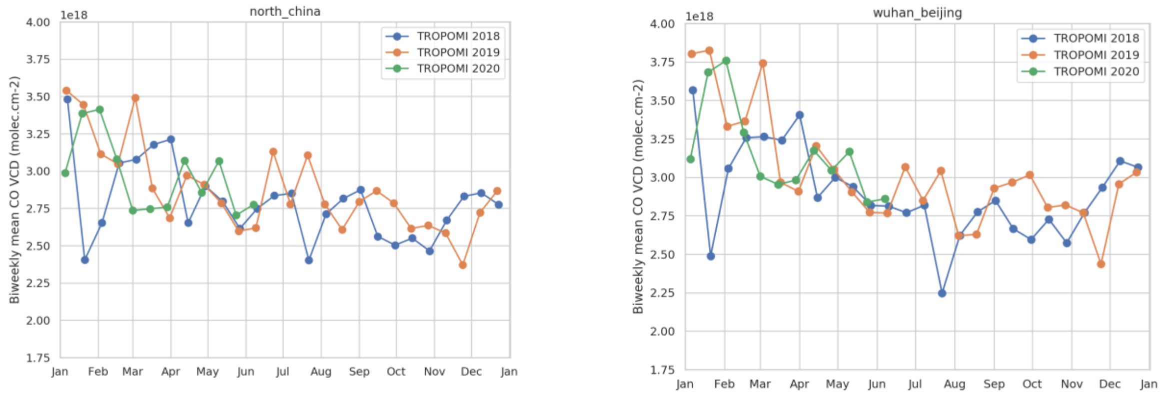

Figure 3.2.8: Time series of TROPOMI CO retrievals from 2018-2020 over Northern China [41.42, 103.99, 34.63, 121.91] (left panel) and the corridor between Beijing and Wuhan [42.33, 112.99, 29.64, 117.09] (right panel).

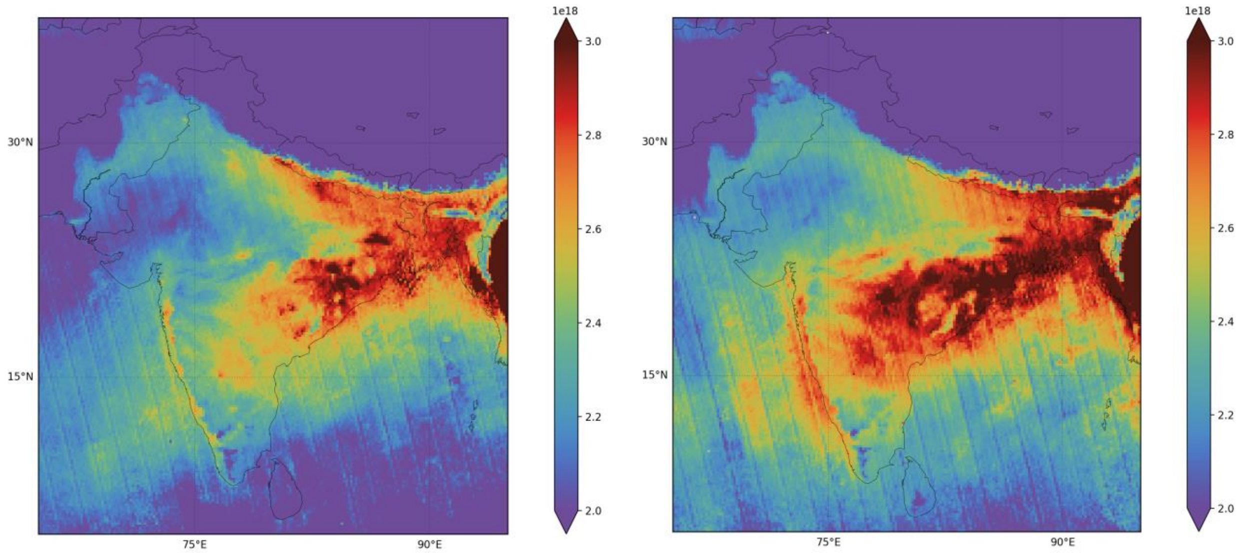

Figure 3.2.9: Monthly averages of the TROPOMI CO retrievals for April 2019 (left panel) and April 2020 (right panel) over India. Vertical column densities in molecules/cm^2 are shown.

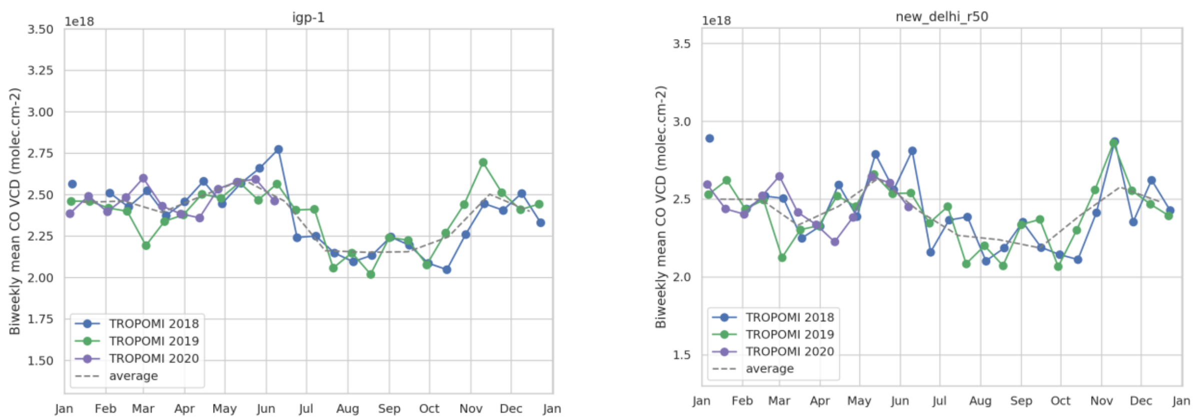

Figure 3.2.10: Time series of TROPOMI CO retrievals from 2018-2020 over the Indo-Gangetic plain plane (left panel) and in a radius of 50km around New Delhi (right panel). The dotted line is the average of all years.

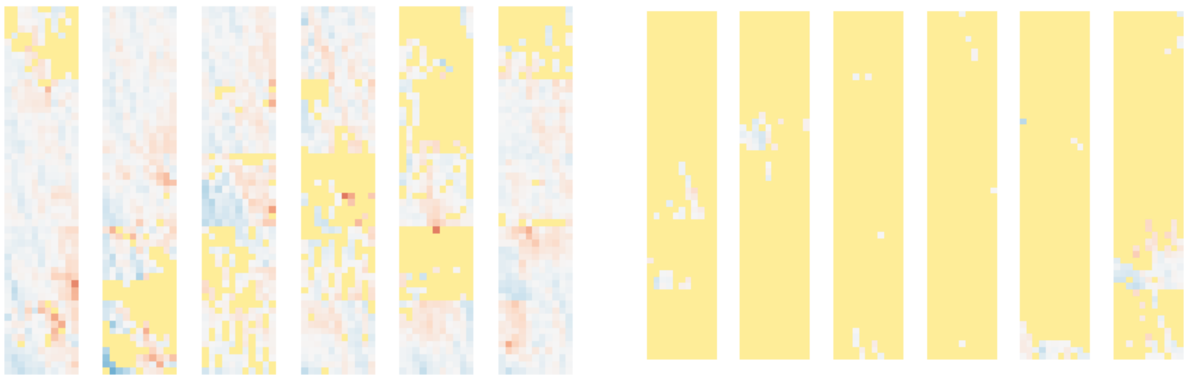

Figure 3.2.11: TROPOMI CO retrievals in a X by X lat/long box centred around New Delhi. From left to right and top to bottom the daily overpasses in April 2020 are shown. (left panel) CO retrieval under cloudy and clear-sky conditions (qa_value>0.5), (right panel) only clear-sky retrievals (qa_value>0.7). We removed the background CO concentration for each overpass by subtracting the median of the retrievals. Vertical column densities in molecules/cm^2 are shown.

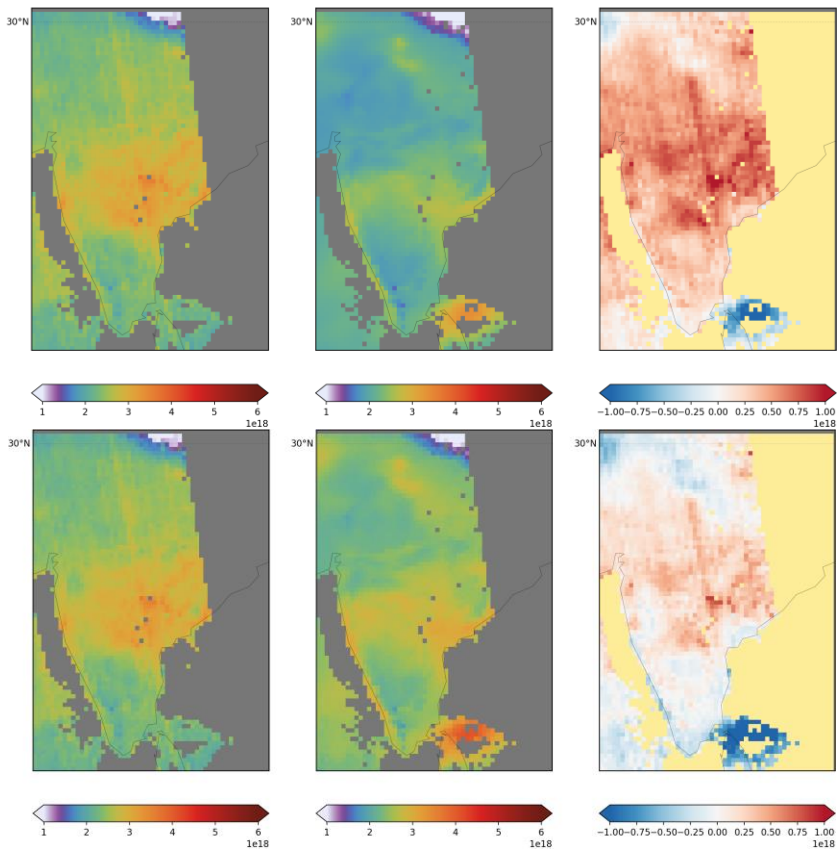

Figure 3.2.12: TROPOMI CO retrievals over India on the 1st of April 2020 (first column). Simulated CO columns of the CAMS IFS control run collated with the TROPOMI overpass (second column). Difference between TROPOMI CO and CAMS (third column). In the second row the CAMS simulation was scaled to have the same mean CO concentration as the TROPOMI measurements. We applied the averaging kernels of the TROPOMI retrieval to the CAMS model. Vertical column densities in molecules/cm^2 are shown.

3.2.2.2 Analysis using the WFMD scientific algorithm (IUP-Bremen)

In order to find out if potential changes in atmospheric CO during the pandemic can be detected from space we have analysed Sentinel-5-Precursor (S5P) scientific WFMD algorithm XCO retrievals (Schneising et al., 2019, 2020a) during October 2017 to June 2020.

We focussed on regional-scales and generated XCO maps (absolute XCO and XCO differences to the previous year) for South East Asia, Europe, and continental US (Figures 3.2.13-16). To better analyse the observed pattern we also performed an additional time series analysis for smaller source region (with substraction of background to remove seasonal cycle and potential global yearly changes) based on weekly data for different years. The time series analysis is performed for the following sub-regions: East China (Figure 3.2.13), Northern Italy (Figure 3.2.14), India (Figure 3.2.15) and the US East Coast (Figure 3.2.16). The source region of interest and the corresponding background region are highlighted in the respective figures.

The spatial maps of XCO differences between COVID-19 and a pre-pandemic period typically show a complex pattern of year 2020 reductions and enhancements and the time series analysis indicates that the differences of 2020 and 2019 are within normal year-to-year variability for all analysed regions.

For example in the case of China, we find a reduction in 2020 relative to 2019 in the analysed source region in the spatial difference map for February and March (Figure 3.2.13). However, the time series analysis suggests that single difference maps are not sufficient to explicitly link such reductions to the COVID-19 lockdown: we find lower values (2020 relative to 2019) in the late lockdown period after about February 10 (2018 is in between), but the exact opposite during the first 2-3 weeks of the lockdown and there are also lower values relative to the year before from October to mid January in a time period without lockdown.

The time series analysis also indicates that the 2019 values were exceptionally high in late February contributing to the reduction in the Chinese source region, which is visible in the XCO difference map (2020FM-2019FM). In the other regions there are no significant time series differences between the years.

It is therefore concluded that there is no unambiguous signature in XCO during the COVID-19 lockdown in 2020 in the analysed regions.

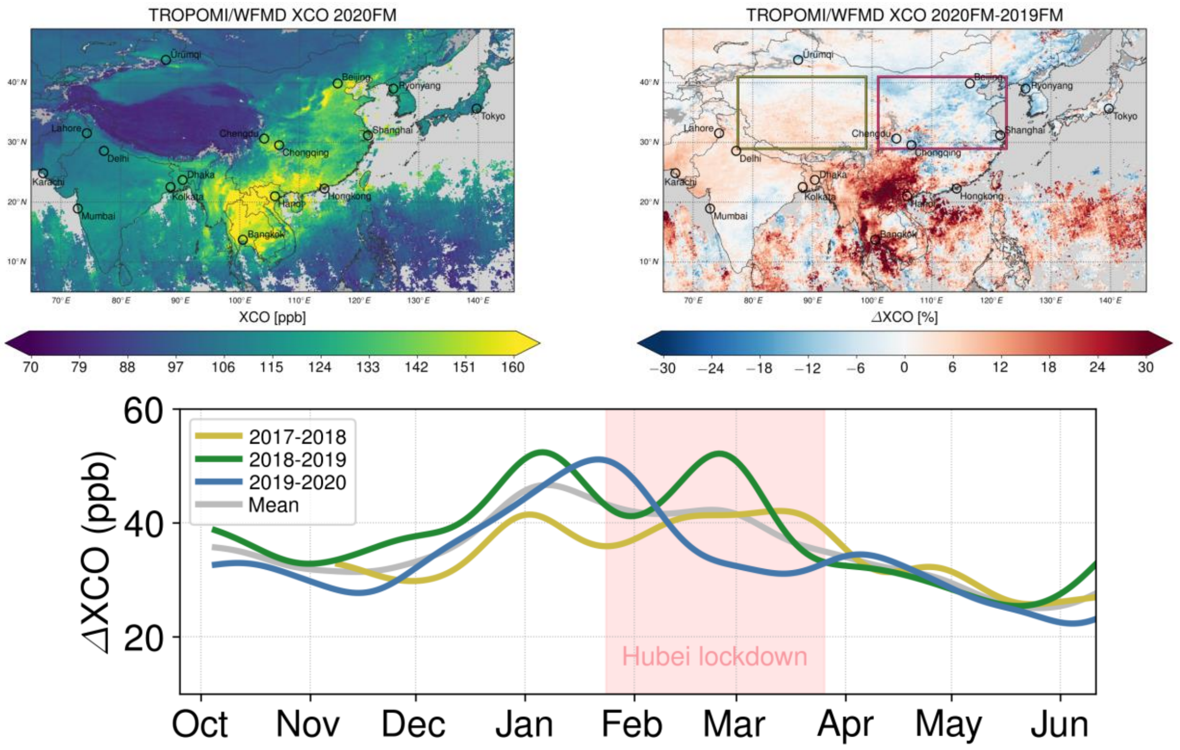

Figure 3.2.13: Top left: XCO over China and surrounding countries for February/March 2020 (2020FM). Top right: XCO difference 2020FM minus 2019FM, the large positive increment in South East Asia is due to wildfires in 2020. Also shown are two rectangular regions: the East China target (or source) region of interest (red) and the corresponding background region (green). Bottom: Time series (weekly resolution) of ΔXCO, which are target minus background (TmB) region differences of consecutive years. Also shown in light red is the Hubei lockdown period from end of January 2020 to end of March 2020. As can be seen from the blue curve, TmB ΔXCO is lower in 2020 compared to 2019 during the late part of the lockdown but there is also a reduction before the lockdown and at the start of the lockdown the TmB curve is even larger for 2020 in comparison to 2019. It is therefore concluded that the year-to-year differences of 2020 and 2019 are within normal variability.

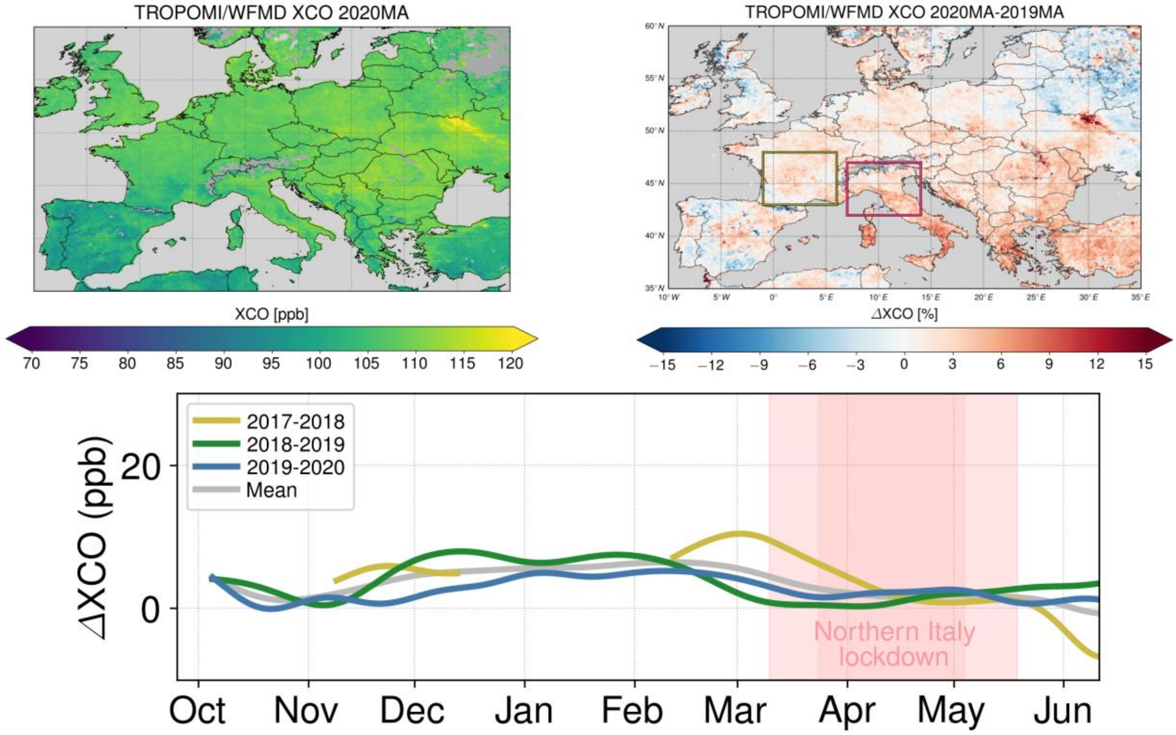

Figure 3.2.14: Similar as Figure 3.2.13 but for Europe and March/April maps focussing on Northern Italy for the time series analysis. The elevated XCO in the Ukraine is due to wildfires in 2020.

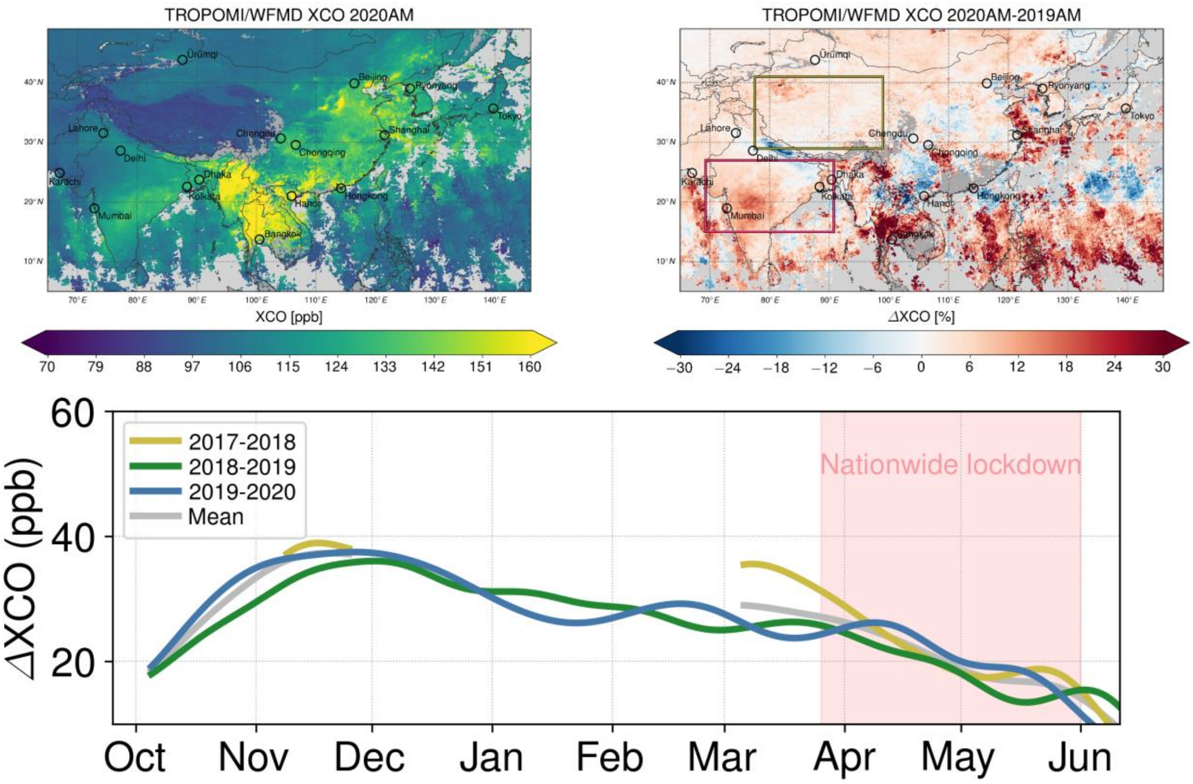

Figure 3.2.15: Similar as Figure 3.2.13 but for India and April/May maps focussing on Northern India for the time series analysis.

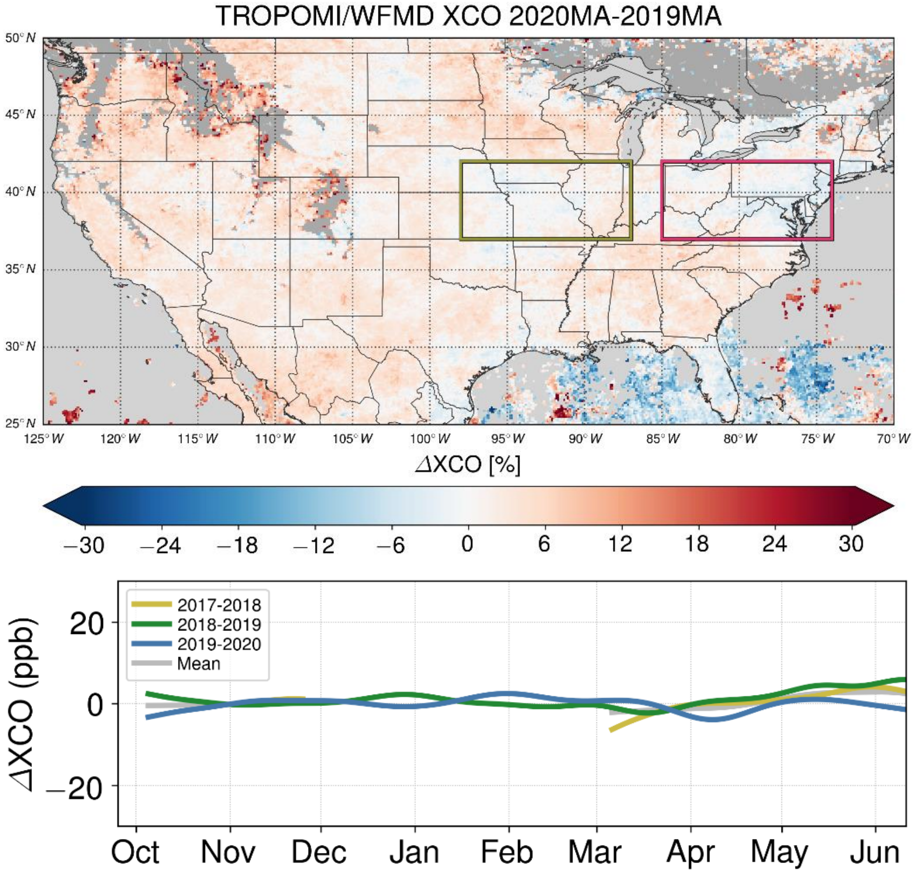

Figure 3.2.16: Similar as Figure 3.2.13 but for the US and a March/April difference map focussing on parts of the US East Coast for the time series analysis.

3.2.3 Formaldehyde (HCHO), glyoxal (CHOCHO) and PAN (BIRA-IASB)

HCHO and CHOCHO are both short-lived indicators of NMVOC emissions as they are largely produced via the oxidation of other NMVOCs either emitted as a result of biogenic processes, large biomass burning events, or anthropogenic activities (Bauwens et al., 2016; Fu et al., 2008; Stavrakou et al., 2009). To a lesser extent, direct emissions of HCHO and CHOCHO from combustion and industrial processes may also occur. In particular, glyoxal is produced from oxidation of aromatics with a much higher yield than HCHO, providing a stronger response to anthropogenic activities (Cao et al., 2018). There are difficulties associated with the investigation of a possible lockdown signature in the satellite HCHO and CHOCHO data sets. Large uncertainties are associated with both of these column retrievals owing to their low optical depth. As mentioned before, HCHO and CHOCHO columns are dominated by biogenic emissions, which explains the observed seasonal pattern of HCHO and CHOCHO column values with a maximum during summertime. Variability in meteorology (temperature changes, winds, precipitations) may lead to changes in column amounts on the same order of magnitude as the expected lockdown-related reduction in anthropogenic emission changes. Working with large regions allows reducing the noise on the observations, but local effects are not well separated from natural variations and the spatial sampling should be verified to remain comparable for year-to-year, and month-to-month. Working at a finer city scale allows better isolating local effects and reducing sampling issues, but at the expense of a larger noise level, often preventing to conclude on the observed variations.

3.2.3.1 HCHO

Our analysis was primarily based on 3 years of TROPOMI measurements. Observations during the 2020 lockdown period were compared with the values in 2018 and 2019. As will be explained in this section, for HCHO, we could observe a 40% decrease over Northern China during the second half of February, and a similar decrease over New Delhi during the first half of April. In Europe, US or South America, we could not isolate an unambiguous decrease in the atmospheric HCHO columns.

Even for the Chinese and Indian regions, it was not easy to confirm the anthropogenic origin of the observed decrease. The column being at their minimum during the winter time periods, and their uncertainties being larger for large solar zenith angles, signal changes are much more difficult to confirm during winter time than during spring or summer time. Data and methods needed to be carefully adapted. The influence of the temperatures has been taken into account. In the larger Northern China region, the spatial sampling has been carefully checked. Finally, the OMI data records has been used to evaluate the observed changes relative to the HCHO variability.

Data and Method

We use the TROPOMI level-2 HCHO operational data product (RPRO+OFFL, product versions 1.1.[5-8], http://www.tropomi.eu/data-products/formaldehyde; doi: 10.5270/S5P-tjlxfd2). HCHO retrieval algorithm has been fully described in the HCHO ATBD (De Smedt et al., 2018). It is based on the DOAS method, and is directly inherited from the OMI QA4ECV product (https://doi.org/10.18758/71021031). Considering that the bias between OMI and TROPOMI HCHO columns is lower than 10% in most regions (ROCVR http://mpc-vdaf.tropomi.eu/, De Smedt et al., 2021/), we have used the QA4ECV OMI dataset to construct a climatology based on the more recent years (2010-2018) and use it to assess the interannual and seasonal variability. Furthermore, we use the strong correlation between HCHO columns and surface temperatures (Zhu et al., 2017) to introduce a temperature correction based on data from 2005-2020 for OMI measurements, and 2018-2020 for TROPOMI measurements. In brief, this correction consists of fitting a second-order polynomial through daily HCHO columns reported as a function of the temperature. This analysis is performed for each region and on the OMI and TROPOMI time series separately. On this basis, the temperature-induced variations in HCHO are subtracted from the time series using local daily temperatures specified by ERA5-Land 2m data meteorological sets (Copernicus C3S ERA5-Land reanalysis, 2019) up to December 2020. This mainly leaves HCHO anomalies, which are not related to temperature fluctuations. Finally, a polynomial obtained using a climatology of surface temperatures is added to the differential HCHO columns, in order to reintroduce the natural seasonal cycle, assuming the same temperature every year. Note that the difference with uncorrected HCHO columns is generally small (less than 10%), but can be significant when looking for small effects such as those induced by COVID-related emission changes.

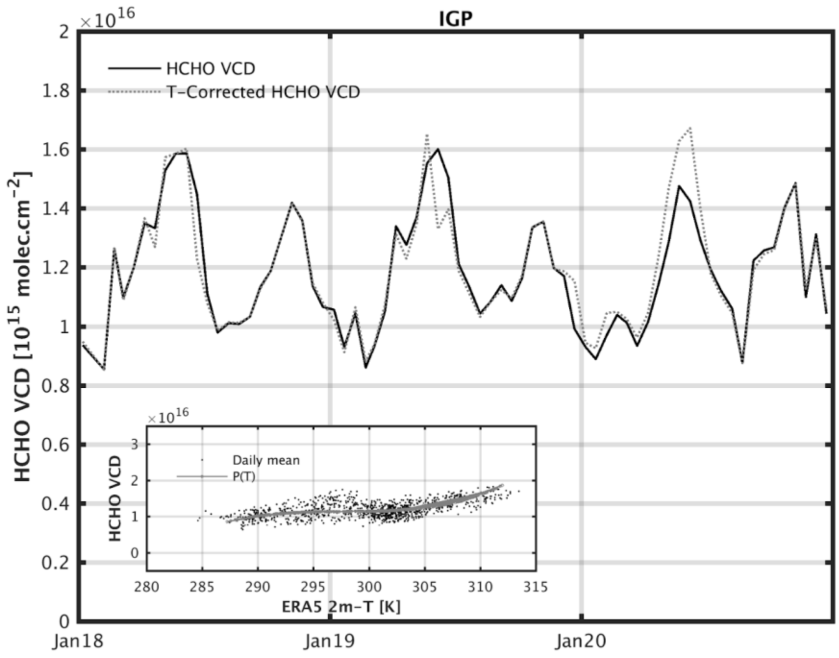

Figure 3.2.17: Example of temperature correction of the HCHO tropospheric columns in the Indogangetic Plain. The dashed line presents the HCHO columns after correction using climatological temperatures. The correlation between the local daily temperatures from ERA5 and the HCHO columns is shown inset.

Results

Figure 3.2.18 and Figure 3.2.19 present monthly maps of TROPOMI HCHO columns, respectively over Eastern China in February 2019 and 2020, and over Asia in April 2019 and 2020. On those maps, the most visible decrease is found over the Indo Gangetic plain in April.

Figure 3.2.20 shows the seasonal cycles for tropospheric HCHO column amounts of TROPOMI in Northern China and New Delhi, but also over Milan, Barcelona, Paris and New York. The different coloured curves show the bi-weekly medians of the daily mean tropospheric columns. OMI data sets allow for comparison of TROPOMI observations to a climatological seasonal cycle built using OMI data from 2010 to 2018, as indicated by the black dashed curves. The associated error bars represent the interannual variability as estimated from OMI. For each region or city, the corresponding surface temperature and precipitations are presented below the HCHO columns. For the Northern China and New-Delhi cases (first line), the "surface-temperature-corrected" HCHO columns are also shown.

For Northern China, the temperatures and the amount of precipitation in February were close to normal values. The interannual variability as estimated from the OMI data sets is estimated to be in the range of $1.2x10^{15}$ molec.cm^{-2} (~12%). However, a minimum is visible in late February 2020, with columns significantly lower than 2019 and lower than the OMI climatology (about -40%). The differences are also larger than what can be explained by the typical interannual variability.
In India, the temperatures in April and May 2020 were lower than average, and the precipitations were heavier. During the first part of April (coinciding with the phase 1 lockdown), a reduction in HCHO column concentrations is observed for the IGP and is even more pronounced over New Delhi (respectively -20% and -40 % compared to the OMI climatology). In both cases, the anomaly is larger than the interannual variations generally observed during this period. Neither a change in temperature nor the amount of precipitation can explain the observed column decrease during phase 1. In addition, the effect appears even more pronounced over New Delhi than in the IGP, which gives confidence in the anthropogenic nature of the reduction. During the second part of April and May, the temperature correction reduces strongly the observed reduction and prevent to attribute the observed diminution only to a decrease of the pollution levels.
The time series over Milan or Paris do not show a decrease in the HCHO columns during the lock down period. Only over Barcelona, a punctual decrease is observed during the second part of April and might be related to the lockdown, although the same effect is not observed in Madrid and is difficult to explain. Over New York, a decrease seems to be observed in May 2020, and later in September, outside the peak due to biogenic emissions in summer time. But this decrease is within the interannual variability.

In Table 5, we provide the annual averages of the HCHO columns, corrected for the surface temperature variation, for certain cities or regions. New York and San Francisco present a significant decrease of the annual concentrations (more than 10%), despite the strong fire emissions in August/September 2020. This is particular to the US cities. In China or India, the decrease was of short duration and did not significantly impact the annual levels, while in Europe or South America, no decrease can be detected on the short or on the long term.

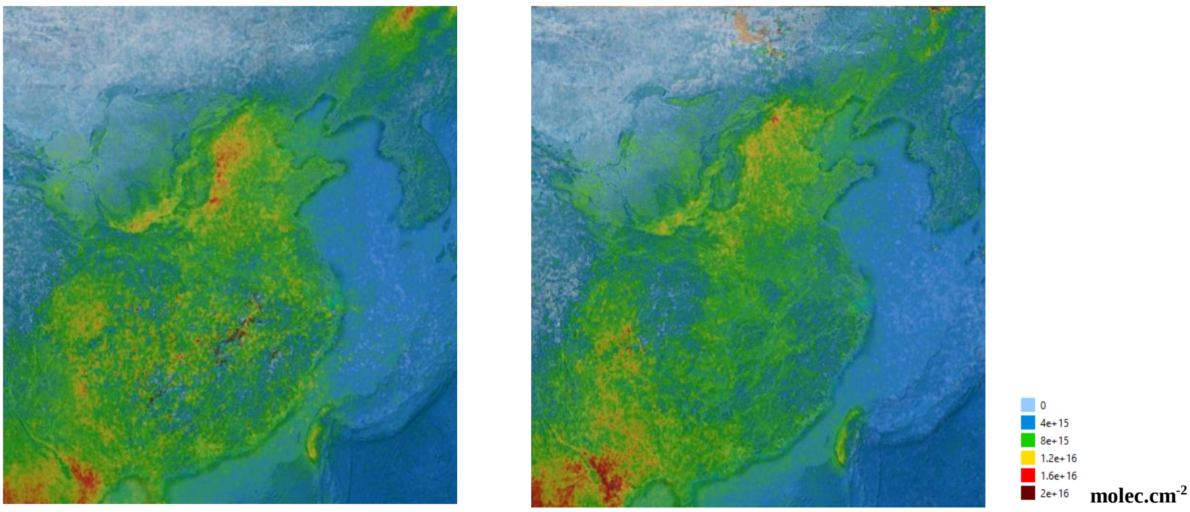

Figure 3.2.18: TROPOMI HCHO tropospheric columns averaged over Eastern China in Feb. 2019 and Feb. 2020.

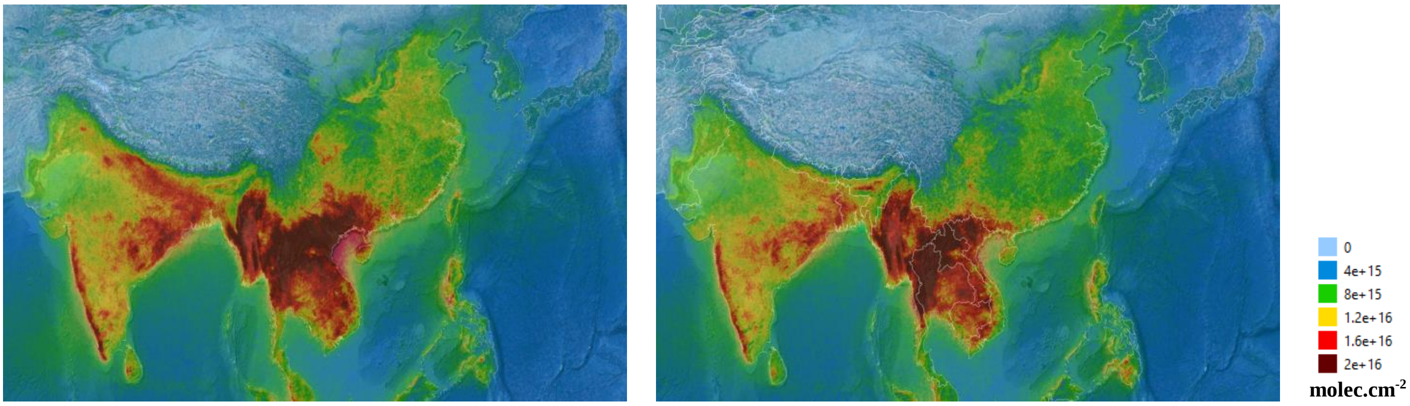

Figure 3.2.19: TROPOMI HCHO tropospheric columns averaged over Asia in Apr. 2019 and Apr. 2020.

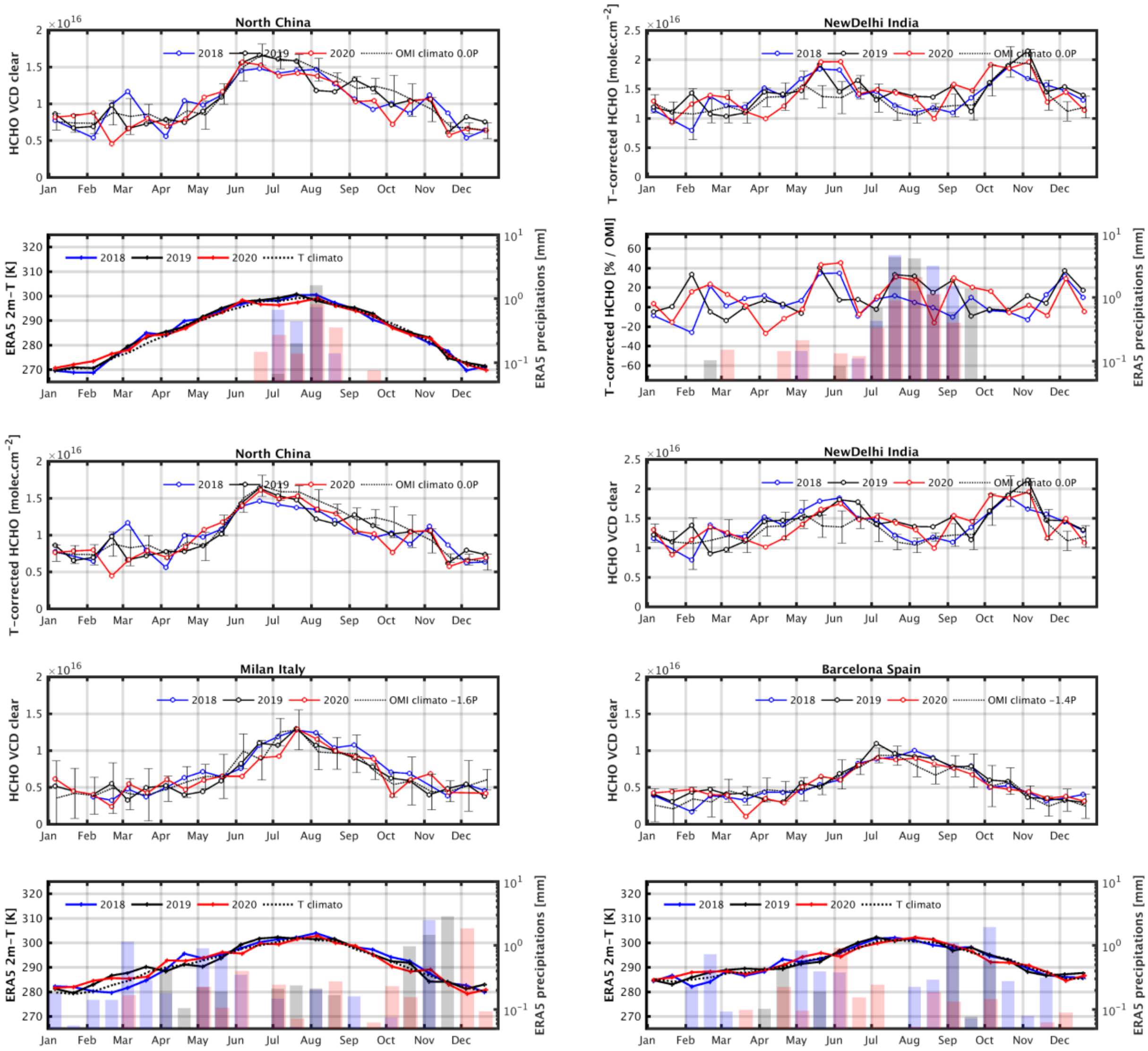

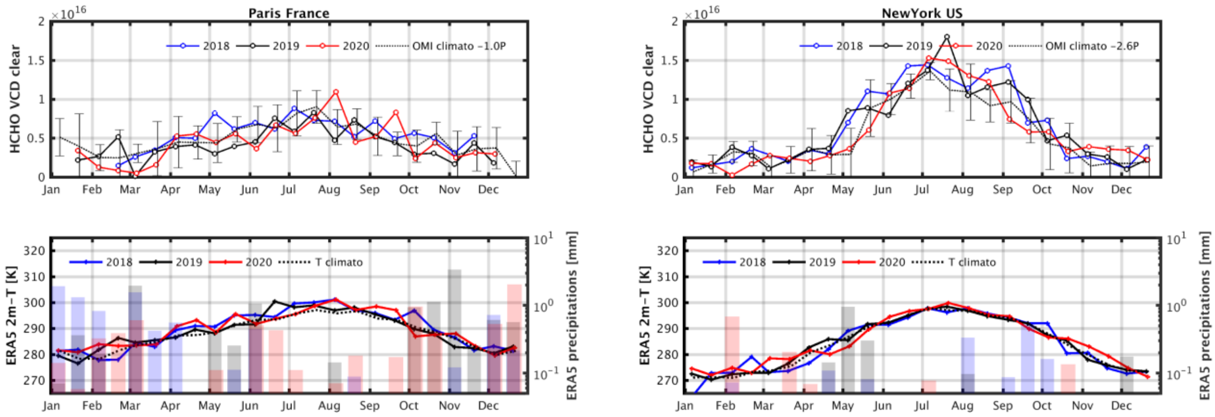

Figure 3.2.20: Biweekly averaged of HCHO tropospheric columns as retrieved from TROPOMI in 2018 (blue), 2019 (black) and 2020 (red) in a selection of cities or regions. For each region, the corresponding diagram of surface temperature and precipitations is presented (lower plot). For the Northern China and New-Delhi cases (first line), the "surface-temperature-corrected" HCHO columns are also shown. In all figures, the OMI climatology is shown (dashed black line), and the error bars represent the interannual variability.

Table 5: Annually averaged "surface-temperature-corrected" HCHO tropospheric columns as retrieved from TROPOMI in 2018, 2019 and 2020 in a selection of cities or regions.

Annual Mean HCHO [x10^{15} molec.cm^{-2}]	**2018**	**2019**	**2020**
New Delhi	13.9	14.4	14
North China	9.9	10.0	9.3
Center East China	9.5	9.6	9.1
South China	9.5	10.0	10.1
Roma	4.6	4.4	4.8
Milan	6.1	5.5	5.7
Barcelona	4.4	5.2	4.4
Madrid	4.4	4.2	3.4
Paris	4.9	4.0	4.0
New York	4.2	4.1	3.7
San Francisco	5.2	4.9	4.3
Buenos Aires	5.7	6.2	6.1
Sao Paulo	8.8	9.2	9.4

3.2.3.2 CHOCHO

This analysis relies on the S5p TROPOMI glyoxal tropospheric column product that is being developed as part of the GLYRETRO project within the S5p+Innovation program (primary activity of this contract). Details on the algorithm and validation results are available in the GLYRETRO ATBD (Lerot et al., 2020) and Verification Report (Alvarado et al., 2020), available on the project website (https://glyretro.aeronomie.be/) and are also comprehensively described in Lerot et al. (2021). The methodology to search for possible lockdown signature is similar to that of HCHO, except that a temperature correction is not applicable to glyoxal since the glyoxal column/temperature correlation is weaker due to higher yields from other type of emissions than biogenic sources. We focused on the highly polluted area of China and Northern India where the glyoxal columns are large and originate to a significant part from anthropogenic sources.

Figure 3.2.21 compares the monthly mean glyoxal fields from 2019 and 2020 in China and India during their respective strictest lockdown phases (i.e. February and April). A clear low bias is visible in those two countries in 2020 compared to 2019. In India, localized elevated glyoxal signals are also much less visible during the local lockdown. In February 2019, southern part of China has been poorly sampled from space because of persistent cloud contamination. For this reason, we restrain the analysis to the Northern part of China.

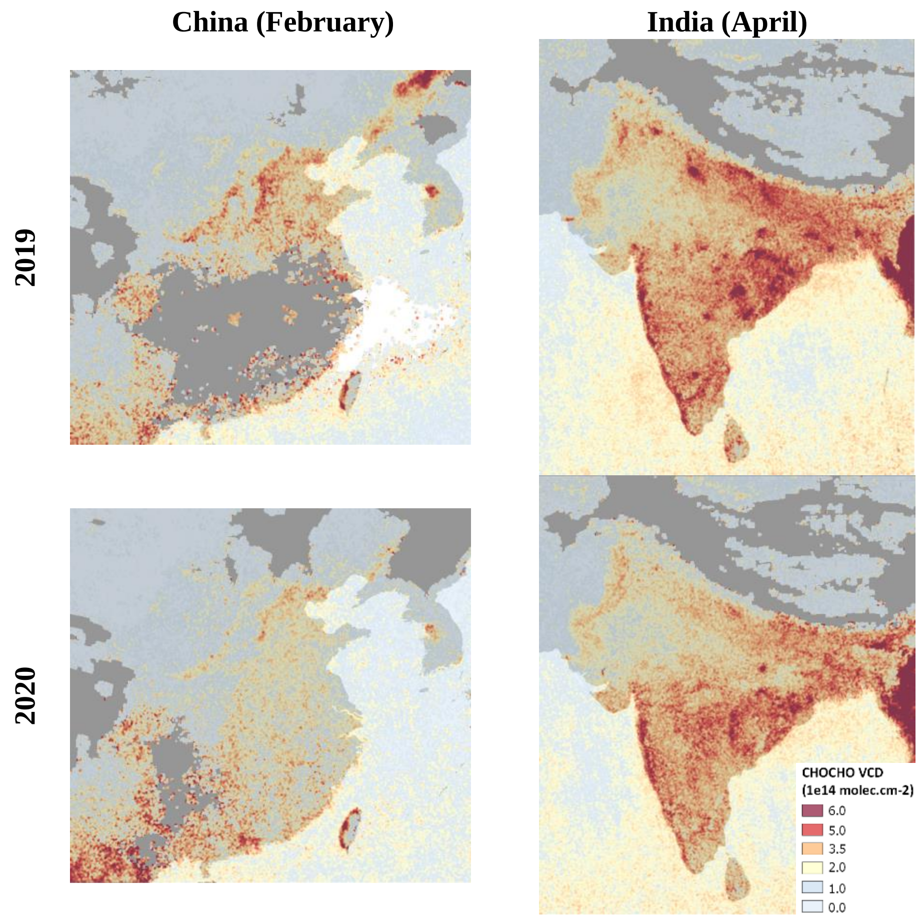

Figure 3.2.21: Comparison of the 2019 and 2020 monthly mean TROPOMI CHOCHO tropospheric columns over Eastern China and India for the months of February and April, respectively.

Figure 3.2.22 and Figure 3.2.23compare the time series of biweekly medians of TROPOMI glyoxal columns in Northern China and Northern India for 2018, 2019 and 2020 separately. For comparison, OMI climatological columns based on the years 2010-2018 are also drawn along with estimates of the corresponding interannual variability. In China, the CHOCHO interannual variability is estimated to be in the range of $1x10^{14}$ molec.cm^{-2} (~30%). A clear minimum is visible in the CHOCHO 2020 time series in late February, with columns significantly lower than 2018 and 2019 (~-50%). The discussion on meteorological parameters from section 3.2.3.1 is also valid for glyoxal, and no change in those parameters can explain the low bias in late February. Note that a small reduction of the column amounts starts already in late January but similar reductions are observed in other years in phase with the yearly Chinese New Year holidays during which anthropogenic emissions also drop. Interestingly while the columns usually rebound shortly after the holidays, they further decrease this year. Note however that compared to the OMI climatology, the differences are smaller and within the 2010-2018 inter-annual variability. Drawing firm conclusions based on the glyoxal observations alone is therefore difficult. On the other hand, since reductions are also identified for other species during the same period and are also reproduced for glyoxal by model simulations based on a COVID-19-optimized inventory (see section 3.2.3.3), their lockdown-related origin is very likely.

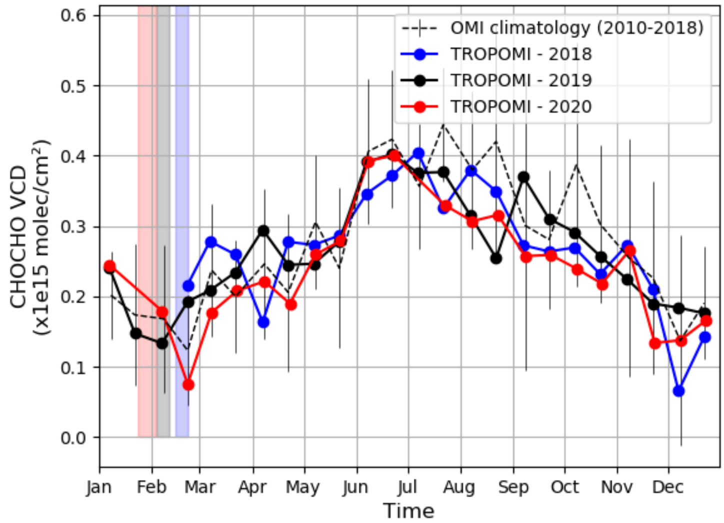

Figure 3.2.22: Biweekly mean CHOCHO tropospheric columns as retrieved from TROPOMI in 2018 (blue), 2019 (black) and 2020 (red) in Northeastern China. The dashed black curve shows climatological glyoxal columns as derived from the OMI data set using the period 2010-2018. The error bars give an estimate of the inter-annual variability (1-sigma standard deviation). The colored rectangles indicate the yearly Chinese New Year holidays, during which anthropogenic emissions typically drop.

In the Indo-Gangetic Plains, glyoxal columns show a clear COVID-19 signal in late March/early April, which can't be explained by change in temperature or precipitation. Note the temperatures have been lower in 2020 compared to 2019, but only from the second part of April. In addition, the number of fires has been lower in May 2020, which can explain partly the persistent low bias in the 2020 glyoxal columns. The reduction of CHOCHO during the lockdown period over the IGP is slightly larger than the $1x10^{14}$ molec.cm^{-2} [or -25%] interannual variability as determined from the OMI CHOCHO climatology. When we zoom in over New Delhi (within a radius of 50km), the detected low bias is even more pronounced (-50%) and 2020/2019 differences are clearly larger than the interannual variability there, which gives confidence in the anthropogenic nature of the reduction.

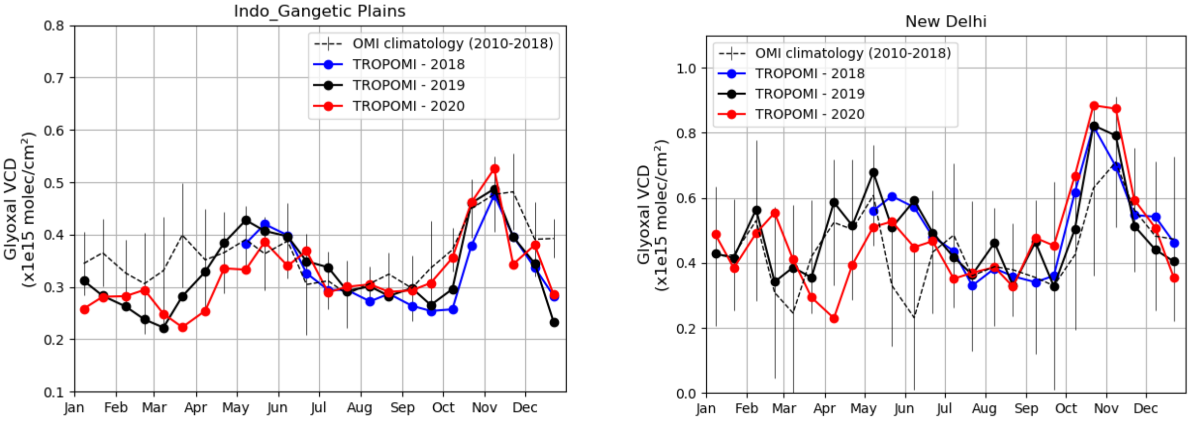

Figure 3.2.23: Biweekly mean CHOCHO tropospheric columns as retrieved from TROPOMI in 2018 (blue), 2019 (black) and 2020 (red) in the Indo-Gangetic Plains (left panel) and over New Delhi (right panel). The dashed black curve shows climatological glyoxal columns as derived from the OMI data set using the period 2010-2018. The error bars give an estimate of the inter-annual variability (1-sigma standard deviation).

3.2.3.3 Comparison with VOC changes over China simulated with the CTM MAGRITTEv1.1

Here we use satellite observations of HCHO, CHOCHO, and peroxyacetyl nitrate (PAN) in February 2019 and 2020 and analyze their distributions against model simulations. The first two compounds are measured by TROPOMI, while PAN is retrieved from the observations of the Infrared Atmospheric Sounding Interferometer (IASI, Clerbaux et al., 2009), carried on the Metop platforms.

In contrast to NO_x, which have strong direct emissions, HCHO, CHOCHO and PAN are predominantly secondary in origin. In Northern China, their wintertime columns are lower than in summer, due to reduced photochemical activity and biogenic NMVOC emissions (Fischer et al., 2014; Stavrakou et al., 2016; Franco et al., 2018; Li et al., 2018). This explains the noisier and more uncertain columns in winter. Despite these limitations, a good agreement between observed and model distributions of the 2020-to-2019 column ratios is found in February Figure 3.2.24).

The observed HCHO and CHOCHO ratio distributions are similar, with values lower than 1 in central-eastern China (between ~28° and 38°N), and values higher than 1 in the southern part (<25°N) as well as in northern China (between 40° and 43°N). This latitudinal gradient is reproduced by the model, with lower-than-one values, largely due to the drop in anthropogenic VOC emissions between 2020 and 2019, by 25% on average in eastern China, and by 33% in the YRD region. The stronger column reduction for CHOCHO than for HCHO is explained by the larger contribution of anthropogenic sources to the CHOCHO budget.

Due to secondary formation, both HCHO and CHOCHO are observed away from the emission source, a pattern well represented in the model (Figure 3.2.24). The higher biomass burning emission in 2020 over Myanmar (18-23°N, 96-102°E, Figure 3.1.10c) leads to HCHO and CHOCHO model columns enhanced by 12% and 23%, respectively, in fair agreement with the observed enhancement (15% for HCHO and 34% for CHOCHO). However, the data suggest an underestimation of biomass burning emissions over northern Vietnam, as well as an underestimation of CHOCHO formation in agricultural fires, which are a commonplace practice in this region for clearing the fields after harvesting (Biswas et al., 2015). In eastern China (Figure 3.1.13), the use of the CONFORM emissions in R1 leads to a decrease of 7% and to 18% in HCHO and CHOCHO column ratio, respectively, in comparison with the R2 experiment using baseline emissions for 2020. The stronger impact of emission reduction on CHOCHO than on HCHO is due to the larger contribution of anthropogenic VOCs to the abundance of CHOCHO (25% at global scale) compared to HCHO (7%).

PAN is formed by oxidation of non-methane volatile organic compounds (NMVOCs) in the presence of NOx. Since most NMVOCs can be PAN precursors, a diversity of NMVOC emissions sources are responsible for PAN formation. In Northern China, the anthropogenic sources are dominant outside the growing season. Note that modelling PAN chemistry is challenging since the formation of PAN implicates many stages of NMVOC oxidation and the yields can be very different from one NMVOC to another (Fischer, 2014).

Similar to HCHO and CHOCHO, the observations of the PAN column ratios show a pronounced north-south gradient, which is qualitatively well represented in the model (Figure 3.2.24), although the observed changes are larger (

Table 6). In consistency with the model, the largest decrease is found in the NCP, in response to the anthropogenic emission decreases. The higher column ratios in southern China might be due to a combination of higher biomass burning over Myanmar and higher isoprene emission fluxes over South-eastern China in 2020 (Figure 3.1.10d). Isoprene is a major precursor of PAN, responsible for ~37% of its formation on the global scale (Fischer et al., 2014). While the enhanced fires in Myanmar result in higher modeled PAN columns in February 2020 in this region, their effect is not visible over the source region according to IASI, suggesting that fire events might actually play little role in the PAN formation (Fischer et al., 2014).

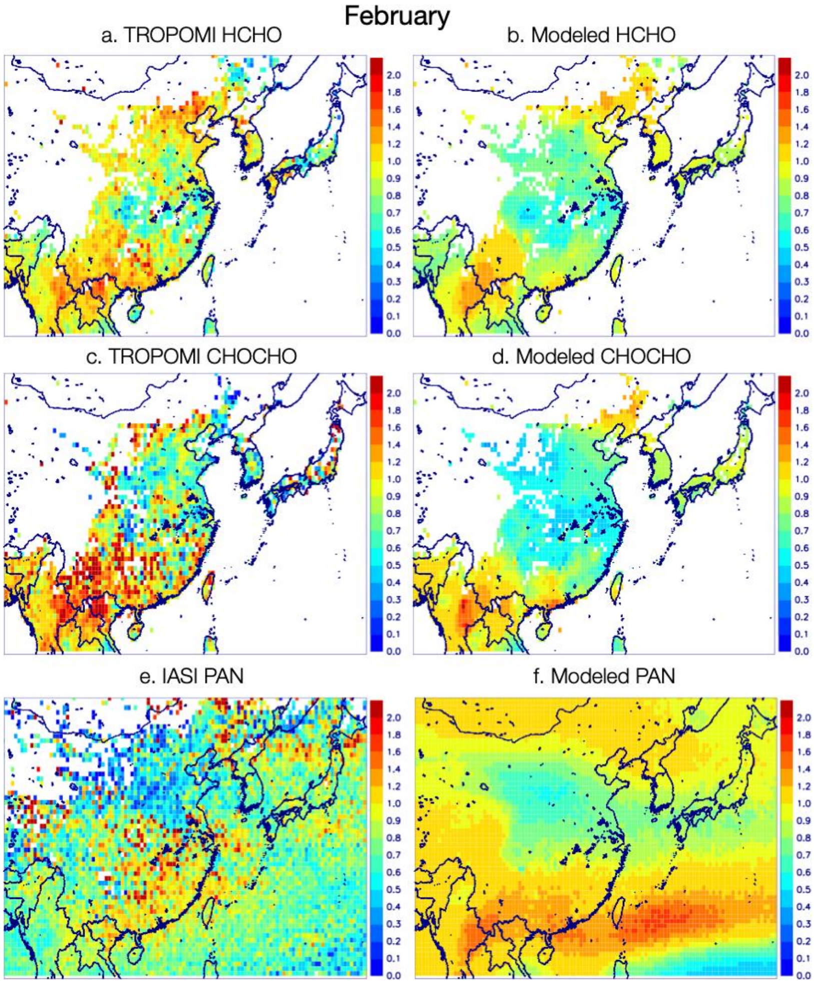

Figure 3.2.24: (a, b) HCHO column ratio, February 2020 divided by February 2019, according to satellite data (left) and to MAGRITTEv1.1 (right). (c, d) Idem for CHOCHO. (e, f) Idem for PAN. Invalid data and areas with very low VOC emissions (less than 5×10^{10} molec.cm^{-2}s^{-1}) are left blank in panels a-d.

Table 6: Percentage changes of monthly columns between 2020 and the same month in 2019 ((2020-2019)/2019), based on observed and modelled columns from simulations R1 (CONFORM emissions), R1H and R1L (high and low CONFORM emissions), and R2 (baseline emissions). All values are calculated for the eastern China region shown in Figure 3.1.13delimited by 22-42°N, 108-125°E.

HCHO changes	TROPOMI	R1	R1H	R1L	R2
February	-6.9	-20.3	-18.2	-22.5	-13.2
CHOCHO changes	TROPOMI	R1	R1H	R1L	R2
February	-13.2	-33.6	-28.4	-38.7	-15.0
PAN changes	IASI	R1	R1H	R1L	R2
February	-17.9	-10.9	-7.0	-14.4	1.3

4 Impact of lockdown measures on climate gases

4.1 Carbon dioxide (CO_2) (IUP-Bremen)

The COVID-19 pandemic resulted in reduced anthropogenic carbon dioxide (CO_2) emissions during 2020 in large parts of the world. We report results from a first attempt to determine whether a regional-scale reduction of anthropogenic CO_2 emissions during the COVID-19 pandemic can be detected using space-based observations of atmospheric CO_2. For details the reader is referred to Buchwitz et al., 2021 (and references given therein), which is shortly summarized in this section.

For this purpose, we have analysed a small ensemble of satellite retrievals of column-averaged dry-air mole fractions of CO_2, i.e. XCO_2. We focus on East China because COVID-19 related CO_2 emission reductions are expected to be largest there early in the pandemic. We analysed four XCO_2 data products from the satellites Orbiting Carbon Observatory-2 (OCO-2) and Greenhouse gases Observing SATellite (GOSAT) (see Table 7).

We use a data-driven approach that does not rely on a priori information about CO_2 sources and sinks and ignores atmospheric transport. Our approach utilises the computation of XCO_2 anomalies, ΔXCO_2, from the satellite Level 2 data products using a method called DAM (Daily Anomalies via (latitude band) Medians) (Figure 4.1.1). DAM removes large-scale, daily XCO_2 background variations, yielding XCO_2 anomalies that correlate with the location of major CO_2 source regions such as East China.

We analysed satellite data between January 2015 and May 2020 and compared monthly XCO_2 anomalies in 2020 with corresponding monthly XCO_2 anomalies of previous years. In order to link the XCO_2 anomalies to East China fossil fuel (FF) emissions, we used XCO_2 and corresponding FF emissions from NOAA's (National Oceanic and Atmospheric Administration) CarbonTracker version CT2019 from 2015 to 2018. Using this CT2019 data set, we found that the relationship between target region ΔXCO_2 and the FF emissions of the target region is approximately linear and we quantified slope and offset via a linear fit.

We use the empirically obtained linear equation to compute ΔXCO_2^{FF}, an estimate of the target region FF emissions, from the satellite-derived XCO_2 anomalies, ΔXCO_2. We focus on October to May periods to minimize contributions from biospheric carbon fluxes and quantified the error of our FF estimation method for this period by applying it to CT2019. We found that the relative difference of the retrieved FF emissions and the CT2019 FF emissions is approximately 5% (1-sigma).

We applied our method to NASA's (National Aeronautics and Space Administration) OCO-2 XCO_2 data product (version 10r) and to three GOSAT products. We focus on estimates of the relative change of East China monthly emissions in 2020 relative to previous months.

Our results (Figure 4.1.2) show considerable month-to-month variability (especially for the GOSAT products) and significant differences across the ensemble of satellite data products analysed. The ensemble mean indicates an emission reduction by approximately 10% ± 10% in March and April 2020. However, our results show considerable month-to-month variability and significant differences across the ensemble of satellite data products analysed. For example, OCO-2 suggests a much smaller reduction (1%–2% ± 2 %).

The large uncertainty and the differences of the results obtained for the individual ensemble members indicates that it is challenging to reliably detect and to accurately quantify the emission reduction. There are several reasons for this including the weak signal (the expected regional XCO_2 reduction is only on the order of 0.1-0.2 ppm), the sparseness of the satellite data, remaining biases and limitations of our relatively simple data-driven analysis approach. Inferring COVID-19 related information on regional-scale CO_2 emissions using current satellite XCO_2 retrievals likely requires, if at all possible, a more sophisticated analysis method including detailed transport modelling and considering a priori information on anthropogenic and natural CO_2 surface fluxes.

Table 7: Overview of the satellite XCO_2 Level 2 (L2) input data products. (#) These products are available via the Copernicus Climate Data Store (CDS) until end of 2019. Year 2020 data will be made available via the CDS in 2021.

Satellite	Algorithm	Product version	Product ID	References	Data provider and data access information
OCO-2	ACOS	v10r	CO_2_OC2_ACOS	O'Dell et al., 2018; Kiel et al., 2019; Osterman et al., 2020	Product "OCO_2_L2_Lite_FP 10r" obtained from NASA's Earthdata GES DISC website: https://disc.gsfc.nasa.gov/datasets?keywords=OCO-2%20v10r&page=1
GOSAT	UoL-FP	v7.3	CO_2_GOS_OCFP	Cogan et al., 2012; Boesch et al., 2019	Generated by Univ. Leicester (#)
GOSAT	RemoTeC	v2.3.8	CO_2_GOS_SRFP	Butz et al., 2011; Wu et al., 2019	Generated by SRON (#)
GOSAT	FOCAL	v1.0	CO_2_GOS_FOCA	Noël et al., 2020	Generated by IUP, Univ. Bremen

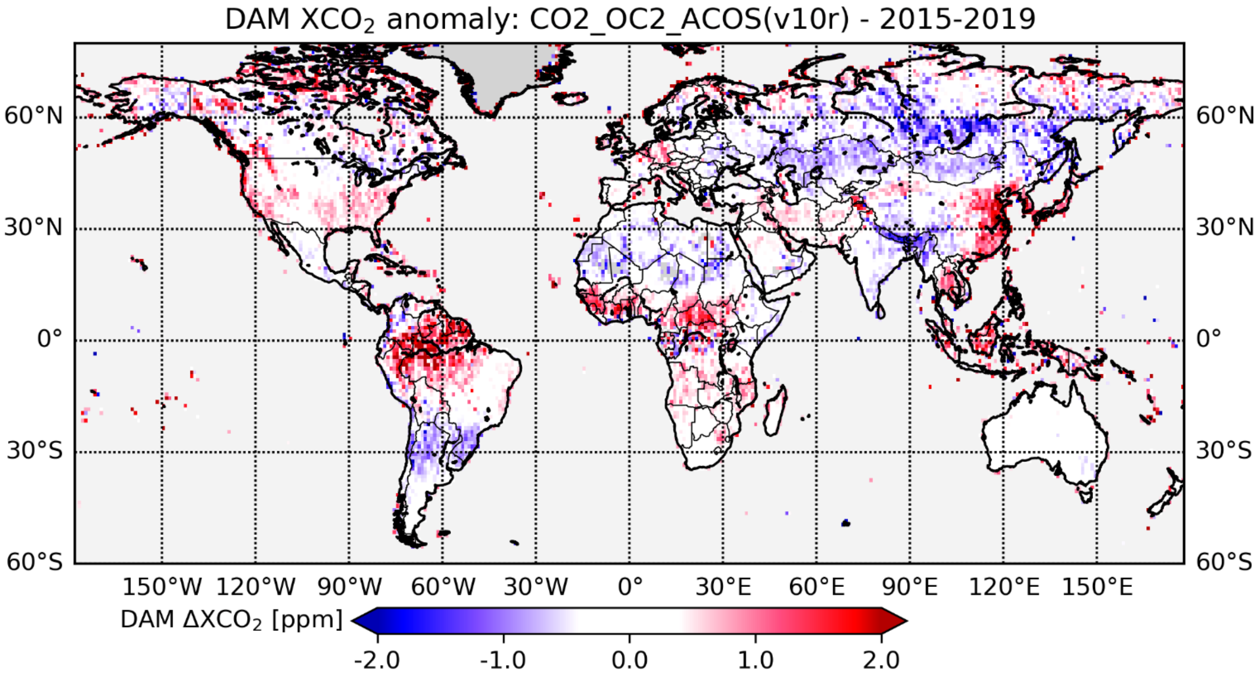

Figure 4.1.1: DAM XCO_2 anomaly map at 1° x 1° resolution generated from OCO-2 Level 2 XCO_2 (v10r, land) for 2015 to 2019.

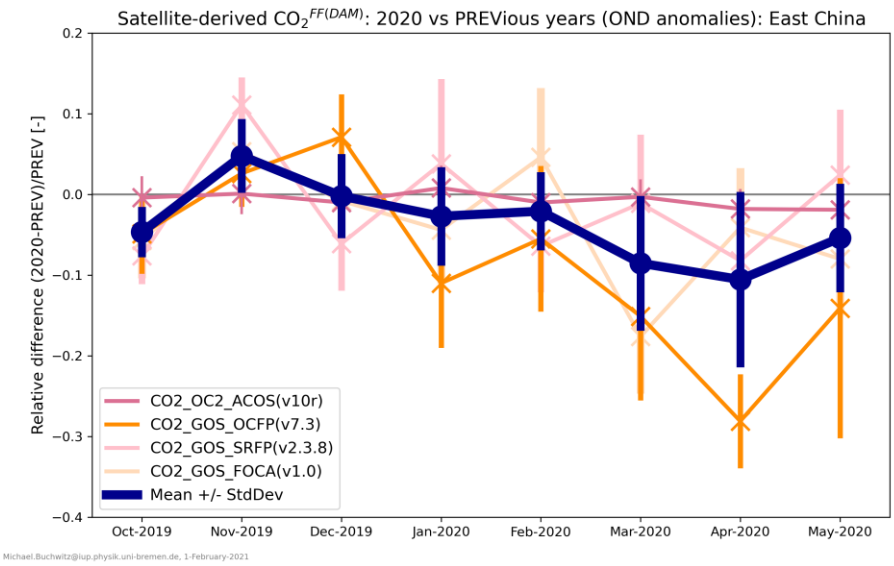

Figure 4.1.2: Overview of the ensemble-based CO_2 emission reduction results for January-May 2020 relative to October-December 2019 and previous years via reddish colours for each of the four analysed satellite XCO_2 data products (see Table 7). The corresponding ensemble mean value and its uncertainty is shown in dark blue. The uncertainty has been computed as standard deviation of the ensemble members.

4.2 Methane (CH_4) (IUP-Bremen)

In order to find out if potential changes in atmospheric methane during the pandemic can be detected from space we have analysed Sentinel-5-Precursor (S5P) scientific WFMD algorithm XCH_4 retrievals (Schneising et al., 2019, 2020b) during October 2017 to June 2020.

We focussed on regional-scales and generated XCH_4 maps (absolute XCH_4 and XCH_4 differences to the previous year) for South East Asia, Europe, and continental US (Figures 4.2.1-4). To better analyse the observed pattern we also performed an additional time series analysis for smaller source region (with substraction of background to remove seasonal cycle and global yearly increase) based on weekly data for different years. The time series analysis is performed for the following sub-regions: East China (Figure 4.2.1), Northern Italy (Figure 4.2.2), India (Figure 4.2.3) and the US East Coast (Figure 4.2.4). The source region of interest and the corresponding background region are highlighted in the respective figures.

The spatial maps of XCH_4 differences between COVID-19 and a pre-pandemic period typically show a complex pattern of year 2020 reductions and enhancements and the time series analysis indicates that the differences of 2020 and 2019 are within normal year-to-year variability for all analysed regions.

For example, in the case of the source region time series for East China, we find lower values (2020 relative to 2019) in the lockdown period before March (2018 is in between), but the reduction already starts before lockdown. For all regions the magnitude of differences during the lockdown period is comparable to differences in other periods, , e.g. in the case of the US East Coast source region, we find a reduction in 2020 relative to 2019 between March and May, which is also reflected in the spatial difference map (Figure 4.2.4), but there is a similar reduction between December and February, which cannot be linked to COVID-19 limitations.

It is therefore concluded that there is no unambiguous signature in XCH_4 during the COVID-19 lockdown in 2020 in the analysed regions.

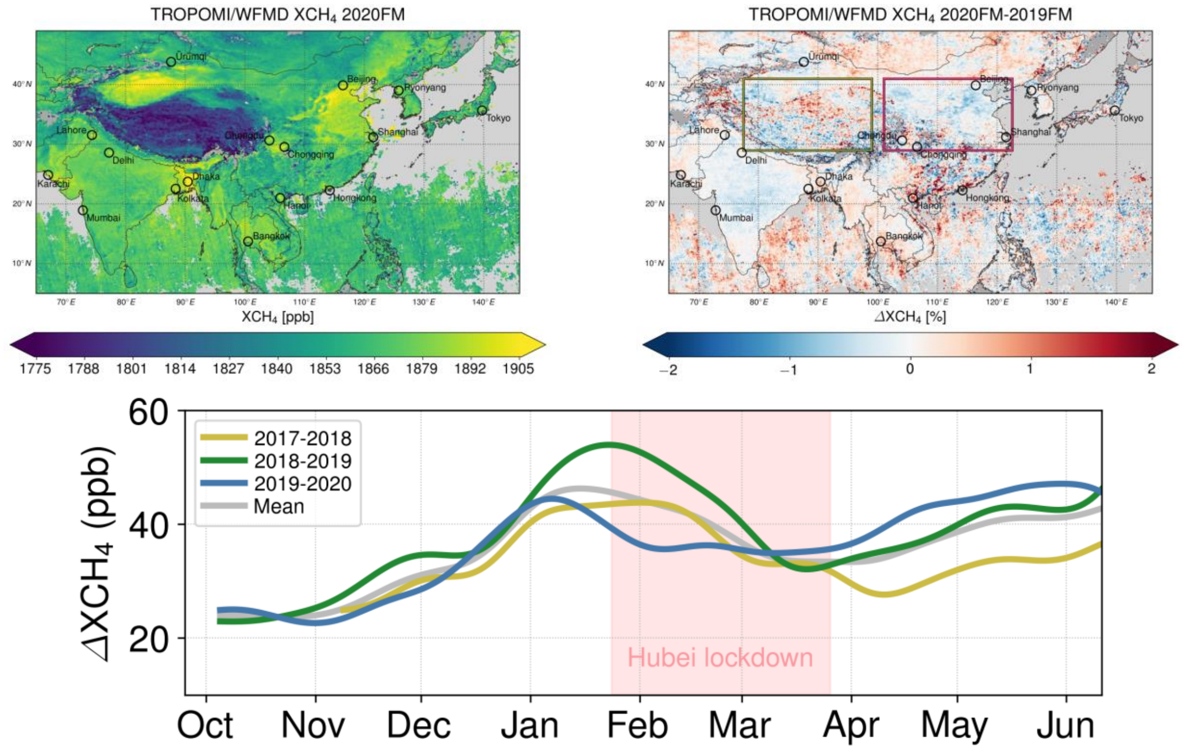

Figure 4.2.1: Top left: XCH_4 over China and surrounding countries for February/March 2020 (2020FM). Top right: XCH_4 difference 2020FM minus 2019FM. Also shows are two rectangular regions: the East China target (or source) region of interest (red) and the corresponding background region (green). Bottom: Time series (weekly resolution) of ΔXCH_4, which are target minus background (TmB) region differences of consecutive years. Also shown in light red is the Hubei lockdown period from end of January 2020 to end of March 2020. As can be seen from the blue curve, TmB ΔXCH_4 is lower in 2020 compared to 2019 in the lockdown period before March but the reduction starts already before the lockdown. Furthermore, the magnitude is similar to other periods. It is therefore concluded that the year 2020 to 2019 difference is within normal variability.

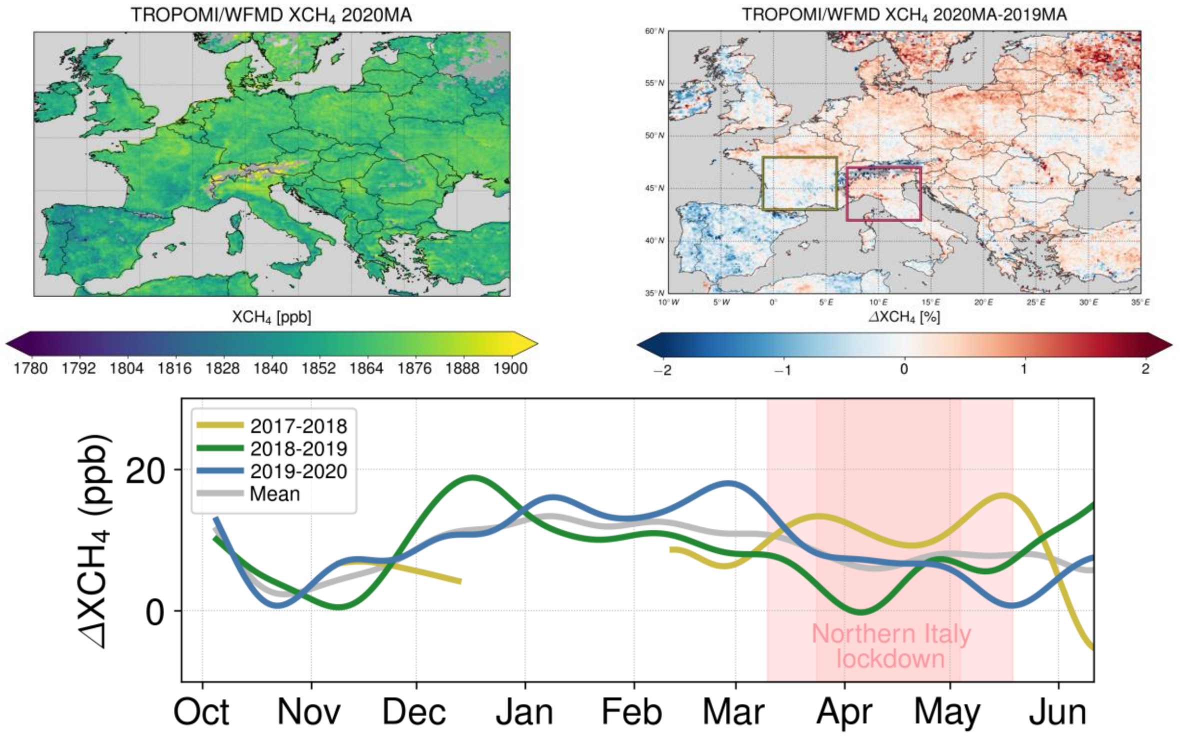

Figure 4.2.2: Similar as Figure 4.2.1 but for Europe and March/April maps focussing on Northern Italy for the time series analysis.

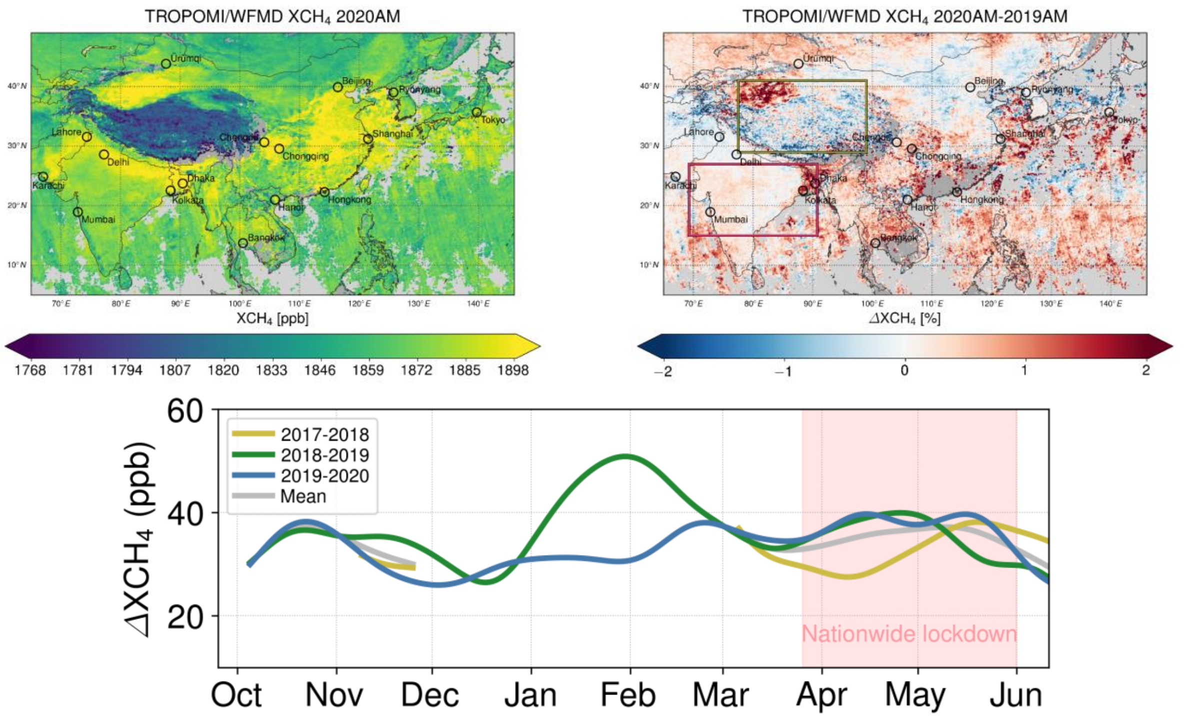

Figure 4.2.3: Similar as Figure 4.2.1 but for India and April/May maps focussing on Northern India for the time series analysis.

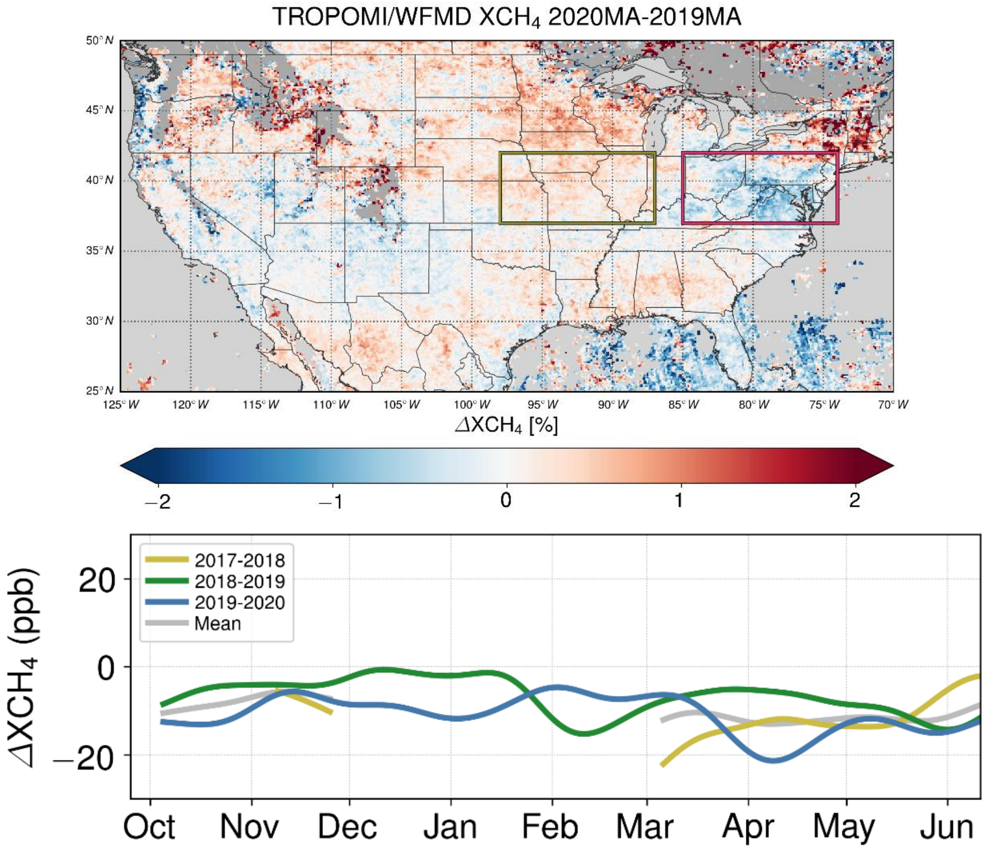

Figure 4.2.4: Similar as Figure 4.2.1 but for the US and a March/April difference map focussing on parts of the US East Coast for the time series analysis.

5 Dissemination and outreach

A large effort from the ICOVAC team has been devoted to contributing to outreach. A large number of interviews, web stories and press releases have been prepared by the consortium before and during the project. The various press releases led to many article in the international press (e.g. in Belgium, Italy, India) Those articles have been published in various international media, including:

- Physics Today (https://physicstoday.scitation.org/do/10.1063/PT.6.2.20200501a/full/).
- Tagesschau (https://www.tagesschau.de/investigativ/ndr/stickoxid-corona-101.html)
- Four BIRA-IASB press releases (https://aeronomie.be/en/news/2020/tropomi-observes-impact-corona-virus-air-quality-china, https://aeronomie.be/en/news/2020/corona-does-not-necessarily-imply-less-pollution, https://aeronomie.be/en/news/2020/satellites-see-worldwide-decrease-nitrogen-dioxide-pollution-result-covid-19-crisis-china, https://aeronomie.be/en/news/2020/covid-19-air-pollution-returns-lockdowns-are-lifted)
- AGU press release (https://news.agu.org/press-release/covid-19-lockdowns-significantly-impacting-global-air-quality/)
- ESA eo4society press release (https://eo4society.esa.int/2020/05/14/is-the-global-covid-19-related-drop-in-NO_2-pollution-coming-to-an-end/)

- ESA web story (ESA web story https://www.esa.int/Applications/Observing_the_Earth/Copernicus/Sentinel-5P/Sulphur_dioxide_concentrations_drop_over_India_during_COVID-19)
- Nature News: Why pollution is plummeting in some cities — but not others, https://www.nature.com/articles/d41586-020-01049-6
- Dutch news items, e.g. https://nos.nl/artikel/2328537-lucht-flink-schoner-door-coronamaatregelen.html; https://www.nemokennislink.nl/publicaties/corona-klaart-de-lucht/
- KNMI web stories: https://www.knmi.nl/kennis-en-datacentrum/achtergrond/afname-luchtvervuiling-tijdens-coronacrisis; https://www.knmi.nl/over-het-knmi/nieuws/afname-luchtvervuiling-boven-nederland; https://www.knmi.nl/kennis-en-datacentrum/uitleg/tropomi-metingen-van-stikstofdioxide-NO_2 ; https://www.knmi.nl/over-het-knmi/nieuws/toename-luchtvervuiling-na-opheffen-lockdown
- “Dados de satélite apontam piora da poluição em SP em período de menor isolamento“, https://g1.globo.com/bemestar/coronavirus/noticia/2020/04/30/dados-de-satelite-apontam-piora-da-poluicao-em-sp-em-periodo-de-menor-isolamento.ghtml
- ESA web story: “Global air pollution maps now available”, https://www.esa.int/ESA_Multimedia/Images/2020/06/Global_air_pollution_maps_now_available#.XuIOZllucSw.link
- ESA Web story: “Air pollution in a post-COVID-19 world” https://www.esa.int/Applications/Observing_the_Earth/Copernicus/Sentinel-5P/Air_pollution_in_a_post-COVID-19_world
- Popular science web story at Scientias.nl (in Dutch): “Minder luchtvervuiling na de Coronacrisis, maar voor hoelang nog?”, https://www.scientias.nl/minder-luchtvervuiling-na-de-coronacrisis-maar-voor-hoelang-nog/
- Daily Science, La qualité de l’air, impactée pas la crise du COVID-19 (https://dailyscience.be/11/05/2020/la-qualite-de-lair-impactee-par-la-crise-du-covid-19-2)
- Medical News Today, The dual effects of COVID-19 lockdown on air quality (https://www.medicalnewstoday.com/articles/the-dual-effects-of-covid-19-lockdowns-on-air-quality)
- Science News, Emissions dropped during the COVID-19 pandemic. The climate impact won’t last (https://www.sciencenews.org/article/covid-19-coronavirus-greenhouse-gas-emissions-climate-change)
- Green Report, Con il lockdown da COVID-19 calo ‘senza precedente’ per l’inquinamento del mondo (https://www.greenreport.it/news/economia-ecologica/con-il-lockdown-da-covid-19-calo-senza-precedenti-per-linquinamento-nel-mondo)
- BBC Science Studios, T. Stavrakou interviewed by Greta Thunberg about the effects of COVID-19 on air quality in the frame of a BBC One docuseries ‘Greta Thunberg : A Year to Change the World’ (broadcast in May in US/UK, in June/July in Belgium).
- Several members of the consortium contributed to the preparation of a MOOC module on the impact of the COVID-19 lockdowns on the air quality and climate produced by Imperative Space.

The study activities realized so far are summarized in the following peer-reviewed papers published or in preparation:

Published articles:

- Bauwens, M., Compernolle, S., Stavrakou, T., Müller, J. -F., Gent, J., Eskes, H., Levelt, P. F., A, R., Veefkind, J. P., Vlietinck, J., Yu, H. and Zehner, C.: Impact of Coronavirus Outbreak on NO_2 Pollution Assessed Using TROPOMI and OMI Observations, Geophys. Res. Lett., 47(11), doi:10.1029/2020GL087978, 2020.
- Buchwitz, M., Reuter, M., Noël, S., Bramstedt, K., Schneising, O., Hilker, M., Fuentes Andrade, B., Bovensmann, H., Burrows, J. P., Di Noia, A., Boesch, H., Wu, L., Landgraf, J., Aben, I., Retscher, C., O'Dell, C. W., and Crisp, D.: Can a regional-scale reduction of atmospheric CO_2 during the COVID-19 pandemic be detected from space? A case study for East China using satellite XCO_2 retrievals, Atmos. Meas. Tech., 14, 2141–2166, https://doi.org/10.5194/amt-14-2141-2021, 2021.
- J. Ding, R.J. van der A, H.J. Eskes, B. Mijling, T. Stavrakou, J.H.G.M. van Geffen, J.P. Veefkind, Chinese NO_x emission reductions and rebound as a result of the COVID-19 crisis quantified through inversion of TROPOMI NO_2 observations, Geophysical Research Letters, 46, e2020GL089912, doi:10/1029/2020GL089912, 2020.
- Gaubert, B., Bouarar, I., Doumbia, T., Liu, Y., Stavrakou, T., Deroubaix, A., et al., Global changes in secondary atmospheric pollutants during the 2020 COVID-19 pandemic. Journal of Geophysical Research: Atmospheres, 126, e2020JD034213, https://doi.org/10.1029/2020JD034213, 2021.
- Gkatzelis, G.I., Gilman, J.B., Brown, S.S., Eskes, H., Gomes, A.R., Lange, A.C., McDonald, B.C., Peischl, J., Petzold, A., Thompson, C.R., Kiendler-Scharr, A. 2021. The global impacts of COVID-19 lockdowns on urban air quality: A critical review and recommendations. Elementa: Science of the Anthropocene 9(1). DOI: https://doi.org/10.1525/elementa.2021.00176
- Griffin, D., McLinden, C. A., Racine, J., Moran, M. D., Fioletov, V., Pavlovic, R., Mashayekhi, R., Zhao, X. and Eskes, H.: Assessing the Impact of Corona-Virus-19 on Nitrogen Dioxide Levels over Southern Ontario, Canada, Remote Sens., 12(24), 4112, doi:10.3390/rs12244112, 2020.
- Koukouli, M.-E., Skoulidou, I., Karavias, A., Parcharidis, I., Balis, D., Manders, A., Segers, A., Eskes, H. and van Geffen, J.: Sudden changes in nitrogen dioxide emissions over Greece due to lockdown after the outbreak of COVID-19, Atmos. Chem. Phys., 21(3), 1759–1774, doi:10.5194/acp-21-1759-2021, 2021.
- Liu, F., Page, A., Strode, S. A., Yoshida, Y., Choi, S., Zheng, B., Lamsal, L. N., Li, C., Krotkov, N. A., Eskes, H., van der A, R., Veefkind, P., Levelt, P. F., Hauser, O. P. and Joiner, J.: Abrupt decline in tropospheric nitrogen dioxide over China after the outbreak of COVID-19, Sci. Adv., 6(28), eabc2992, doi:10.1126/sciadv.abc2992, 2020.
- Liu, Y., Wang, T., Stavrakou, T., Elguindi, N., Doumbia, T., Granier, C., Bouarar, I., Gaubert, B. and Brasseur, G. P.: Diverse response of surface ozone to COVID-19 lockdown in China, Sci. Total Environ., 147739, doi:10.1016/j.scitotenv.2021.147739, 2021.
- Miyazaki, K., Bowman, K., Sekiya, T., Jiang, Z., Chen, X., Eskes, H., et al. (2020). Air quality response in China linked to the 2019 novel coronavirus (COVID-19) lockdown. Geophysical Research Letters, 47, e2020GL089252. https://doi.org/10.1029/2020GL089252.
- Miyazaki, Kazuyuki, Kevin Bowman, Takashi Sekiya, Masayuki Takigawa, Jessica L. Neu, Kengo Sudo, Greg Osterman, Henk Eskes, Global tropospheric ozone responses to reduced NOx emissions linked to the COVID-19 world-wide lockdowns, Accepted for publication in Science Advances, April 2021.
- Stavrakou, J. and Bauwens, M.: What can COVID-19 shutdowns teach us about reducing air pollution**?,** Research Outreach, 121, https://doi.org/10.32907/RO-121-1140323852, 2021.
- Wang, W., van der A, R., Ding, J., van Weele, M., and Cheng, T.: Spatial and temporal changes of the ozone sensitivity in China based on satellite and ground-

based observations, Atmos. Chem. Phys., 21, 7253–7269, https://doi.org/10.5194/acp-21-7253-2021, 2021.

- Bo Zheng, Guannan Geng, Philippe Ciais, Steven J. Davis, Randall V. Martin, Jun Meng, Nana Wu, Frederic Chevallier, Gregoire Broquet, Folkert Boersma, Ronald van der A, Jintai Lin, Dabo Guan, Yu Lei, Kebin He, Qiang Zhang, Satellite-based estimates of decline and rebound in China's CO_2 emissions during COVID-19 pandemic, Sci. Adv. 2020, Vol. 6, no. 49, DOI: 10.1126/sciadv.abd4998

Articles in preparation or in review:

- Bouarar, I., B. Gaubert, G. P. Brasseur, W. Steinbrecht, T. Doumbia, S. Tilmes, Y. Liu, T. Stavrakou, A. M. Deroubaix, S. Darras, C. Granier, F. G. Lacey, J.-F. Müller, X. Shi, N. Elguindi, and T. Wang: Ozone Anomalies in the Free Troposphere during the COVID-19 Pandemic, ***Geophys. Res. Lett.*,** in review.
- Doumbia, T., C. Granier, N. Elguindi, I. Bouarar, S. Darras, G. Brasseur, B. Gaubert, Y. Liu, X. Shi, T. Stavrakou, S. Tilmes, F. Lacey, A. Deroubaix, and T. Wang: Changes in global air pollutant emissions during the Covid-19 pandemic: a dataset for atmospheric chemistry modelling, Earth Syst. Sci. Data Discuss.**,** https://doi.org/10.5194/essd-2020-348, in review, 2021.
- Levelt, P.F., Deborah C. Stein Zweers, Ilse Aben, Maite Bauwens, Tobias Borsdorff, Isabelle De Smedt, Henk J. Eskes, Christophe Lerot, Diego G. Loyola, Fabian Romahn, Trissevgeni Stavrakou, Nicolas Theys, Michel Van Roozendael, J. Pepijn Veefkind, Tijl Verhoelst, Air Quality Impacts of COVID-19 Lockdown Measures using high-resolution observations of multiple trace gases from S5P/TROPOMI, to be submitted.
- Lange, K., Richter, A., and Burrows, J. P.: Variability of nitrogen oxide emission fluxes and lifetimes estimated from Sentinel-5P TROPOMI observations, Atmos. Chem. Phys. Discuss. [preprint], https://doi.org/10.5194/acp-2021-273, in review, 2021.
- Stavrakou, T., J.-F. Müller, M. Bauwens, T. Doumbia, N. Elguindi, S. Darras, C. Granier, I. De Smedt, C. Lerot, B. Franco et al.: Atmospheric Impacts of COVID-19 on NO_x and VOC levels over China based on TROPOMI and IASI satellite data and modeling, submitted.

Project activities and findings have also been communicated at conferences and meetings:

- Buchwitz M. et al.: Can a COVID-19 related regional-scale CO_2 emission reduction be detected from space using satellite XCO_2 retrievals?: A case study for East China, AGU Fall Meeting 2020.
- Ding J. et al.: COVID-effects on China NOx emissions OMI/TROPOMI workshop 2020.
- Ding J. et al.: NOx Emissions Reduction and Rebound in China Due to the COVID-19 Crisis, IGAC/AMIGO workshop: Changes in Atmospheric Composition During the COVID-19 Lockdowns, 3 November 2020.
- Eskes H. et al.: TROPOMI NO_2 Algorithm Overview & updates, OMI/TROPOMI workshop 2020.
- Eskes H. et al.: The Impacts of COVID-19 Lockdowns on NO_2 as Measured by Sentinel-5P TROPOMI: impacts of Weather and Implications for Emissions and Chemistry, AGU Fall Meeting 2020.
- Eskes H. et al.: The Impacts of COVID-19 Lockdowns on NO_2 as Measured by Sentinel-5P TROPOMI, AMS, 11-15 January 2021.

- Eskes, H., Levelt, P., Stein, D., DeSmedt, I., Aben, I., van Roozendael, M., Stavrakou, J., Bauwens, M., Lerot, C., Veefkind, P., Borsdorff, T., Verhoelst, T., Loyola, D., and Romahn, F.: Air Quality Impacts of COVID-19 Lockdown Measures using high-resolution observations of multiple trace gases from S5P/TROPOMI, EGU General Assembly 2021, online, 19–30 Apr 2021, EGU21-13216, https://doi.org/10.5194/egusphere-egu21-13216, 2021.
- Eskes, H., P. Veefkind, J. van Geffen, B. Mijling, R. van der A, J. Ding, P. Levelt, K. Miyazaki, C. Lerot, Reductions of NO_2 Air Pollution during Covid-19 lockdowns, as Observed by Sentinel-5P TROPOMI, GAW Symposium 2021, 28 June - 2 July.
- Lange K. et al.: Variability of nitrogen oxide emission fluxes and lifetimes estimated by Sentinel-5P TROPOMI observations, AGU Fall Meeting 2020.
- Lerot C. et al.: The ICOVAC project: an ESA initiative to study the impacts of COVID-19 lockdown measures on Air quality and Climate, AGU Fall Meeting 2020.
- Levelt P. et al.: Impact of COVID-19 Lockdown Measures on Air Quality as Observed by the TROPOMI/S5p Instrument, AGU Fall Meeting 2020.
- Mijling B. et al.: COVID-19 impact on NO_2 in European cities, OMI/TROPOMI workshop 2020.
- Stavrakou T. et al.: Covid-19 Shutdowns as an Unplanned Atmospheric Composition Experiment, AGU Fall Meeting 2020, invited.
- Stavrakou, T., Müller, J.-F., Bauwens, M., Doumbia, T., Elguindi, N., Darras, S., Claire Granier, C. G., Yiming Liu, Y. L., Shi, X., Bouarar, I., Brasseur, G., Wang, T., Eskes, H., De Smedt, I., Clarisse, L., Coheur, P. F., and Franco, B.: Covid-19-related air composition changes over China based on TROPOMI and IASI observations, in situ data and model simulations, EGU General Assembly 2021, online, 19–30 Apr 2021, EGU21-12942, https://doi.org/10.5194/egusphere-egu21-12942, 2021.
- Theys N. et al.: Improved TROPOMI SO_2 columns using a Covariance-Based Retrieval Algorithm (COBRA), OMI/TROPOMI workshop 2020.

6 References

Al-Haschimi, A., Aposolou, A. and Ricci, M. (2020). China's path to normalisation in the aftermath of the COVID-19 pandemic. Economic Bulletin Articles, 6 (1), https://EconPapers.repec.org/RePEc:ecb:ecbart:2020:0006:1

Alvarado, L., M.A., A. Richter, Lerot, C: GLYoxal Retrievals from TROPOMI (GLYRETRO) Valdiation Report, S5p+Innovation – theme 1 (CHOCHO), 5p+I_CHOCHO_BIRA_VR, issue 1.1, 19 November 2020, available at https://glyretro.aeronomie.be/.

Barré, J., Petetin, H., Colette, A., Guevara, M., Peuch, V.-H., Rouil, L., Engelen, R., Inness, A., Flemming, J., Pérez García-Pando, C., Bowdalo, D., Meleux, F., Geels, C., Christensen, J. H., Gauss, M., Benedictow, A., Tsyro, S., Friese, E., Struzewska, J., Kaminski, J. W., Douros, J., Timmermans, R., Robertson, L., Adani, M., Jorba, O., Joly, M., and Kouznetsov, R.: Estimating lockdown-induced European NO_2 changes using satellite and surface observations and air quality models, Atmos. Chem. Phys., 21, 7373–7394, https://doi.org/10.5194/acp-21-7373-2021, 2021.

Bauwens, M., Stavrakou, T., Müller, J.-F., De Smedt, I., Van Roozendael, M., van der Werf, G. R., Wiedinmyer, C., Kaiser, J. W., Sindelarova, K. and Guenther, A.: Nine years of global hydrocarbon emissions based on source inversion of OMI formaldehyde observations, Atmos. Chem. Phys., 16(15), 10133–10158, doi:10.5194/acp-16-10133-2016, 2016.

Bauwens, M., Compernolle, S., Stavrakou, T., Müller, J. -F., Gent, J., Eskes, H., Levelt, P. F., A, R., Veefkind, J. P., Vlietinck, J., Yu, H. and Zehner, C.: Impact of Coronavirus Outbreak on NO_2 Pollution Assessed Using TROPOMI and OMI Observations, Geophys. Res. Lett., 47(11), doi:10.1029/2020GL087978, 2020.

Beirle, S., Boersma, K. F., Platt, U., Lawrence, M. G., and Wagner, T.: Megacity emissions and lifetimes of nitrogen oxides probed from space, Science, 333, 1737–1739, 2011.

Biswas, S., Vadrevu, K. P., Lwin, Z. M., Lasko, K. & Justice, C. O. (2015). Factors Controlling Vegetation Fires in Protected and Non-Protected Areas of Myanmar. PLoS One, 10 (4), doi: 10.1371/journal.pone.0124346

Boesch, H., Anand, J., and Di Noia, A.: Product User Guide and Specification (PUGS) – ANNEX A for products CO_2_GOS_OCFP, CH_4_GOS_OCFP & CH_4_GOS_OCPR (v7.2, 2009-2018), 3-Nov-2019, pp. 33, http://wdc.dlr.de/C3S_312b_Lot2/Documentation/GHG/PUGS/C3S_D312b_Lot2.3.2.3-v1.0_PUGS-GHG_ANNEX-A_v3.1.pdf, 2019.

Borsdorff, T., aan de Brugh, J., Hu, H., Nédélec, P., Aben, I., and Landgraf, J.: Carbon monoxide column retrieval for clear-sky and cloudy atmospheres: a full-mission data set from SCIAMACHY 2.3 µm reflectance measurements, Atmos. Meas. Tech., 10, 1769–1782, https://doi.org/10.5194/amt-10-1769-2017, 2017.

Borsdorff, T., Hasekamp, O. P., Wassmann, A., & Landgraf, J., Insights into Tikhonov regularization: Application to trace gas column retrieval and the efficient calculation of total column averaging kernels. Atmospheric Measurement Techniques, 7(2), 523– 535, 2014.

Borsdorff, T., aan de Brugh, J., Hu, H., Hasekamp, O., Sussmann, R., Rettinger, M., Hase, F., Gross, J., Schneider, M., Garcia, O., Stremme,W., Grutter, M., Feist, D. G., Arnold, S. G., De Mazière, M., Kumar Sha, M., Pollard, D. F., Kiel, M., Roehl, C., Wennberg, P. O.,Toon, G. C., and Landgraf, J.: Mapping carbon monoxide pollution from space down to city scales with daily global coverage, Atmo-spheric Measurement Techniques Discussions, 2018, 1–19, https://doi.org/10.5194/amt-2018-132, https://www.atmos-meas-tech-discuss.10net/amt-2018-132/, 2018a.

Borsdorff, T., de Brugh, J. A., Hu, H., Aben, I., Hasekamp, O., and Landgraf, J.: Measuring Carbon Monoxide With TROPOMI: First Results and a Comparison With ECMWF-IFS Analysis Data, Geophysical Research Letters, 45, 2826–2832,https://doi.org/10.1002/2018GL077045, https://agupubs.onlinelibrary.wiley.com/doi/abs/10.1002/2018GL077045, 2018b.

Borsdorff, T., aan de Brugh, J., Pandey, S., Hasekamp, O., Aben, I., Houweling, S., and Landgraf, J.: Carbon monoxide air pollution on sub-city scales and along arterial roads detected by the Tropospheric Monitoring Instrument, Atmospheric Chemistry and Physics, 19,3579–3588, https://doi.org/10.5194/acp-19-3579-2019, https://www.atmos-chem-phys.net/19/3579/2019/, 2019.

Borsdorff, T., García Reynoso, A., Maldonado, G., Mar-Morales, B., Stremme, W., Grutter, M., and Landgraf, J.: Monitoring CO emissions of the metropolis Mexico City using TROPOMI CO observations, Atmos. Chem. Phys., 20, 15761–15774, https://doi.org/10.5194/acp-20-15761-2020, 2020.

Brasseur, G. P., Xie, Y., Petersen, A. K., Bouarar, I., Flemming, J., Gauss, M., et al. (2019). Ensemble forecasts of air quality in eastern China - Part 1: Model description and implementation of the MarcoPolo-Panda prediction system, version 1, *Geosci. Model Dev.*, 12, 33-67, https://doi.org/10.5194/gmd-12-33-2019.

Buchwitz, M., Reuter, M., Noël, S., Bramstedt, K., Schneising, O., Hilker, M., Fuentes Andrade, B., Bovensmann, H., Burrows, J. P., Di Noia, A., Boesch, H., Wu, L., Landgraf, J., Aben, I., Retscher, C., O'Dell, C. W., and Crisp, D.: Can a regional-scale reduction of atmospheric CO_2 during the COVID-19 pandemic be detected from space? A case study for East China using satellite XCO_2 retrievals, Atmos. Meas. Tech., 14, 2141-2166, https://doi.org/10.5194/amt-14-2141-2021, 2021.

Butz, A., Guerlet, S., Hasekamp, O., Schepers, D., Galli, A., Aben, I., Frankenberg, C., Hartmann, J.-M., Tran, H., Kuze, A., Keppel-Aleks, G., Toon, G., Wunch, D., Wennberg, P., Deutscher, N., Griffith, D., Macatangay, R., Messerschmidt, J., Notholt, J., and Warneke, T.: Toward accurate CO_2 and CH_4 observations from GOSAT, Geophys. Res. Lett., doi:10.1029/2011GL047888, 2011.

Cao, H., Fu, T.-M., Zhang, L., Henze, D. K., Miller, C. C., Lerot, C., Abad, G. G., De Smedt, I., Zhang, Q., van Roozendael, M., Hendrick, F., Chance, K., Li, J., Zheng, J. and Zhao, Y.: Adjoint inversion of Chinese non-methane volatile organic compound emissions using space-based observations of formaldehyde and glyoxal, Atmos. Chem. Phys., 18(20), 15017–15046, doi:10.5194/acp-18-15017-2018, 2018.

Clerbaux, C., Boynard, A., Clarisse, L., George, M., Hadji-Lazaro, J., Herbin, H., et al. (2009). Monitoring of atmospheric compo-sition using the thermal infrared IASI/MetOp sounder. Atmospheric Chemistry and Physics, 9, 6041–6054

Cogan, A. J., Boesch, H., Parker, R. J., Feng, L., Palmer, P. I., Blavier, J.-F. L., Deutscher, N. M., Macatangay, R., Notholt, J., Roehl, C., Warneke, T., and Wunsch, D.: Atmospheric carbon dioxide retrieved from the Greenhouse gases Observing SATellite (GOSAT): Comparison with ground-based TCCON observations and GEOS-Chem model calculations, J. Geophys. Res., 117, D21301, doi:10.1029/2012JD018087, 2012.

De Smedt, I., Theys, N., Yu, H., Danckaert, T., Lerot, C., Compernolle, S., Van Roozendael, M., Richter, A., Hilboll, A., Peters, E., Pedergnana, M., Loyola, D., Beirle, S., Wagner, T., Eskes, H., van Geffen, J., Boersma, K. F., and Veefkind, P.: Algorithm theoretical baseline for formaldehyde retrievals from S5P TROPOMI and from the QA4ECV project, Atmos. Meas. Tech., 11, 2395–2426, https://doi.org/10.5194/amt-11-2395-2018, 2018.

De Smedt, I., Pinardi, G., Vigouroux, C., Compernolle, S., Bais, A., Benavent, N., Boersma, F., Chan, K.-L., Donner, S., Eichmann, K.-U., Hedelt, P., Hendrick, F., Irie, H., Kumar, V., Lambert, J.-C., Langerock, B., Lerot, C., Liu, C., Loyola, D., Piters, A., Richter, A., Rivera Cárdenas, C. I., Romahn, F., Ryan, R. G., Sinha, V., Theys, N., Vlietinck, J., Wagner, T., Wang, T., Yu, H., and Van Roozendael, M.: Comparative assessment of TROPOMI and OMI formaldehyde observations against MAX-DOAS network column measurements, Atmos. Chem. Phys. Discuss. [preprint], https://doi.org/10.5194/acp-2021-378, in review, 2021.

Ding, J., van der A, R. J., Mijling, B., Levelt, P. F., & Hao, N. (2015). NOx emission estimates during the 2014 Youth Olympic Games in Nanjing. *Atmos. Chem. Phys*., 15(16), 9399-9412. doi:10.5194/acp-15-9399-2015.

Doumbia, T., Granier, C., Elguindi, N., Bouarar, I., Darras, S., Brasseur, G., et al. (2021). Changes in global air pollutant emissions during the COVID-19 pandemic: a dataset for atmospheric chemistry modeling. Earth System Science Data Discussions [preprint], https://doi.org/10.5194/essd-2020-348.

de Foy, B., Krotkov, N. A., Bei, N., Herndon, S. C., Huey, L. G., Martínez, A. P., Molina, L. T.: Hit from both sides: tracking industrial and volcanic plumes in Mexico City with surface measurements and OMI SO_2 retrievals during the MILAGRO field campaign. Atmos. Chem. Phys., 9, 9599–9617, https://doi.org/10.5194/acp-9-9599-2009, 2009.

Elguindi, N., Granier, C., Stavrakou, T., Darras, S., Bauwens, M., Cao, H., et al. (2020). Intercomparison of magnitudes and trends in anthropogenic surface emissions from bottom-up inventories, top-down estimates and emission scenarios. Earth's Future, 8, e2020EF001520.

Ekienabor, E. (2020). Coronavirus (Covid-19): The Lockdown Strategy in Nigeria. Preprints 2020, 2020050201, doi: 10.20944/preprints202005.0201.v1.

Fischer, E. V., Jacob, D. J., Yantosca, R. M., Sulprizio, M. P., Millet, D. B., Mao, J., et al. (2014). Atmospheric peroxyacetyl nitrate (PAN): a global budget and source attribution. Atmospheric Chemistry and Physics, 14, 2679–2698, https://doi.org/10.5194/acp-14-2679-2014

Franco, B., Clarisse, L., Stavrakou, T., Müller, J.-F., Van Damme, M., Whitburn, S., et al. (2018). A general framework for global retrievals of trace gases from IASI: application to methanol, formic acid, and PAN. Journal of Geophysical Research, 123, 13963–13984

Fu, T.-M. T.-M., Jacob, D. J., Wittrock, F., Burrows, J. P., Vrekoussis, M. and Henze, D. K.: Global budgets of atmospheric glyoxal and methylglyoxal, and implications for formation of secondary organic aerosols, J. Geophys. Res., 113(D15), D15303, doi:10.1029/2007JD009505, 2008.

Gaubert, B., Bouarar, I., Doumbia, T., Liu, Y., Stavrakou, T., Deroubaix, A., et al., Global changes in secondary atmospheric pollutants during the 2020 COVID-19 pandemic. Journal of Geophysical Research: Atmospheres, 126, e2020JD034213, https://doi.org/10.1029/2020JD034213, 2021.

Gkatzelis, G.I., Gilman, J.B., Brown, S.S., Eskes, H., Gomes, A.R., Lange, A.C., McDonald, B.C., Peischl, J., Petzold, A., Thompson, C.R., Kiendler-Scharr, A. 2021. The global impacts of COVID-19 lockdowns on urban air quality: A critical review and recommendations. Elementa: Science of the Anthropocene 9(1). DOI: https://doi.org/10.1525/elementa.2021.00176

Goldberg, D. L., S. C. Anenberg, D. Griffin, C. A. McLinden, Z. Lu, D. G. Streets: Disentangling the impact of the COVID-19 lockdowns on urban NO_2 from natural variability. Geophys. Res. Lett., 47, 2020.

Granier, C., Darras, S., Denier van der Gon, H., Doubalova, J., Elguindi, N., Bo, G., Gauss, M., Jalkanen, J.-P., Kuenen, J. et al. (2019). The Copernicus Atmosphere Monitoring Service global and regional emissions [Research Report] Copernicus At-mosphere Monitoring Service

Hersbach, H., Bell, B., Berrisford, P., Hirahara, S., Horanyi, A., Munoz-Sabater, J. et al. (2020). The ERA5 global reanalysis. Quarterly Journal of the Royal Meteorological Society, 146, 1999-2049, https://doi.org/10.1002/qj.3803

Holloway, T., Levy, H., and Kasibhatla, P., Global distribution of carbon monoxide, J. Geophys. Res., 118, 10490-10505, doi:10.1002/jgrd.50823, 2013.

Inness, A., Ades, M., Agustí-Panareda, A., Barré, J., Benedictow, A., Blechschmidt, A.-M., Dominguez, J. J., Engelen, R., Eskes, H., Flemming, J., Huijnen, V., Jones, L., Kipling, Z., Massart, S., Parrington, M., Peuch, V.-H., Razinger, M., Remy, S., Schulz, M., and Suttie, M.: The CAMS reanalysis of atmospheric composition, Atmos. Chem. Phys., 19, 3515–3556, https://doi.org/10.5194/acp-19-3515-2019, 2019.

Kiel, M., O'Dell, C. W., Fisher, B., Eldering, A., Nassar, R., MacDonald, C. G., and Wennberg, P. O.: How bias correction goes wrong: measurement of XCO_2 affected by erroneous surface pressure estimates, Atmos. Meas. Tech., 12, 2241–2259, https://doi.org/10.5194/amt-12-2241-2019, 2019.

Landgraf, J., aan de Brugh, J., Borsdorff, T., Houweling, S., and O., H.: Algorithm Theoretical Baseline Document for Sentinel-5 Precursor:Carbon Monoxide Total Column Retrieval, Atbd, SRON, Sorbonnelaan 2, 3584 CA Utrecht, The Netherlands, 2016a.

Landgraf, J., aan de Brugh, J., Scheepmaker, R., Borsdorff, T., Hu, H., Houweling, S., Butz, A., Aben, I., and Hasekamp, O.: Carbonmonoxide total column retrievals from TROPOMI shortwave infrared measurements, Atmospheric Measurement Techniques, 9, 4955–4975, https://doi.org/10.5194/amt-9-4955-2016, https://doi.org/10.5194%2Famt-9-4955-2016, 2016b.

Lange, K., Richter, A., and Burrows, J. P.: Variability of nitrogen oxide emission fluxes and lifetimes estimated from Sentinel-5P TROPOMI observations, Atmos. Chem. Phys. Discuss. [preprint], https://doi.org/10.5194/acp-2021-273, in review, 2021

Lerot, C., T. Stavrakou, M. Van Roozendael, L. M.A. Alvarado, A. Richter: GLYoxal Retrievals from TROPOMI (GLYRETRO) ATBD, S5p+Innovation – theme 1 (CHOCHO), 5p+I_CHOCHO_BIRA_ATBD, issue 2.1, 16 November 2020, https://glyretro.aeronomie.be/.

Lerot, C., Hendrick, F., Van Roozendael, M., Alvarado, L. M. A., Richter, A., De Smedt, I., Theys, N., Vlietinck, J., Yu, H., Van Gent, J., Stavrakou, T., Müller, J.-F., Valks, P., Loyola, D., Irie, H., Kumar, V., Wagner, T., Schreier, S. F., Sinha, V., Wang, T., Wang, P., and Retscher, C.: Glyoxal tropospheric column retrievals from TROPOMI, multi-satellite intercomparison and ground-based validation, Atmos. Meas. Tech. Discuss. [preprint], https://doi.org/10.5194/amt-2021-158, in review, 2021.

Li, J., Zhang, M., Tang, G., Wu, F., Alvarado, L. M. A., Vrekoussis, M., Richter, A., Burrows, J. P. (2018). Investigating missing sources of glyoxal over China using a regional air quality model (RAMS-CMAQ). Journal of Environmental Sciences, 71, 108–118, https://doi.org/10.1016/j.jes.2018.04.021

Liu, Y., and Wang, T. (2020). Worsening urban ozone pollution in China from 2013 to 2017–Part 1: The complex and varying roles of meteorology. Atmos. Chem. Phys., 20(11), 6305-6321.

Liu, F., Page, A., Strode, S. A., Yoshida, Y., Choi, S., Zheng, B., Lamsal, L. N., Li, C., Krotkov, N. A., Eskes, H., van der A, R., Veefkind, P., Levelt, P. F., Hauser, O. P. and Joiner, J.: Abrupt decline in tropospheric nitrogen dioxide over China after the outbreak of COVID-19, Sci. Adv., 6(28), eabc2992, doi:10.1126/sciadv.abc2992, 2020.

Masaki, T., Nakamura, S., Newhouse, D.: How is the COVID-19 crisis affecting nitrogen dioxide emissions in Sub-Saharan Africa? Poverty and Equity Notes, No. 21. World Bank, Washington, DC, World Bank. https://openknowledge.worldbank.org/handle/10986/33801, 2020.

Menut, L., Bessagnet, B., Khvorostyanov, D., Beekmann, M., Blond, N., Colette, A., et al. (2013). CHIMERE 2013: A model for regional atmospheric composition modelling. Geoscientific Model Development, 6(4), 981–1028. https://doi.org/10.5194/gmd-6-981-2013.

Mijling, B., and van der A, R. J. (2012). Using daily satellite observations to estimate emissions of short-lived air pollutants on a mesoscopic scale. Journal of Geophysical Research: Atmospheres, 117(D17). doi:10.1029/2012JD017817.

Müller, J.-F., Stavrakou, T. and Peeters, J. (2019). Chemistry and deposition in the Model of Atmospheric composition at Global and Regional scales using Inversion Techniques for Trace Gas Emissions (MAGRITTE v1.1). Part A. Chemical mechanism. Geoscientific Model Development, 12, 2307-2356, https://doi.org/10.5194/gmd-12-2307-2019

Noël, S., M. Reuter, M. Buchwitz, J. Borchardt, M. Hilker, H. Bovensmann, J. P. Burrows, A. Di Noia, H. Suto, Y. Yoshida, M. Buschmann, N. M. Deutscher, D. G. Feist, D. W. T. Griffith, F. Hase, R. Kivi, I. Morino, J. Notholt, H. Ohyama, C. Petri, J. R. Podolske, D. F. Pollard, M. Kumar Sha, K. Shiomi, R. Sussmann, Y. Té, V. A. Velazco, and T. Warneke, XCO_2 retrieval for GOSAT and GOSAT-2 based on the FOCAL algorithm, submitted to Atmos. Meas. Tech., 2020.

O'Dell, C. W., Eldering, A., Wennberg, P. O., Crisp, D., Gunson, M. R., Fisher, B., Frankenberg, C., Kiel, M., Lindqvist, H., Mandrake, L., Merrelli, A., Natraj, V., Nelson, R. R., Osterman, G. B., Payne, V. H., Taylor, T. R., Wunch, D., Drouin, B. J., Oyafuso, F., Chang, A., McDuffie, J., Smyth, M., Baker, D. F., Basu, S., Chevallier, F., Crowell, S. M. R., Feng, L., Palmer, P. I., Dubey, M., García, O. E., 15 Griffith, D. W. T., Hase, F., Iraci, L. T., Kivi, R., Morino, I., Notholt, J., Ohyama, H., Petri, C., Roehl, C. M., Sha, M. K., Strong, K.,Sussmann, R., Te, Y., Uchino, O., and Velazco, V. A.: Improved Retrievals of Carbon Dioxide from the Orbiting Carbon Observatory-2 with the version 8 ACOS algorithm, Atmos. Meas. Tech., 11, 6539-6576, https://doi.org/10.5194/amt-11-6539-2018, 2018.

Opacka, B., Müller, J.-F., Stavrakou, T., Bauwens, M., Sindelarova, K., Markova, J. & Guenther, A. (2021). Global and regional impacts of land cover changes on isoprene emissions derived from spaceborne data and the MEGAN model. Atmospheric Chemistry and Physics, 21, 8413–8436, https://doi.org/10.5194/acp-21-8413-2021, 2021.

Osterman, G., O'Dell, C., Eldering A., Fisher, B., Crisp, D., Cheng, C., Frankenberg, C., Lambert, A., Gunson, M., Mandrake, L., Wunch, D.: Orbiting Carbon Observatory-2 & 3 (OCO-2 & OCO-3) Data Product User's Guide, Operational Level 2 Data Versions 10 and Lite File Version 10 and VEarly, Technical Report National Aeronautics and Space Administration, Jet Propulsion Laboratory, California Institute of Technology, Pasadena, California, USA, Version 1.0, Revision A, June 8, 2020, Data Release: 10 (OCO-2), VEarly (OCO-3), https://docserver.gesdisc.eosdis.nasa.gov/public/project/OCO/OCO_2_OCO3_B10_DUG.pdf, 2020.

Petersen, A. K., Brasseur, G. P., Bouarar, I., Flemming, J., Gauss, M., Jiang, F., et al (2019). Ensemble forecasts of air quality in eastern China - Part 2: Evaluation of the MarcoPolo-Panda prediction system, version 1. Geosci. Model Dev.. 12, 1241-1266, https://doi.org/10.5194/gmd-12-1241-2019.

Pommier, M., McLinden, C. A., and Deeter, M.: Relative changes in CO emissions over megacities based on observations from space, Geophysical research letters, 40, 3766–3771, 2013.

Schneising, O., Buchwitz, M., Reuter, M., Bovensmann, H., Burrows, J. P., Borsdorff, T., Deutscher, N. M., Feist, D. G., Griffith, D. W. T., Hase, F., Hermans, C., Iraci, L. T., Kivi, R., Landgraf, J., Morino, I., Notholt, J., Petri, C., Pollard, D. F., Roche, S., Shiomi, K., Strong, K., Sussmann, R., Velazco, V. A., Warneke, T., and Wunch, D.: A scientific algorithm to simultaneously retrieve carbon monoxide and methane from TROPOMI onboard Sentinel-5 Precursor, Atmos. Meas. Tech., 12, 6771-6802, https://doi.org/10.5194/amt-12-6771-2019, https://doi.org/10.5194/amt-12-6771-2019, 2019.

Schneising, O., Buchwitz, M., Reuter, M., Bovensmann, H., and Burrows, J. P.: Severe Californian wildfires in November 2018 observed from space: the carbon monoxide perspective, Atmos. Chem. Phys., 20, 3317-3332, https://doi.org/10.5194/acp-20-3317-2020, 2020a.

Schneising, O., Buchwitz, M., Reuter, M., Vanselow, S., Bovensmann, H., and Burrows, J. P.: Remote sensing of methane leakage from natural gas and petroleum systems revisited, Atmos. Chem. Phys., 20, 9169-9182, https://doi.org/10.5194/acp-20-9169-2020, 2020b.

Shi, X. and Brasseur, G. P.: The Response in Air Quality to the Reduction of Chinese Economic Activities during the COVID-19 Outbreak, Geophys. Res. Lett., doi:10.1029/2020GL088070, 2020.

Tan, P.-H., Chou, C., Liang, J.-Y., Chou, C. C.-K., *and* Shiu, C.-J.: Air pollution 'holiday effect' resulting from the Chinese New Year. Atmos. Environ., 43*(*13*)*, 2114–2124, 2009.

Stavrakou, T., Müller, J.-F., De Smedt, I., Van Roozendael, M., Kanakidou, M., Vrekoussis, M., Wittrock, F., Richter, A. and Burrows, J. P.: The continental source of glyoxal estimated by the synergistic use of spaceborne measurements and inverse modelling, Atmos. Chem. Phys., 9(21), 8431–8446 [online] Available from: http://www.atmos-chem-phys.net/9/8431/2009/, 2009.

Stavrakou, T., Müller, J.-F., Bauwens, M., De Smedt, I., Lerot, C., Van Roozendael, M., et al. (2016). Substantial Underestimation of Post-Harvest Burning Emissions in the North China Plain Revealed by Multi-Species Space Observations. Scientific Reports, 6, 32307, https://doi.org/10.1038/srep32307

Stavrakou, T., Müller, J.-F., Bauwens, M., De Smedt, I., Van Roozendael, M. & Guenther, A. (2018). Impact of short-term climate variability on volatile organic compounds emissions assessed using OMI satellite formaldehyde observations. Geophysical Research Letters, 45, 1621-1629, http://doi.org/10.1029/2018GL078676

Theys, N., Fioletov, V., Li, C., De Smedt, I., Lerot, C., McLinden, C., Krotkov, N., Griffin, D., Clarisse, L., Hedelt, P., Loyola, D., Wagner, T., Kumar, V., Innes, A., Ribas, R., Hendrick, F., Vlietinck, J., Brenot, H., and Van Roozendael, M.: A Sulfur Dioxide Covariance-Based Retrieval Algorithm (COBRA): application to TROPOMI reveals new emission sources, Atmos. Chem. Phys. Discuss. [preprint], https://doi.org/10.5194/acp-2021-294, in review, 2021.

Valin, L., Russell, A., and Cohen, R.: Variations of OH radical in an urban plume inferred from NO_2 column measurements, Geophysical Research Letters, 40, 1856–1860, 2013.

van Geffen, J., Boersma, K. F., Eskes, H., Sneep, M., Ter Linden, M., Zara, M., Veefkind, J. P., S5P TROPOMI NO_2 slant column retrieval: method, stability, uncertainties and comparisons with OMI. Atmos. Meas. Tech., *13*(3), 1315-1335, 2020.

van der A, R. J., Mijling, B., Ding, J., Koukouli, M. E., Liu, F., Li, Q., et al. (2017). Cleaning up the air: effectiveness of air quality policy for SO_2 and NO_x emissions in China. *Atmos. Chem. Phys.*, 17(3), 1775-1789. doi:10.5194/acp-17-1775-2017.

van der Werf, G. R., Randerson, J. T., Giglio, L., van Leeuwen, T. T., Chen, Y., Rogers, B. M., Mu, M., van Marle, M. J. E., Morton, D. C., Collatz, G. J., Yokelson, R. J. & Kasibhatla, P. S. (2017). Global fire emissions estimates during 1997–2016. Earth System Science Data, 9, 697–720, https://doi.org/10.5194/essd-9-697-2017

Veefkind, J.P., Aben, I., McMullan, K., Forster, H., de Vries, J., Otter, G., Claas, J., Eskes, H.J., de Haan, J.F., Kleipool, Q., van Weele, M., Hasekamp, O., Hoogeveen, R., Landgraf, J., Snel, R., Tol, P., Ingmann, P., Voors., R., Kruizinge, B., Vink, R., Visser, H., and Levelt, P.F., TROPOMI on the ESA Sentinel-5 Precursor : A GMES mission for global observations of the atmospheric composition for climate, air quality and ozone layer applications, Remote Sensing of Environment, 120, 70-83, 2012.

Wu, L., Aben, I., and Hasekamp, O. P.: Product User Guide and Specification (PUGS) – ANNEX B for products CO_2_GOS_SRFP, CH_4_GOS_SRFP (v2.3.8, 2009-2018), 29-Nov-2019, pp. 26, http://wdc.dlr.de/C3S_312b_Lot2/Documentation/GHG/PUGS/C3S_D312b_Lot2.3.2.3-v1.0_PUGS-GHG_ANNEX-B_v3.1.pdf, 2019.

Zhang, Y., Cao, F. (2015) Fine particulate matter (PM2.5) in China at a city level. Sci Rep 5, 14884. https://doi.org/10.1038/srep14884

Zhu, L., Jacob, D. J., Mickley, L. J., Marais, E. A., Cohan, D. S., Yoshida, Y., Chance, K. V. (2014). Anthropogenic emissions of highly reactive volatile organic compounds in eastern Texas inferred from oversampling of satellite (OMI) measurements of HCHO columns. Environ. Res. Lett., 9(11), 114004.

Annex A

Coordinates of the 59 Indian powerplants used to analyze the SO_2 column reduction during the local COVID-19 lockdown.

Longitude (degree)	Latitude (degree)	Power plant name
82.6719	24.0983	VINDH_CHAL S
69.5532	22.8230	MUNDRA TPP
69.5281	22.8158	MUNDRA UMPP
82.6275	23.9784	SASAN UMPP
79.9671	21.4129	TIRORA TPP
82.7915	24.0270	RIHAND
85.0740	21.0966	TALCHER STPS
82.2930	22.1300	SIPAT STPS
79.2900	20.0063	CHANDRAPUR_C
82.7891	24.2010	ANPARA
82.6858	22.3881	KORBA STPS
79.4560	18.7572	R_GUNDEM STP
79.0960	21.2414	KORADI
83.4513	22.0987	TAMNAR TPP
79.3978	21.1797	MOUDA STPS
87.8940	24.7720	FARAKKA STPS
82.7068	24.1033	SINGRAULI ST
75.2372	29.9240	TALWANDI SAB
77.6078	28.6030	DADRI (NCTPP
82.4091	21.9603	AKALTARA TPP
77.3422	16.3532	RAICHUR
76.7195	15.1932	BELLARY TPS
77.0357	24.6217	CHHABRA TPS
88.1046	24.3696	SAGARDIGHI T
77.3568	16.2949	YERMARUS TPP
79.4417	11.5576	NEYVELI ST I
81.8525	21.4499	RAIKHEDA
82.6888	22.4118	KORBA-WEST
79.1160	21.2818	K_KHEDA II
87.1311	23.4639	MEJIA
81.0668	23.3026	SANJAY GANDH
81.9045	24.1500	NIGRI
87.8713	22.4157	KOLAGHAT
75.8425	21.0483	BHUSAWAL
82.8000	24.2007	ANAPARA "C"
81.7865	23.0655	ANUPUR TPP
83.1889	21.9114	BARADARHA TP
84.9843	21.1238	DERANG
79.7515	11.5214	ITPCL TPP
86.6610	23.6220	RAGHUNATHPUR
79.5748	18.8372	SINGARENI TP
76.5317	22.0971	Shri Singaji
82.9803	24.4448	OBRA-A
73.5574	21.2093	UKAI_Coal
79.8265	18.3835	KAKATIYA TPP
83.1215	21.8858	UCHPINDA TPP

87.4513	23.8285	BAKRESWAR
85.2671	20.8700	KAMALANGA
86.7600	23.8209	MAITHON RB T
87.2043	23.5800	DURGAPUR STE
80.6936	17.6219	K_GUDEM NEW
82.6022	22.0708	MARWA TPP
87.1311	23.4639	MEJIA TPS EX
83.2331	21.9846	RAIGARH TPP
76.8763	29.3975	PANIPAT
82.7188	22.3828	KORBA-EAST
77.8138	11.7696	METTUR
83.4573	21.7570	LARA
88.1400	22.4673	BUDGE BUDGE